ADAPTIVE INTERVAL TYPE-2 FUZZY LOGIC CONTROL OF MARINE VESSELS

XUETAO CHEN

NATIONAL UNIVERSITY OF SINGAPORE

2013

ADAPTIVE INTERVAL TYPE-2 FUZZY LOGIC CONTROL OF MARINE VESSELS

XUETAO CHEN

(*B.Eng, HIT*)

A THESIS SUBMITTED

FOR THE DEGREE OF DOCTOR OF PHILOSOPHY

DEPARTMENT OF ELECTRICAL AND COMPUTER ENGINEERING

NATIONAL UNIVERSITY OF SINGAPORE

2013

Acknowledgements

It is my great pleasure to thank all the people who enabled me to perform this work.

Firstly, I am extremely grateful to my supervisor, Assoc. Prof. Woei Wan Tan, for her outstanding guidance and continuous support on my research and life during my Ph.D study. Without her commitment and dedication, I would not have honed my research skills and capabilities as well as I did in the past four years. The numerous discussions with her throughout the course of this research have been most fulfilling and have given me a deeper insight in fuzzy logic and control theory.

Jointly, I would like to thank Assoc. Prof. Woei Wan Tan, Assoc. Prof. Che Sau Chang and Prof. Tien Fang Fwa for the opportunity to participate in the idea conceptualization and grant proposal writing at Center for Maritime Studies of NUS. I salute them for their exemplary efforts in building relationships with both academia and industry and dedication to the Maritime and Offshore industry. Special thanks to Assoc. Prof. Stephane Bressan and Dr. Baljeet Singh Malhotra, I have learnt a lot from discussions with them.

My appreciation goes to Prof. Qingguo Wang, Assoc. Prof. Cheng Xiang and Assoc. Prof. Kok Kiong Tan in my thesis committee, for their kind advice and guidance on my thesis.

I also wish to take this opportunity to thank professors in Department of Electrical

and Computer Engineering of NUS for building up my fundamentals in control theory.

My gratitude goes to Dr. Teck Wee Chua and Dr. Maowen Nie for their help and technical troubleshooting during the initial phases and later comradeship. Sincere thanks goes to many colleagues and friends in the Advanced Control Technology Laboratory, Control and Simulations Laboratory and Center for Maritime Studies, with special mention of Dr. Yang Yang, Dr. Lichun Shao, Dr. Han Yan, Mr. Xingguo Shao, Dr. Huaping Dai, Dr. Xinhua Wang, Mr. Gangquan Dai, Mr. Chao Yu, Dr. Keng Peng Tee, Mr. Xiangxu Dong, Ms. Xiaolian Zheng, Ms. Lingling Cao, Mr. Yue Yang, Dr. Dong Yang, Dr. Zhuo Sun, Dr. Jianfeng Zheng and Dr. Hongtao Hu for the lively discussions, sharing of ideas and happiness along the journey. Also my sincere thanks to all who have helped in one way or another in the completion of this thesis.

Last but not least, I would like to express my gratitude to my parents Liang Chen and Guoxian Ding, my brother and sister in law Xuehui Chen and Yajing Tong, and my girl friend Xue Wang for their unquestioning love, trust and encouragement. They have always been there for me, stood by me through the good times and the bad.

Contents

Summary

With the demand for fossil fuels increasing over the years, the exploration and exploitation of these energy sources have been moving from land to the deep sea. This results in an increased focus on the marine control systems which are essential to guarantee that the sea operations such as deep sea oil drilling, oil production, storage and offloading, and cable/pipe laying are performed as planned. To increase the safety and efficiency of the sea operations, more advanced marine control systems are needed for dynamic positioning (DP) and trajectory tracking control of marine vessels. The main purpose of the research in this thesis is to develop advanced strategies for DP and tracking control of marine vessels in the harsh marine environment and alleviate some of the challenges of dealing with complex hydrodynamic disturbances.

DP is an essential system for floating vessels such as drilling rigs, floating production, storage and offloading systems, crane vessels and multi-purpose vessels. For DP of floating vessels under time-varying hydrodynamic disturbances, this thesis presents an indirect adaptive interval type-2 (IT2) fuzzy logic controller (FLC). Approximation-based adaptive control technique in combination with IT2 fuzzy logic system (FLS) is employed in the design of the controller to reject the hydrodynamic disturbances without the need for exact information. The stability of the design is demonstrated through passive and Lyapunov analyses where the sufficient condition,

under which the semiglobally asymptotic convergence of the regulation errors is guaranteed, is proposed. Rigorous analysis shows that the resultant closed-loop system is passive. Comparative simulations with linear proportional derivative controller and adaptive type-1 FLC are carried out. The proposed technique is found to be effective, robust, and has better performance. In a DP system, filtering and state estimation are important features, as the position and heading measurements are corrupted by oscillatory motion due to first-order wave disturbances. Moreover, in most cases the measurements of the vessel velocities are not available. This thesis then presents a passive adaptive IT2 fuzzy observer for DP of floating vessels under time-varying hydrodynamic disturbances. The approximation-based adaptive technique is also used to handle the time-varying hydrodynamic disturbances. The stability of the observer error dynamics is explored through passive and Lyapunov analyses. It shows that the estimation errors of the observer error dynamics are semiglobally uniformly ultimately bounded. The adaptive observer includes features like estimations of both the low frequency displacements and velocities of the vessels from noisy displacement measurements and wave filtering. Simulation studies with a container ship demonstrate the satisfactory performance of the proposed observer. A comparative study of the proposed observer against a passive nonlinear observer shows the proposed observer has better disturbance rejection property.

Another major application of automatic control technique in the offshore and marine industry is trajectory tracking. Trajectory tracking control is very important for surface vessels which perform operations such as dredging, towing, and cable and pipe laying. For tracking control of surface vessels under time-varying hydro-

dynamic disturbances, the thesis first presents an indirect adaptive IT2 FLC as well as a direct adaptive IT2 FLC. In the tracking control problem, the approximation-based adaptive control technique again shows its efficiency in handling time-varying hydrodynamic disturbances. Although designed from different points of view, both indirect and direct adaptive IT2 FLC yield similar and passive closed-loop systems. The semiglobal asymptotic convergence of the tracking errors in the closed-loop systems is shown through Passive and Lyapunov analyses. A comparative study of the proposed techniques against their adaptive type-1 counterparts was conducted. The proposed adaptive IT2 fuzzy techniques are found to be effective, robust, and reduce the integral of time-weighted absolute tracking errors for the indirect adaptive FLC by at least 21.9% and 18.0% for the direct adaptive case compared to type-1 FLCs. However, the indirect and direct adaptive IT2 FLCs require the velocities of the vessels measurable. To relax this requirement and improve the reliability of the control systems, a fault-tolerant adaptive backstepping IT2 FLC is designed. The combination of backstepping control and approximation-based adaptive technique allows the proposed controller to be able to accommodate certain faults in the plant and the controller itself. These faults could be the changes of the loading conditions and trimming of the vessels, and failure of some parts of the control law. In the output feedback controller, the unmeasurable velocities are estimated by a high-gain observer to get a stable output feedback closed-loop system. Using backstepping and Lyapunov synthesis, semiglobal uniform boundedness of the output feedback closed-loop signals is guaranteed. Simulation results demonstrate that the output feedback controller is effective in reducing the tracking errors, and able to accommodate the

faults in the plant and the controller.

List of Figures

List of Tables

Chapter 1

Introduction

As the major source of energy powering the world, fossil fuels have been contributing to the growth of the global economy. With the demand for fossil fuels increasing over the years, the exploration and exploitation of these energy sources have been moving from land to the deep sea. This has brought about an era of offshore oil and gas industry. Offshore oil and gas industry involves different kinds of equipments to perform various missions. One crucial equipment is marine vessels, which include drilling rigs, shuttle tankers, cable/pipe layers, floating production, storage, and offloading systems (FPSOs), crane and heavy lift vessels, and multi-purpose vessels. A marine vessel may comprise sub-systems such as the main structure, marine control system, power system, propulsion system, measurement system, equipment system and auxiliary system. Among all these systems, the marine control system is essential to guarantee that sea operations such as deep sea oil drilling, installation and intervention, oil production, storage and offloading, and cable/pipe laying are performed as planned. To increase the safety and efficiency of the sea operations, more advanced marine control systems are necessary. One main factor that impedes the performance of marine control systems is the hydrodynamic disturbances generated by wind-induced waves and associated uncertainties. To handle the complex hydrodynamic disturbances and the uncertainties, advanced control algorithm is applied

to marine control system design in dynamic positioning (DP) and tracking control of these marine vessels.

In the remainder of this chapter, a detailed exposition of the background and motivation, as well as the objectives and scope, and organization of this thesis are provided. For clarity of presentation, the background and motivation is separated into two parts, namely Marine Control Systems and Interval Type-2 Fuzzy Logic. In each part, the related works and background knowledge that motivate the research in this thesis are discussed in detail.

1.1 Marine Control Systems

The history of vessel control starts with the invention of the gyrocompass in 1908. The gyrocompass was the basic instrument in the first feedback control system for heading control of vessels, and today these devices are known as autopilots. In 1970s, local area vessel positioning systems like hydro acoustic reference systems, hyperbolic radio navigation systems, and local electromagnetic distance measuring systems were introduced. These systems together with new results in feedback control resulted in new applications like DP systems for vessels. In 1994, Navstar GPS was declared fully operational although the first satellite was launched in 1974. Today, GPS receivers are standard component in tracking control systems. Marine control systems and their applications to marine vessels have become more and more popular due to the developments in computer science, propulsion systems and modern sensor technology. Other examples of commercially available systems are: attitude control systems

for underwater vehicles, fin and rudder-roll stabilization systems, buoyancy control systems including trim and heel correction systems, propeller and thruster control systems, and energy and power managements systems. In the following subsections autopilots, DP systems and tracking control systems are described in details. After that, a basic configuration of marine control systems for different control objectives is introduced.

1.1.1 Autopilots

The autopilot or automatic pilot is a device which is used to control an aircraft, ship or other vehicles without constant human intervention. The earliest autopilots could do no more than maintain a fixed heading (course-keeping) and they are still in use by smaller boats during routine cruising nowadays. For vessels, course-keeping is the first application. However, modern autopilots can conduct more complex maneuvers like turning, docking operations and even control inherently unstable vessels, e.g. submarines and some large oil tankers.

The history of autopilot for vessel started with Elmer Sperry (1860-1930), who constructed the first automatic ship steering mechanism for course keeping in 1911 [1]. This device, which is referred to as the "Metal Mike", was a gyroscope-guided autopilot or a mechanical helmsman. Later in 1922, Nicholas Minorsky (1885-1970) presented a detailed analysis of a position feedback control system where he formulated a three-term control law which today is known as Proportional Integral Derivative (PID) control [2]. These three different behaviors were motivated by observing

the way in which a helmsman steered a ship. The autopilot systems of Sperry and Minorsky are both single-input single-output control systems, where they compare the desired heading with the measured heading and compute the rudder command. In 1960-1961 the Kalman filter was publised by Kalman [3] and Kalman and Bucy [4]. Two years later in 1963, the theory of Linear Quadratic Regulator controller was developed, which motivated the application of Linear Quadratic Gaussian (LQG) in autopilot design [5–7]. With the help of LQG control technique, the autopilot system became multi-input multi-output system, and the heading and position of a ship could be controlled simultaneously. In addition to LQG and H_∞ control, other design techniques have been applied to ship autopilot design to obtain better control performance, for instance nonlinear control theory [8].

1.1.2 Dynamic Positioning Systems

A DP system is defined by the class societies e.g. Det Norske Veritas (DNV), American Bureau of Shipping (ABS) and Lloyd's Register (LRS or Lloyd's), as a system that maintains a vessels's position and heading exclusively by means of active thrusters. This is obtained either by installing tunnel thrusters in addition to the main propellers, or by using azimuth thrusters, which can produce thrust in different directions. In offshore oil and gas industry, dynamic positioning finds very wide applications. It is almost applicable to all the service vessels. Besides, it is also widely applied to merchant vessels, cruise ships, yachts and fisheries to assist their docking and driving operations.

The great success of PID-based autopilots, and the development of local area positioning systems suggested that three decoupled PID controllers could be used to control the motion of a ship in the surge, sway and yaw axes exclusively by means of thrusters and propellers. The idea was tested in the 1960s, and the invention was referred to as a DP system. The first DP system was designed using conventional PID controller in cascade with low pass and notch filters to suppress the wave-induced motion components [9]. The drawback of the PID controller in cascade with low pass and notch filters is that additional phase lag and nonlinearities are introduced in the closed-loop system. In 1976, a new model-based control concept utilizing stochastic optimal control theory and Kalman filtering techniques was employed to reduce these problems by Balchen et al. [10]. The Kalman filter is used to separate the low frequency and wave frequency motion components such that only low frequency motion is fed back. The reason behind this is that the vessel motion is in the low frequency spectrum, and the high frequency wave motion due to first order wave would cause wear and tear of the actuators if it enters the feedback loop. Later extensions and modifications of this work have been reported by many authors such as Balchen et al. [11], Fung and Grimble [12], Fossen et al. [13], Sørensen et al. [14], Volovodov et al [15] and Perez and Donaire [16]. The major drawback of Kalman filter is that the kinematic equations must be linearized about a set of yaw angles, typically 36 operating points in steps of 10°. As a result, it is very difficult and time consuming to tune the parameters of the Kalman filter. In the 1990s nonlinear controls for DP were proposed by several research groups. Stephens et al [17] proposed fuzzy controllers. Aarset et al. [18], Fossen and Grøvlen [19] and Bertin et al. [20] pro-

posed backstepping and nonlinear feedback linearization for DP. As nonlinear control techniques were actively developed in 1990s [21]– [24], the linear Kalman filter became an obstacle in the research community. To surmount this obstacle, a passive nonlinear observer was proposed by Fossen and Strand [25]. One of the motivations for using nonlinear passivity theory was that the passivity theory allows the control algorithms to be decomposed into several simpler subsystems. Correspondingly the number of observer tuning parameters were significantly reduced. As DP technology became more mature, research efforts were put into the integration of vessel control systems and missions by including operational requirements into the design of both the guidance systems and the controllers. Sørensen et al. recommended the concept of optimal setpoint following for DP of deep-water drilling and intervention vessel [26]. Leira et al. extended this work and proposed to use structural reliability criteria of the drilling risers for the setpoint following [27]. Fossen and Strand presented the nonlinear passive weather optimal positioning control systems for ships and rigs [28]. The importance of the DP control system for the closed-loop performance of the station keeping operation is clearly demonstrated in several studies. Morishita and Cornet [29], Morishita et al. [30] and Tannuri et al. [31] have conducted detailed performance studies of the DP operations for shuttle tanker and FPSOs. More recently, Sørensen et al. [32], Nguyen [33]– [35], and Nguyen and Sørensen [36] proposed the design of supervisory switched hybrid controllers for DP that automatically switch controllers according to whether the sea conditions is clam or choppy, and from transit to station keeping operations. The main objective of the supervisory switched control is to integrate a bunch of controllers into a hybrid DP system being

able to control a vessel to operate in varying environmental and operational conditions. When there are time-varying hydrodynamic disturbances in marine vessels as shown in [37, 38], the existing DP controllers may not be able to provide satisfactory performance, and the passive nonlinear observer [25] which models time-varying hydrodynamic disturbances as a first order Markov process may only handle slowly varying component of the time-varying hydrodynamic disturbances. In this thesis, to handle the time-varying hydrodynamic disturbances that are present in marine vessels during DP controller and observer design, adaptive technique is applied. Traditional model-based adaptive control technique is not suitable since it is generally useful only when dealing with systems in which the dynamics are linear in the parameters, the regressors are exactly known, and the uncertainties are parametric and time-invariant [39,40]. Hence, approximation-based adaptive control [41]– [48], which does not require parametric or functional certainty, is adopted to compensate for the disturbances from environment. The approximators in approximation-based adaptive technique utilize a standard regressor function whose configuration is independent of the dynamic characteristics of the vessel model.

1.1.3 Tracking Control Systems

A tracking control system is a system that controls a vessel to track a reference trajectory which is computed from the old to the new position or heading set point. The transformation of the way points to a feasible path or trajectory is generally a nonlinear optimization problem. In order to guide a vessel through a busy water way

or to perform sea operations like dredging operations, towing operations, cable/pipe laying operations, tracking control is necessary.

The successful application of LQG controllers to vessel autopilots and DP systems, and the availability of global navigation systems like GPS and GLONASS resulted in a growing interest for trajectory tracking control [49]– [53]. The controller design problem can be treated as a nonlinear control problem or solved by means of linear theory [52]. When there are time-varying hydrodynamic disturbances presented in marine vessels [37, 38], the trajectory tracking problem with these models for both state feedback and output feedback control is challenging. Faults in automated processes often cause undesired reactions of a controlled plant, and the consequences could be damaging to the plant, to personnel or the environments. In order to improve the reliability of automated processes, fault-tolerant control has been proposed and studied as illustrated in [54] and [55]. As a passive fault-tolerant approach, backstepping control has been applied in vessel control problems as shown in [51] and [56]. Augmentation of active fault-tolerant components to the backstepping control would improve its performance. In this thesis, to accommodate faults such as changes of the loading conditions and trimming of the vessels, and failure of some parts of the control law in the controller, fault-tolerant tracking control of vessels is investigated.

1.1.4 Basic Configuration

Various methods have been proposed for designing marine control systems used for DP and trajectory tracking. While the design methodologies may differ, the basic

configurations are more or less based on the same principles [57], as exemplified in Fig. 1.1. The functions of the main components are described below.

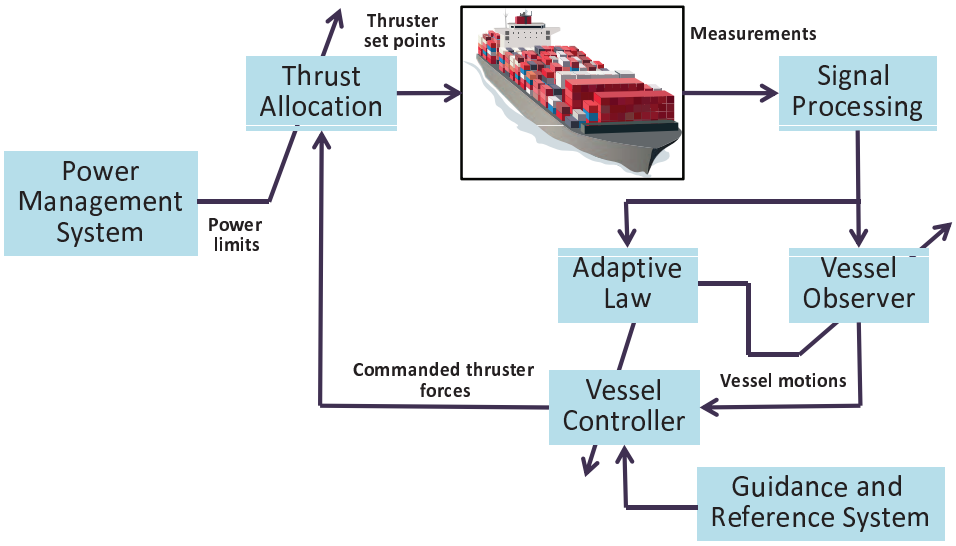

Figure 1.1: Basic configuration of marine control systems.

- Signal processing. All signals from the sensors should be analyzed and checked by a separate signal processing module. This includes testing of the individual signals and signal voting and weighting when redundant measurements are available. The individual signal quality verification should comprise tests for frozen signals, signal range and variance, and signal wild points. If an erroneous signal is detected, the signal is rejected and not used. The resultant signals from each sensor group should not contain any steps or discontinuities when utilized in the system in order to ensure a safe operation.

- Vessel observer. When measurements of parts of the vessel states are not available, estimates of these vessel states must be computed from available

measurements through a state observer. In accurate DP control, the influence of first order wave would be significant. The oscillatory motion due to the first order wave should not enter the feedback loop, because the wave frequency motion will cause wear and tear in the propulsion system and there is no need to reject the oscillatory wave frequency motion. In this case, the so called wave filtering techniques are used to separates the position and heading measurements into a low frequency and a wave frequency position and heading part. For vessels which are not traveling in low speed, the influence of first order wave would not be so significant.

- Vessel controller. The controller is a set of algorithms that determine the necessary control forces and moments to be provided by the propulsion system in order to satisfy a certain control objective. The desired control objective is usually in conjunction with the guidance and reference system. Examples of control objectives are DP, trajectory tracking, path following, maneuvering etc. The inputs of the feedback controller are the outputs from the measurement system or state observer. The outputs of the feedback controller are the commands of the actuation system.

- Guidance and reference system. This system computes the reference position, velocity and acceleration of a vessel to be used by the control system. These data are usually provided to the human operator. The basic components of a guidance system are motion sensors, weather sensors and a computer. The computer collects and processes the data, and then feeds the results to the

control system. In many cases, optimization techniques are used to compute the optimal trajectory for the vessel to follow. This might include features like fuel optimization, minimum time navigation, weather routing, collision avoidance, formation control and schedule meeting.

- Thrust allocation. The high-level feedback controller computes the commanded forces and moments. The thrust allocation module the calculates the corresponding force and direction commands to each thrust device. The low-level thruster controllers will then control the propeller pitch, speed, torque, and power to satisfy the desired thrust demands. This module is also the main link between the control system and the power management system. In any case, the thrust allocation must handle power limitation of the thrusters in order to avoid power system overload or blackout.

- Adaptive law. The parameters in the mathematical model describing the vessel dynamics will change with different environmental and operational conditions. In a model based observer and controller design, the control system should be able to automatically provide necessary corrections of the vessel model and controller gains subject to variations in vessel draught, vessel loading condition, wind area, and sea state. This can be obtained either by nonlinear and adaptive formulations or by other techniques such as gain-scheduling.

This thesis mainly focuses on the modules of vessel observer, vessel controller and adaptive law. The control objective will mainly be DP and trajectory tracking.

1.2 Interval Type-2 Fuzzy Logic

Uncertainty is ubiquitous in the real world to make things different from one another. When dealing with real-world problems, uncertainty can be rarely avoided. There are many sources of uncertainty facing the marine control systems in the real world. Some of them are as follows.

- Uncertainties in inputs to the control systems. Since the sensor measurements are always corrupted with colored noise, caused by a combination of inevitable measurement errors and resolution limits of measuring instruments as well as wind, waves and ocean currents.
- Uncertainties in control actions. They often result from the lack of sufficient power for desired control actions or the changes of the actuator characteristics.
- Uncertainties in control algorithms. The control algorithms may be designed based on mathematical models of vessels, and these models likely contain uncertainties resulting from unmodelled dynamics and changes of operational conditions.

In addition, marine applications are characterized by time-varying environmental disturbances and widely changing sea conditions, which brings about extra unavoidable uncertainties.

Type-1 fuzzy sets, the foundation of fuzzy theory, were introduced as a way of expressing non-probabilistic uncertainties by Zadeh [58] in 1965. Since then, fuzzy theory has been applied to construct different kinds of type-1 fuzzy logic controllers

(FLCs) to control systems where tradition methods may not have good results. After decades of development, the type-1 FLC is now credited with being an adequate methodology for designing robust controllers that are able to deliver a satisfactory performance in face of uncertainty and imprecision [59]– [63]. However, type-1 fuzzy sets are not sufficient for coping with the uncertainties described above. A primary reason is that the membership grade of a type-1 fuzzy set is a crisp value so that the membership function is limited in modeling the shape and position of a fuzzy set. The introduction of type-2 fuzzy sets overcomes this limitation, since for any value of the variables, the membership grades of type-2 fuzzy sets are type-1 fuzzy sets instead of a crisp value. The architecture of type-2 fuzzy sets allows more design freedoms for modeling and coping with uncertainties.

Type-2 fuzzy sets were first defined and discussed by Zadeh [64]. Later, the logical connectives enabling AND and OR in particular were studied by Mizumoto and Tanaka [65] and Dubois and Prade [66]. Gorzalczany [67], Türkşen [68], Schwartz [69] and Klir and Folger [70] promoted the use of interval type-2 (IT2) fuzzy sets, which were referred to as interval-valued fuzzy sets. Gorzalczany may be acknowledged as a pioneer in the development of interval-valued fuzzy sets. For IT2 fuzzy sets to be applied to real applications in rule-based systems, the output signal needs to be a crisp value. Karnik and Mendel [71] proposed a type-reduction algorithm as the first stage for defuzzifing type-2 fuzzy sets by applying the extension principle to a variety of type-1 defuzzifiers. After the notion of an output processing stage of a type-2 fuzzy system was developed, the IT2 fuzzy logic systems (FLSs) were fully defined [72]. After the definitions, the IT2 FLSs have attracted much attention in

the research community [73]– [77]. Research has shown that IT2 FLSs outperforms its type-1 counterparts in several engineering problems [48], [77]– [84]. To better handle the uncertainties in marine control systems, the IT2 FLSs are combined with approximation-based adaptive technique in this thesis.

Type-1 FLSs have been found to be able to approximate continuous nonlinear functions to any desired accuracy over a compact set [85]– [88], thus could be universal approximators in approximation-based adaptive technique. Research by Hao Ying [89]– [91] has shed light on the universal approximation property of IT2 FLSs, but more comprehensive analysis and verification are necessary. As the performance of the control systems designed in this thesis is guaranteed only when the IT2 FLSs adequately approximate the underlying functions, another objective of this thesis is to verify universal approximation property of IT2 FLSs via engineering applications.

1.3 Objectives and Scope of the Thesis

In view of the above review, research gaps for the current study of marine control systems are summarized below. As the marine environment is characterized by time-varying environmental disturbances and widely changing sea conditions, the marine control systems face challenges of complex disturbances and uncertainties. In order to enhance safety and efficiency, and conduct all-year marine operations in harsh environment, more advanced control techniques are required for DP and tracking control. Specifically the active research issues are as follows.

- As accurate modeling of vessels can increase the probability that a control

system, designed based on mathematical vessel model, achieves similar performance in reality, more and more realistic dynamic models for marine vessels have been developed [92]. With the help of new strip theory in hydrodynamics, one of the latest vessel models was presented in [37, 38]. Environmental conditions such as wave, current, and other hydrodynamic forces are taken into consideration by treating them as time-varying hydrodynamic disturbances acting on the vessels. Due to the time-varying hydrodynamic disturbances, few control systems have been designed based on it.

- Based on International Maritime Organization publication, the Classification Societies have issued rules for DP vessels, which shows the fast development and wide applications of DP systems. However, as the new vessel models were presented, available DP systems show their limitation. New controller and observer for the new vessel models are necessary.

- As the development of new vessel models, tracking control of these models for both state feedback and output feedback control is challenging.

- Fault-tolerant control has been widely used in the control of aircrafts, and gained great successes. In order to improve the reliability of marine control systems, fault-tolerant marine control systems are need to be explored.

- As extensions of type-1 FLCs, IT2 FLCs were reported to outperform its counterparts in many applications. But it is not clear yet whether adaptive IT2 FLCs will maintain their better performance when dealing with multi-input multi-output plant like marine vessels.

- The fact that type-1 FLSs are universal approximators has been proved and used in their early research stage. But the similar property for IT2 FLSs is still under study and more effort is required.

In view of the above gaps, the main aim of this study is to apply the combination of approximation-based adaptive technique and IT2 FLSs to marine control systems to handle the time-varying hydrodynamic disturbances and uncertainties in DP and tracking control of marine vessels. The specific objectives of the research are to

- combine approximation-based adaptive technique and IT2 FLSs to handle time-varying hydrodynamic disturbances and uncertainties,
- design stable adaptive IT2 FLC and observer for DP of floating vessels,
- design stable state feedback and output feedback adaptive IT2 FLC for tracking control of surface vessels,
- explore fault-tolerant control of marine vessels,
- investigate the universal approximation property of IT2 FLSs via engineering applications.

The results of this present study may lay the foundation for the application of adaptive IT2 FLC to marine control system. The combination of approximation-based adaptive technique and IT2 FLSs would be a new method to handle time-varying disturbances and uncertainties. The comparative simulations between adaptive IT2 FLCs and its counterparts may contribute to a better understanding of adaptive IT2 FLCs and the approximation property of IT2 FLSs. As a matter of fact, the phrase

"marine control system" has a very broad meaning. It could be divided into low level thrust location and high level plant control. And this study is restricted to high level plant control. As mentioned in Section 1.1, even in high level plant control, marine control system could have different control objectives. This study mainly focuses on DP and trajectory tracking control. Based on the implication method, the IT2 FLSs could be divided into Madani IT2 and TSK IT2. This study concentrates on Madani IT2 FLSs. As simplified forms of type-2 FLSs, IT2 FLSs are central to this study. General type-2 FLSs are excluded from this study due to its computational complexity.

1.4 Organization of the Thesis

The remainder of the thesis is organized as follows. Chapter 2 presents the mathematical models of marine vessels for DP and tracking control. The IT2 fuzzy set and singleton IT2 FLS, which is constructed in the linear in the parameters form, are also introduced in this chapter. Chapter 3 delineates the design and stability analysis of the indirect adaptive IT2 FLC for DP of floating vessels. In Chapter 4, a passive adaptive IT2 fuzzy observer for DP is proposed. The stability property and performance of the observer are explored as well. After that, Chapter 5 presents an indirect as well as a direct adaptive IT2 FLC for tracking control of surface vessels. Although designed from different points of view, both indirect and direct adaptive IT2 FLC yield similar and passive closed-loop systems. A comparative study of the proposed controller against their type-1 counterparts was also conducted in this chapter. Next,

the design and stability analysis of an output feedback fault-tolerant adaptive backstepping IT2 FLC are shown in Chapter 6. Finally, Chapter 7 gives the conclusion remarks of the thesis and suggestions for future work.

Chapter 2

Preliminaries and Design Tools

In this chapter, the modeling of marine vessels and IT2 fuzzy set and system is described in detail. These mathematical preliminaries and design tools will be used throughout this thesis. Firstly, the mathematical models of marine vessels for DP and tracking control are introduced. Then, the type-1 FLS is described to provide a baseline of FLSs. After that, the singleton IT2 FLS is delineated and constructed in the linear in the parameters form.

2.1 Modeling of Marine Vessels

In this section, the process plant models of marine vessels for DP and tracking control are introduced. These models are used to conduct the simulation studies throughout this thesis. The classical model for marine vessel is motivated by Newton's law and represented in component form using the Society of Naval Architects and Marine Engineers (SNAME) notation [93]. After applying nonlinear theory to marine vessel modeling, hundreds of components were included to describe the dynamics of a vessel [94]. Hence, model-based control design became relatively complicated due to large number of hydrodynamic coefficients. These coefficients were difficult to determine accurately. Consequently, it would be beneficial to reduce the number of coefficients

by means of physical properties of marine vessels. In 1991, Fossen derived a compact marine vessel model in 6 degrees of freedom (DOF) using a vectorial setting [95]. This result was further refined by Sagatun and Fossen [96], Fossen [7], and Berge and Fossen [97]. It is highly advantageous to use vectorial setting instead of component form when designing control systems, as system properties like symmetry, skew-symmetry and positiveness of matrices can be incorporated into the stability analysis. In addition, these properties are related to passivity of the rigid-body and hydrodynamic models. Nowadays, the vectorial representation model of marine vessels has been adopted by the international community as a standard model for marine control systems design, whereas the component form model is mostly used in hydrodynamic modeling where isolated effects can be investigated. The modeling of marine vessels can be divided into two parts: kinematics and dynamics. Kinematics treats only geometrical aspects of motion, whereas dynamics is the analysis of the forces causing the motion.

2.1.1 Kinematics

For a marine vessel moving in six DOF, six independent coordinates are defined to determine the position and orientation. The first three coordinates corresponding to position and translational motion are surge, sway and heave, whereas the last three coordinates describing orientation and rotational motion are roll, pitch and yaw. The detailed definition and notation of these coordinates are described in Table. 2.1 and Fig. 2.1. The motions of a marine vessel are conventionally defined and measured with respect to two coordinate frames as shown in Fig. 2.1, namely an earth-fixed

frame and a body-fixed frame.

Table 2.1: The notation of SNAME for marine vessels.

DOF		Positions and Euler angles	Linear and angular velocities
1	motion in the x direction (surge)	x	u
2	motion in the y direction (sway)	y	v
3	motion in the z direction (heave)	z	w
4	rotation about the x axis (roll)	ϕ	p
5	rotation about the y axis (pitch)	θ	q
6	rotation about the z axis (yaw)	ψ	r

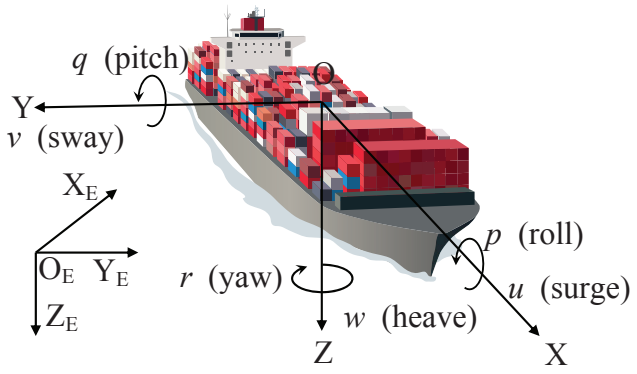

Figure 2.1: Earth-fixed and body-fixed coordinate frames.

The earth-fixed frame, denoted as $X_E Y_E Z_E$, is defined relative to the Earth's reference ellipsoid. For this frame, the X_E axis points towards the north, the Y_E axis points towards the east, and the Z_E axis points downwards normal to the earth's surface. It is mainly used for local guidance and navigation. The body-fixed frame,

denoted as XYZ, is fixed to the hull of the vessel, with X axis pointing to the bow, the Y axis pointing to the starboard, and the Z axis pointing downward. The origin of this frame is normally located at the vessel's center of gravity. Define $\boldsymbol{\eta}' = [x, y, z, \phi, \theta, \psi]^{\mathrm{T}}$ be the vector representing the position and orientation of the vessel with respect to an earth-fixed frame, and let $\boldsymbol{\nu}' = [u, v, w, p, q, r]^{\mathrm{T}}$ denote the translation and rotation velocities of the vessel decomposed in the body-fixed frame. Then, the transformation between the earth-fixed and body-fixed velocity vectors is

$$\dot{\boldsymbol{\eta}}' = \mathbf{J}'(\boldsymbol{\eta}')\boldsymbol{\nu}'. \tag{2.1}$$

where $\mathbf{J}'(\boldsymbol{\eta}')$ is a state dependent transformation matrix, whose detailed definition can be found in [92].

2.1.2 Dynamics

The 6 DOF model of a marine vessel with fluid memory effects introduced in this subsection is based on [37] and [38]. Since the hydrodynamic forces are different for low-speed vessels and non-zero forward speed vessels, the equations of motion for low-speed applications like DP and non-zero forward speed applications like trajectory tracking are different. The equation of motion for DP, which is in body-fixed frame, is given by

$$\mathbf{M}'\dot{\boldsymbol{\nu}}' + \bar{\mathbf{B}}'\boldsymbol{\nu}'_r + \mathbf{G}'\boldsymbol{\eta}' = \boldsymbol{\tau}' + \boldsymbol{\tau}'_{\mathrm{H}}, \tag{2.2}$$

whereas the equation of motion for tracking control is expressed as

$$\mathbf{M}'\dot{\boldsymbol{\nu}}' + \mathbf{C}'_{RB}\boldsymbol{\nu}' + \mathbf{C}'_{A}\boldsymbol{\nu}'_r + \bar{\mathbf{B}}'\boldsymbol{\nu}'_r + \mathbf{G}'\boldsymbol{\eta}' = \boldsymbol{\tau}' + \boldsymbol{\tau}'_{\mathrm{H}}, \tag{2.3}$$

where $\mathbf{M}' = \mathbf{M}'_{RB} + \bar{\mathbf{A}}' \in R^{6\times6}$ is the sum of the system inertia matrix and the added mass matrix. $\mathbf{C}'_{RB} \in R^{6\times6}$ is the Coriolis-Centripetal matrix. $\mathbf{C}'_{A} \in R^{6\times6}$ is the induced matrix of added mass. $\boldsymbol{\nu}'_r = \boldsymbol{\nu}' - \boldsymbol{\nu}'_c \in R^6$ is the relative velocity vector between vessel velocity vector $\boldsymbol{\nu}'$ and sea current velocity vector $\boldsymbol{\nu}'_c$. $\bar{\mathbf{B}}' \in R^{6\times6}$ is the constant infinite frequency potential damping matrix. $\mathbf{G}' \in R^{6\times6}$ is the restoring matrix. $\boldsymbol{\tau}' \in R^6$ is the control force vector produced by the propeller system. $\boldsymbol{\tau}'_{\mathrm{H}} \in R^6$ is a vector of time-varying hydrodynamic forces and moment, and can be expressed by

$$\boldsymbol{\tau}'_{\mathrm{H}} = \boldsymbol{\tau}'_{\mathrm{CFD}} + \boldsymbol{\tau}'_{\mathrm{Wave}} - \boldsymbol{\mu}' \tag{2.4}$$

where $\boldsymbol{\tau}'_{\mathrm{CFD}} \in R^6$ is the cross-flow drag and surge resistance vector. $\boldsymbol{\tau}'_{\mathrm{Wave}} \in R^6$ is the wave load vector, which is computed according to Response Amplitude Operator tables. $\boldsymbol{\mu}' \in R^6$ is computed as follows using a state space model to represent the fluid memory effects.

$$\dot{\boldsymbol{\chi}} = \mathbf{A}_r\boldsymbol{\chi} + \mathbf{B}_r\boldsymbol{\nu}'_r \tag{2.5}$$

$$\boldsymbol{\mu}' = \mathbf{C}_r\boldsymbol{\chi} + \mathbf{D}_r\boldsymbol{\nu}'_r \tag{2.6}$$

where $(\mathbf{A}_r, \mathbf{B}_r, \mathbf{C}_r, \mathbf{D}_r)$ are constant matrices of appropriate dimensions. All the detailed definition and computation of the above matrices and vectors can be found in [92] and [37] and references therein.

2.1.3 Marine System Simulator

The marine system simulator (MSS) [98] is a Simulink-based software package that provides the resources for quick implementation of mathematical models of marine

systems with focus on control system design. It is developed in Norwegian University of Science and Technology with the help of other research groups. Although it is still a undergoing project and requires contribution from marine researchers and professionals all over the world, it has already gained the capability of integrating with the output files of different commercial hydrodynamic codes, so that it could simulate the real situation as closely as possible. The proposed algorithms in this thesis are tested on the MSS platform. The main organization of the software package is [99]:

- Marine GNC Toolbox
- Add-in libraries
- Marine Visualization Toolbox
- Matlab support function

The Marine GNC (guidance navigation and control) Toolbox is the core component of MSS, and most of the other components make use of it. The add-in libraries incorporate further functionality to MSS. At this stage, there are three add-ins, namely Marine Hydro, Marine Propulsion and Marine Systems. The Marine Hydro add-in provides Matlab functions that read the output files of commercial hydrodynamic software such as ShipX-VERES, SEAWAY and WAMIT to make the vessel model more accurate. The Marine Propulsion add-in targets simulation and control design for propellers, rudders and thrusters. The Marine Systems add-in is a Simulink library with complex system ready to simulate. The Marine Visualization Toolbox displays data from simulation, experiments or measurements of marine systems as 3D animations. With further benchmark with model testing of vessels, the MSS has

the potential to outperform the commercial aNySIM software developed by MARIN.

2.2 Type-1 Fuzzy Logic System

2.2.1 Basic Structure

A type-1 fuzzy set A, for a single variable $x \in X$, is defined as

$$A = \{(x, \mu_A(x)) \,|\, x \in X\}, \tag{2.7}$$

where type-1 membership function, $\mu_A(x)$ is constrained to be between 0 and 1 for all $x \in X$, and is a two-dimensional function. A type-1 FLS is constructed completely by type-1 fuzzy sets. It contains four components, namely fuzzifier, rule base, inference engine and defuzzifier, as shown in Fig. 2.2.

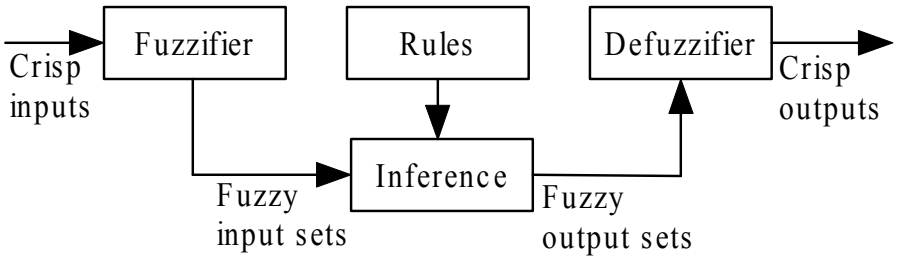

Figure 2.2: A type-1 FLS.

The fuzzifier maps a crisp point $\boldsymbol{x} = (x_1, \ldots, x_n)^T \in X_1 \times X_2 \times \ldots \times X_n \equiv X$ into a fuzzy set A_x in X. The most widely used fuzzifier is the singleton fuzzifier, i.e., A_x is a fuzzy singleton with support $\boldsymbol{x}'$. In other words, $\mu_{A_x}(\boldsymbol{x}) = 1$ for $\boldsymbol{x} = \boldsymbol{x}'$ and $\mu_{A_x}(\boldsymbol{x}) = 0$ for all other $\boldsymbol{x} \in X$ with $\boldsymbol{x} \neq \boldsymbol{x}'$. Nonsingleton fuzzifier, on the other hand, maps $x_i = x_i'$ into a fuzzy number where a membership function is associated

with it. In particular, $\mu_{X_i}(x_i') = 1$ $(i = 1, \ldots, n)$ and $\mu_{X_i}(x_i')$ decreases from unity as x_i moves away from x_i'. Rule base is the heart of a FLS and they can be expressed as a collection of **IF-THEN** statements. The **IF**-part of a rule is its antecedent, and the **THEN**-part of a rule is its consequent. The terms that appear in the antecedents or consequents of rules are associated with type-1 fuzzy sets. Next, the inference engine maps fuzzy input sets to fuzzy output sets according to rule base. It handles the way in which rules are activated and combined. Finally, the defuzzifier transforms the output fuzzy sets into crisp outputs.

2.2.2 Universal Approximation Property

How well does a FLS approximate an unknown function? This is an important question that is asked about all types of function appproximators in the application of approximation-based adaptive control. By using the Stone-Weirstrass theorem, it was firstly proven that a singleton FLS that uses product composition, product implication, Gaussian membership functions, and height defuzzification can uniformly approximate any real continuous nonlinear function to arbitrary degree of accuracy [85]. There is now a very large literature about different kinds of FLSs that are universal approximators, all of which are summarized very well by Kreinovich et al. [100].

Basically, a universal approximation theorem is an existence theorem. It helps to explain why a FLS is so successful in engineering application. However, it does not tell us how to specify a FLS. Currently, the research on the universal approximation

property of FLSs can be classified into two aspects, the qualitative aspect and the quantitative aspect. On the qualitative aspect, the major concerns are to identify various classes of FLSs which have the universal approximation property and to analyze the mechanism as to why such a property is valid [88]. On the quantitative aspect, the main concern is to establish approximation error bounds and to analyze the approximation accuracy for various classes of FLSs [87]. The design degrees of freedom that control the approximation accuracy of a FLS are: number of inputs, number of rules, and number of fuzzy sets for each input variable. Although increasing the number of fuzzy sets for each input could improve the approximation accuracy, it could also result in rule explosion. If there are p inputs, each of which is divided into r overlapping regions, then a complete FLS must contain r^p rules. As resolution parameter r increase, the size of the FLS becomes enormous. So there is a practical tradeoff between resolution and complexity. One way to achieve high resolution and low complexity is to design the FLS using representative data that are collected for a specific application. Another way is to make use of uncertainty. As explained in Section 1.2, this can be done within the framework of IT2 FLSs [74].

Remark 2.1 *It is noted that the universal approximation property of FLSs holds only for compact set. Thus, whenever the universal approximation property is used in this thesis, the signals involved are already assumed to be bounded by a compact set, which could be made as large as deemed necessary in practical applications.*

2.3 Interval Type-2 Fuzzy Set and System

An IT2 FLS is a fuzzy system that uses IT2 fuzzy set and/or IT2 fuzzy logic and inference.

2.3.1 Interval Type-2 Fuzzy Set

A type-2 fuzzy set on a universe of discourse X, denoted as $\tilde{A}$, is characterized by a type-2 membership function $\mu_{\tilde{A}}(x)$ as in

$$\tilde{A} = \{(x, \mu_{\tilde{A}}(x)) | \forall x \in X\} = \{((x, u), f_x(u)) | \forall x \in X, \forall u \in J_x \subseteq [0, 1]\}, \tag{2.8}$$

where $\mu_{\tilde{A}}(x)$, which can also be referred to as a secondary membership function or a secondary set, is a type-1 fuzzy set. $f_x(u)$ is a secondary grade such that $0 \leq f_x(u) \leq 1$. J_x is called primary membership of x. The uncertainty in the primary memberships of a type-2 fuzzy set $\tilde{A}$, consists of a bounded region that is called the footprint of uncertainty (FOU). It is the union of all primary memberships [74]. Fig. 2.3 shows the membership function of a type-2 fuzzy set where relevant definitions are demonstrated. Many choices are possible for the secondary membership functions, and the name that is used to describe the type-2 membership function is associated with the name of the secondary membership function. When $f_x(u) = 1, \forall u \in J_x \subseteq [0, 1]$, then the secondary membership functions are interval sets, and an interval type-2 fuzzy sets may be defined as

$$\tilde{A} = \{(x, \mu_{\tilde{A}}(x)) | \forall x \in X\} = \{((x, u), 1) | \forall x \in X, \forall u \in J_x \subseteq [0, 1]\}. \tag{2.9}$$

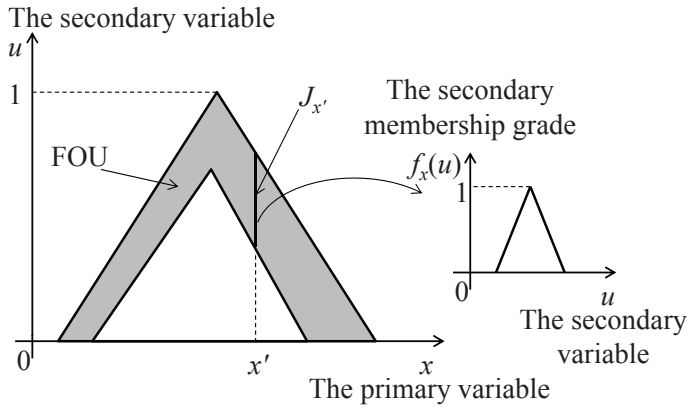

Figure 2.3: Vertical-slice of a type-2 fuzzy set.

Interval secondary membership functions reflect a uniform uncertainty at the primary memberships of x. The secondary membership function of an interval type-2 fuzzy set can be represented just by its domain interval, which is bounded by an upper and a lower membership function. The upper membership function is the upper bound of FOU($\tilde{A}$) and is denoted by $\overline{\mu}_{\tilde{A}}(x), \forall x \in X$, whereas the lower membership function is the lower bound of FOU($\tilde{A}$) and is denoted by $\underline{\mu}_{\tilde{A}}(x), \forall x \in X$. Hence, the interval type-2 fuzzy set (2.9) can be re-expressed by

$$\tilde{A} = \{((x,u),1) | \forall x \in X, \forall u \in [\underline{\mu}_{\tilde{A}}(x), \overline{\mu}_{\tilde{A}}(x)]\}. \tag{2.10}$$

Fig. 2.4 shows the membership function of an IT2 fuzzy set. When compared to the type-1 fuzzy sets, using interval type-2 fuzzy sets has many advantages. Some of these advantages are as follows. As the interval type-2 fuzzy sets include FOUs, they can model and handle the linguistic and numerical uncertainties associated with the inputs and outputs of the FLSs, and hence can handle the difficulty associated with determining the exact membership functions for the fuzzy sets [78, 101]. Using

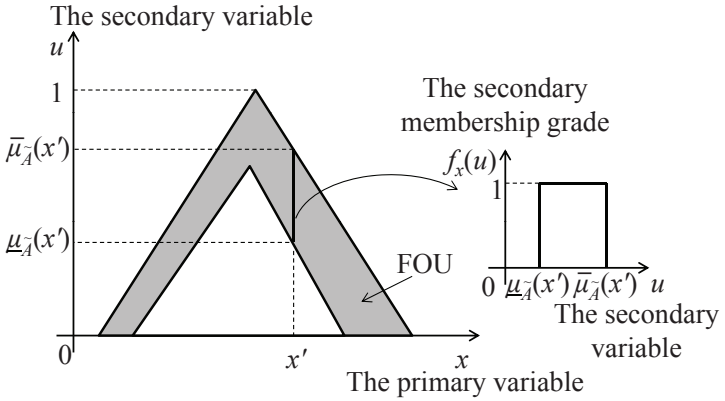

Figure 2.4: Vertical-slice of an interval type-2 fuzzy set.

interval type-2 fuzzy sets to represent inputs and outputs of the FLSs will result in the reduction of the fuzzy rules as the uncertainty in FOU of the interval type-2 fuzzy sets covers the same range as type-1 fuzzy sets with smaller number of labels. The rule reduction will be greater when the number of the inputs increases [79]. An interval type-2 fuzzy set can be interpreted as a combination of numerous embedded type-1 fuzzy sets [75, 102]. Using such a large number of type-1 fuzzy sets to describe the inputs or outputs allows for a detailed description of the control surface.

2.3.2 Interval Type-2 Fuzzy Logic System

In this thesis, a singleton IT2 FLS whose general configuration is depicted in Fig. 2.5 is considered. The main structural difference between an IT2 FLS and a type-1 FLS lies in that the defuzzifier block of a type-1 FLS is replaced by the output porcessing block in an IT2 FLS, which consists of a type-reducer followed by a defuzzifier. Consequently, there are five components in an IT2 FLS, namely fuzzifier, rule base, fuzzy inference engine, type-reducer, and defuzzifier.

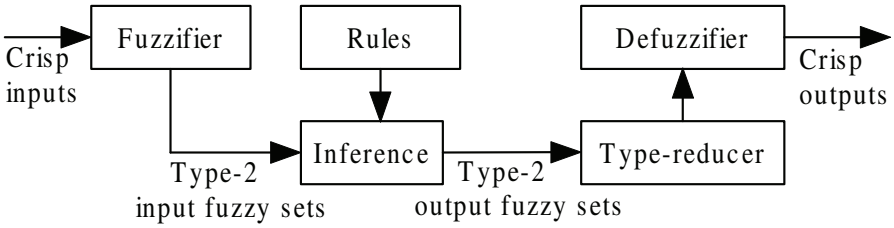

Figure 2.5: A singleton interval type-2 FLS.

2.3.2.1 Fuzzification

The fuzzifier maps a crisp point $\mathbf{x} = (x_1, \ldots, x_n) \in \mathbf{U} \subset R^n$ into a set of IT2 fuzzy sets $\tilde{A}_{x_i}$ $(i = 1, 2, \ldots, n)$ in $\mathbf{U}$. In the singleton fuzzification, the input fuzzy set $\tilde{A}_{x_i}$ has only a single point of nonzero membership as follows.

$$\mu_{\tilde{A}_{x_i}}(x_i) = \begin{cases} 1; & x_i = x_i' \\ 0; & x_i \neq x_i' \end{cases} \tag{2.11}$$

2.3.2.2 Rule Base

The fuzzy rule base in IT2 FLSs remains the same as in type-1 FLSs and consists of a group of fuzzy **IF-THEN** rules. The rules can be extracted from numerical data or provided by experts. Consider an IT2 FLS having n inputs and one output, then the lth rule in the rule base can be written as

$$R^l : \text{IF } x_1 \text{ is } \tilde{F}_1^l \text{ and } \cdots \text{and } x_n \text{ is } \tilde{F}_n^l \text{ THEN } y \text{ is } \tilde{G}^l, \tag{2.12}$$

where $l = 1, 2, \ldots, M$, x_i $(i = 1, 2, \ldots, n)$ and y are the inputs and output to the IT2 FLS respectively, $\tilde{F}_i^l$ and $\tilde{G}^l$ are labels of antecedent and consequent fuzzy sets in $\mathbf{U}_i$ and R, respectively. This rule represents a type-2 relation between the input space

U and output space R.

2.3.2.3 Fuzzy Inference Engine

The fuzzy inference engine combines fuzzy **IF-THEN** rules and provides a mapping from input IT2 fuzzy sets in **U** to output IT2 fuzzy set in R. Each rule is interpreted as a fuzzy implication. Using the extended sup-star compositional rule of inference, the output consequent set corresponding to rule R^l of a singleton IT2 FLS can be expressed as

$$\mu_{\tilde{B}^l}(y) = \mu_{\tilde{G}^l}(y) \sqcap \left[\sqcap_{i=1}^{n} \mu_{\tilde{F}_i^l}(x_i')\right], \tag{2.13}$$

where the firing set $\sqcap_{i=1}^{n} \mu_{\tilde{F}_i^l}(x_i') \equiv F^l(\boldsymbol{x}')$ is an interval type-1 fuzzy set, i.e.,

$$F^l(\boldsymbol{x}') = \left[\underline{f}^l(\boldsymbol{x}'), \overline{f}^l(\boldsymbol{x}')\right] \tag{2.14}$$

$$\underline{f}^l(\boldsymbol{x}') = \underline{\mu}_{\tilde{F}_1^l}(x_1') \bigstar \cdots \bigstar \underline{\mu}_{\tilde{F}_n^l}(x_n') \tag{2.15}$$

$$\overline{f}^l(\boldsymbol{x}') = \overline{\mu}_{\tilde{F}_1^l}(x_1') \bigstar \cdots \bigstar \overline{\mu}_{\tilde{F}_n^l}(x_n'), \tag{2.16}$$

where $\underline{\mu}_{\tilde{F}_i^l}(x_i')$ and $\overline{\mu}_{\tilde{F}_i^l}(x_i')$ are the lower and upper membership grade of IT2 fuzzy set $\tilde{F}_i^l$, respectively, symbol $\bigstar$ denotes the t-norm corresponding to the conjunction "and" in (2.12). Fig. 2.6 describes the input and antecedent operation for a singleton IT2 FLS that has two inputs. The fired output consequent set $\mu_{\tilde{B}^l}(y)$ for the lth rule can be written as

$$\mu_{\tilde{B}^l}(y) = \{(b^l, 1) | b^l \in \left[\underline{f}^l \bigstar \underline{\mu}_{\tilde{G}^l}(y), \overline{f}^l \bigstar \overline{\mu}_{\tilde{G}^l}(y)\right]\}, \tag{2.17}$$

where $\underline{\mu}_{\tilde{G}^l}$ and $\overline{\mu}_{\tilde{G}^l}$ are the lower and upper membership grades of consequent fuzzy set, $\tilde{G}^l$.

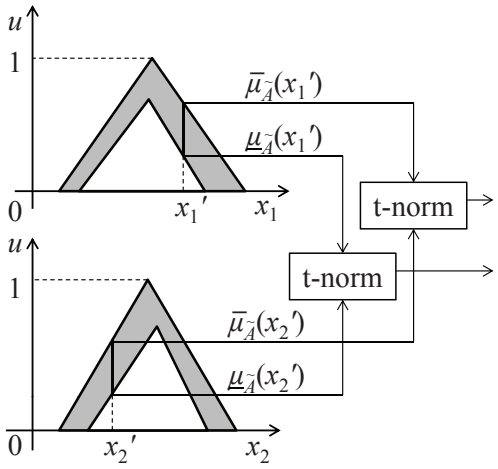

Figure 2.6: Pictorial description of input and antecedent operation for a singleton interval type-2 fuzzy logic system.

2.3.2.4 Type-reduction and Defuzzification

The type-reduction operator acts on the IT2 fuzzy set representing the output of the inference engine to generate a type-1 fuzzy set. This type-1 fuzzy set is then defuzzified to obtain crisp output. Many kinds of type-reduction methods are available, such as centroid, center of sums, height and center of sets type-reduction. In this thesis, center of sets type-reduction is used, as it has reasonable computational complexity. Assume maximum t-conorm, product t-norm, and product implication are used. Then the result of the type-reduction process is an interval type-1 fuzzy set $[y_l', y_r']$, whose left end point y_l' and right end point y_r' can be computed using the Karnik-Mendel iterative procedure [74]. Under the assumption that the consequent

sets are singletons y^i $(i = 1, \ldots, M)$, y'_l and y'_r can be expressed as

$$y'_l = \frac{\sum_{i=1}^{L} \overline{f}^i y^i + \sum_{i=L+1}^{M} \underline{f}^i y^i}{\sum_{i=1}^{L} \overline{f}^i + \sum_{i=L+1}^{M} \underline{f}^i} \tag{2.18}$$

$$y'_r = \frac{\sum_{i=1}^{R} \underline{f}^i y^i + \sum_{i=R+1}^{M} \overline{f}^i y^i}{\sum_{i=1}^{R} \underline{f}^i + \sum_{i=R+1}^{M} \overline{f}^i}. \tag{2.19}$$

where L denotes the left switch point, and R denotes the right switch point. It is noted that the y^i $(i = 1, \ldots, M)$ in (2.18) and (2.19) are arranged in ascending order and $[\underline{f}^i, \overline{f}^i]$ are the corresponding weights of y^i. The standard Karnik-Mendel algorithm is an efficient algorithm that searches for the switch points L and R. The detailed procedure of the Karnik-Mendel iterative algorithm may be stated as

- Step 1: Arrange y^i $(i = 1, \ldots, M)$ in ascending order and relabel them as $y^1 < y^2 < \cdots < y^M$. Let $[\underline{f}^i, \overline{f}^i]$ be the corresponding weight of y^i;
- Step 2: Set

  $$f^i = \frac{\underline{f}^i + \overline{f}^i}{2}$$

  for $i = 1, \ldots, M$ and then compute

  $$y_c = \frac{\sum_{i=1}^{M} y^i f^i}{\sum_{i=1}^{M} f^i};$$

- Step 3: Find the switch point $k \in [1, M-1]$ such that

  $$y^k \leq y_c \leq y^{k+1};$$

- Step 4: Set f^i as
  - for y'_l computation:

    $$f^i = \begin{cases} \overline{f}^i; & \text{for } i \leq k \\ \underline{f}^i; & \text{for } i > k \end{cases}$$

– for y'_r computation:

$$f^i = \begin{cases} \underline{f}^i; & \text{for } i \leq k \\ \overline{f}^i; & \text{for } i > k \end{cases}$$

and compute

$$y'_c = \frac{\sum_{i=1}^{M} y^i f^i}{\sum_{i=1}^{M} f^i};$$

- Step 5: if $y'_c = y_c$, stop. k is the actual switch point L (R) and $y'_l = y_c$ $(y'_r = y_c)$. Otherwise, set $y_c = y'_c$ and go to Step 3.

According to [103, 104], the standard Karnik-Mendel algorithm can be represented in vector form. Let $\mathbf{y} = (y^1, \ldots, y^M)^{\mathrm{T}}$ represent the original consequent values, and let $\hat{\mathbf{y}} = (\hat{y}^1, \ldots, \hat{y}^M)^{\mathrm{T}}$ denote the reordered sequences, where $\hat{y}^1 \leq \hat{y}^2 \leq \ldots \leq \hat{y}^M$. The formula linking $\mathbf{y}$ and $\hat{\mathbf{y}}$ is

$$\hat{\mathbf{y}} = \mathbf{Q}\mathbf{y}, \tag{2.20}$$

where $\mathbf{Q}$ is a $M \times M$ permutation matrix with elementary vectors as columns, and these vectors are permuted to re-order the elements in $\mathbf{y}$ such that the elements in $\hat{\mathbf{y}}$ are in ascending order. The original rule firing strength $\underline{\mathbf{f}} = (\underline{f}^1, \underline{f}^2, \ldots, \underline{f}^M)^{\mathrm{T}}$ and $\overline{\mathbf{f}} = (\overline{f}^1, \overline{f}^2, \ldots, \overline{f}^M)^{\mathrm{T}}$ are accordingly reordered. To compute the end points, the new orders for $\underline{\mathbf{f}}$ and $\overline{\mathbf{f}}$ are $\mathbf{Q}\underline{\mathbf{f}}$ and $\mathbf{Q}\overline{\mathbf{f}}$ respectively. The left end point y'_l of the interval type-reduced set can be computed as

$$\begin{aligned} y'_l =& \frac{\sum_{i=1}^{L} (\mathbf{Q}\overline{\mathbf{f}})_i \hat{y}^i + \sum_{i=L+1}^{M} (\mathbf{Q}\underline{\mathbf{f}})_i \hat{y}^i}{\sum_{i=1}^{L} (\mathbf{Q}\overline{\mathbf{f}})_i + \sum_{i=L+1}^{M} (\mathbf{Q}\underline{\mathbf{f}})_i} \\ =& \frac{\overline{\mathbf{f}}^{\mathrm{T}}\mathbf{Q}^{\mathrm{T}}\mathbf{E}_1^{\mathrm{T}}\mathbf{E}_1\mathbf{Q}\mathbf{y} + \underline{\mathbf{f}}^{\mathrm{T}}\mathbf{Q}^{\mathrm{T}}\mathbf{E}_2^{\mathrm{T}}\mathbf{E}_2\mathbf{Q}\mathbf{y}}{\mathbf{p}_l^{\mathrm{T}}\mathbf{Q}\overline{\mathbf{f}} + \mathbf{g}_l^{\mathrm{T}}\mathbf{Q}\underline{\mathbf{f}}}, \end{aligned} \tag{2.21}$$

where

$$\begin{aligned}
\mathbf{p}_l &= (\underbrace{1,1,\ldots,1}_{L},0,\ldots,0)^{\mathrm{T}} \in R^{M\times 1} \\
\mathbf{g}_l &= (0,\ldots,0,\underbrace{1,1,\ldots,1}_{M-L})^{\mathrm{T}} \in R^{M\times 1} \\
\mathbf{E}_1 &= (\mathbf{e}_1,\mathbf{e}_2,\ldots,\mathbf{e}_L,\mathbf{0},\ldots,\mathbf{0})^{\mathrm{T}} \in R^{L\times M} \\
\mathbf{E}_2 &= (\mathbf{0},\ldots,\mathbf{0},\boldsymbol{\varepsilon}_1,\boldsymbol{\varepsilon}_2,\ldots,\boldsymbol{\varepsilon}_{M-L})^{\mathrm{T}} \in R^{(M-L)\times M}
\end{aligned}$$

and where $\mathbf{e}_i \in R^L$ and $\boldsymbol{\varepsilon}_i \in R^{M-L}$ are elementary vectors [104]. Similarly, the output y'_r can be expressed as

$$\begin{aligned}
y'_r =& \frac{\sum_{i=1}^{R}(\mathbf{Q}\underline{\mathbf{f}})_i\hat{y}^i + \sum_{i=R+1}^{M}(\mathbf{Q}\overline{\mathbf{f}})_i\hat{y}^i}{\sum_{i=1}^{R}(\mathbf{Q}\underline{\mathbf{f}})_i + \sum_{i=R+1}^{M}(\mathbf{Q}\overline{\mathbf{f}})_i} \\
=& \frac{\underline{\mathbf{f}}^{\mathrm{T}}\mathbf{Q}^{\mathrm{T}}\mathbf{E}_3^{\mathrm{T}}\mathbf{E}_3\mathbf{Q}\mathbf{y} + \overline{\mathbf{f}}^{\mathrm{T}}\mathbf{Q}^{\mathrm{T}}\mathbf{E}_4^{\mathrm{T}}\mathbf{E}_4\mathbf{Q}\mathbf{y}}{\mathbf{p}_r^{\mathrm{T}}\mathbf{Q}\underline{\mathbf{f}} + \mathbf{g}_r^{\mathrm{T}}\mathbf{Q}\overline{\mathbf{f}}},
\end{aligned} \tag{2.22}$$

where

$$\begin{aligned}
\mathbf{p}_r &= (\underbrace{1,1,\ldots,1}_{R},0,\ldots,0)^{\mathrm{T}} \in R^{M\times 1} \\
\mathbf{g}_r &= (0,\ldots,0,\underbrace{1,1,\ldots,1}_{M-R})^{\mathrm{T}} \in R^{M\times 1} \\
\mathbf{E}_3 &= (\mathbf{e}_1,\mathbf{e}_2,\ldots,\mathbf{e}_R,\mathbf{0},\ldots,\mathbf{0})^{\mathrm{T}} \in R^{R\times M} \\
\mathbf{E}_4 &= (\mathbf{0},\ldots,\mathbf{0},\boldsymbol{\varepsilon}_1,\boldsymbol{\varepsilon}_2,\ldots,\boldsymbol{\varepsilon}_{M-R})^{\mathrm{T}} \in R^{(M-R)\times M}
\end{aligned}$$

and where $\mathbf{e}_i \in R^R$ and $\boldsymbol{\varepsilon}_i \in R^{M-R}$ are elementary vectors. Finally, the interval type-1 fuzzy set is defuzzified to generate the system output by means of computing the average of y'_l and y'_r. Hence the defuzzified output is

$$y' = \frac{y'_l + y'_r}{2}. \tag{2.23}$$

Defining the consequent parameters $\boldsymbol{\theta} = \mathbf{y} = (y^1,\ldots,y^M)^{\mathrm{T}}$ as adjustable parameters, then (2.23) can be written as

$$y' = \boldsymbol{\phi}^{\mathrm{T}}\boldsymbol{\theta} \tag{2.24}$$

where

$$\begin{aligned}\boldsymbol{\phi}^{\mathrm{T}} = & \frac{\overline{\mathbf{f}}^{\mathrm{T}}\mathbf{Q}^{\mathrm{T}}\mathbf{E}_1^{\mathrm{T}}\mathbf{E}_1\mathbf{Q} + \underline{\mathbf{f}}^{\mathrm{T}}\mathbf{Q}^{\mathrm{T}}\mathbf{E}_2^{\mathrm{T}}\mathbf{E}_2\mathbf{Q}}{2(\mathbf{p}_l^{\mathrm{T}}\mathbf{Q}\overline{\mathbf{f}} + \mathbf{g}_l^{\mathrm{T}}\mathbf{Q}\underline{\mathbf{f}})} \\ & + \frac{\underline{\mathbf{f}}^{\mathrm{T}}\mathbf{Q}^{\mathrm{T}}\mathbf{E}_3^{\mathrm{T}}\mathbf{E}_3\mathbf{Q} + \overline{\mathbf{f}}^{\mathrm{T}}\mathbf{Q}^{\mathrm{T}}\mathbf{E}_4^{\mathrm{T}}\mathbf{E}_4\mathbf{Q}}{2(\mathbf{p}_r^{\mathrm{T}}\mathbf{Q}\underline{\mathbf{f}} + \mathbf{g}_r^{\mathrm{T}}\mathbf{Q}\overline{\mathbf{f}})}\end{aligned} \tag{2.25}$$

is a regressive vector. As illustrated in (2.24), the singleton IT2 FLS using maximum t-conorm, product t-norm, product implication, and center of sets type-reduction can be expressed as a linear in the parameters model. In addition, as shown in (2.21) and (2.22), the Karnik-Mendel algorithm is embedded in (2.24).

Chapter 3

Dynamic Positioning via Adaptive IT2 Fuzzy Control

One major application of automatic control technique in the offshore and marine industry is DP. DP systems are widely used in situations where mooring or anchoring is not feasible due to deep water, congested structures such as pipelines on the sea bottom or other economical issues. DP systems maintain floating structures in fixed position and heading for marine operation purpose exclusively by means of active propellers and thrusters. The objective of this chapter is to position and orientate the DP vessels to a fixed placement via attached thruster systems, which actually is a regulation problem. To fulfill this objective, an indirect adaptive IT2 FLC for DP vessels under time-varying hydrodynamic disturbances is proposed. It overcomes the limitations of model-based adaptive control technique to provide an effective control algorithm for the newly developed vessel model [37, 38]. The combination of approximation-based adaptive technique and IT2 FLS allows us to handle time-varying hydrodynamic disturbances without the need for exact information about the disturbances. Besides, the DP problem is treated as an engineering application to investigate the approximation property of IT2 FLS.

The remainder of this chapter is organized as follows. The design and stability

analysis of the indirect adaptive IT2 FLC for DP is delineated in Section 3.1. Section 3.2 describes the simulation results of the closed-loop system. Comparisons with other controllers are also shown in this section. Finally, conclusions of this chapter are drawn in Section 3.3.

3.1 Adaptive Fuzzy Logic Controller Design

In this section, the process plant model is first simplified to facilitate the controller design. Then, an indirect adaptive IT2 FLC for DP is proposed. Using Lyapunov synthesis, the sufficient condition under which the regulation errors will semiglobally asymptotically converge to zero, is proposed.

3.1.1 Control Plant Model

The models of marine vessels may be classified into two categories [57], namely a process plant model and a control plant model. The process plant model, which simulates the real plant dynamics as closely as possible including process disturbance, sensor outputs and control inputs, is used for numerical analysis and simulation to study the performance and stability of the closed-loop system. The control plant model, which is a simplified form of the complicated process plant model, is used for controller design and theoretical stability analysis (e.g., in the sense of Lyapunov). In this thesis, the time-varying disturbances and uncertainties in the process plant model are lumped together in the control plant model and then handled by IT2 FLSs. The process plant model (2.1) and (2.2) for DP described in Section 2.1 is simplified on

the basis of the following assumptions to facilitate the controller design and analytical stability analysis.

Assumption 3.1 *The motions along the heave, roll, and pitch directions are not controlled. A conventional marine vessel is not equipped with actuators in roll and pitch axes, which suggests that the roll and pitch motions cannot be regulated. Moreover, a conventional vessel is metacentric stable, which means that there are restoring force and moments along heave, roll and pitch, thus this assumption is appropriate.*

Assumption 3.2 *The state variables of the vessel, i.e. displacements and velocities along surge, sway, and yaw, are measured by its own on-board devices such as gyro system, GPS, and accelerometers. Due to the development of the modern integration system of inertial sensors and satellite navigation system, this assumption is also appropriate.*

Assumption 3.3 *The influence of sea current $\boldsymbol{\nu}_c'$ is ignored. This assumption simplifies the theoretical analysis. Its appropriateness would be tested in the simulation studies.*

Applying Assumptions 3.1-3.3 to (2.1) and (2.2), the following control plant model for DP is obtained.

$$\dot{\boldsymbol{\eta}} = \mathbf{J}(\boldsymbol{\eta})\boldsymbol{\nu} \tag{3.1}$$

$$\mathbf{M}\dot{\boldsymbol{\nu}} + \bar{\mathbf{B}}\boldsymbol{\nu} = \boldsymbol{\tau} + \boldsymbol{\tau}_{\mathrm{H}}(\boldsymbol{\nu}) \tag{3.2}$$

where $\boldsymbol{\eta} = [x, y, \psi]^{\mathrm{T}}$ is the displacement vector along surge, sway, and yaw axes, whereas $\boldsymbol{\nu} = [u, v, r]^{\mathrm{T}}$ is the velocity vector. $\mathbf{J}(\boldsymbol{\eta}) \in R^{3\times 3}$ is the rotation matrix.

Note that $\mathbf{J}\mathbf{J}^{\mathrm{T}} = \mathbf{I}$ ($\mathbf{I}$ is the identity matrix). $\mathbf{M} \in R^{3\times3}$ is the system inertia matrix including the added mass. $\bar{\mathbf{B}} \in R^{3\times3}$ is the potential damping matrix. $\boldsymbol{\tau} \in R^3$ and $\boldsymbol{\tau}_{\mathrm{H}}(\boldsymbol{\nu}) \in R^3$ are three dimensional versions of $\boldsymbol{\tau}'$ and $\boldsymbol{\tau}'_{\mathrm{H}}$ respectively.

3.1.2 Control and Adaptive Law

Indirect adaptive fuzzy control is an adaptive fuzzy controller that uses fuzzy logic systems to provide an estimation of the plant model. It can incorporate fuzzy descriptions of some parts of the plant in the model. Here, the hydrodynamic disturbances $\boldsymbol{\tau}_{\mathrm{H}}$ in the plant model (3.2) are estimated by singleton IT2 FLSs (2.24) as

$$\boldsymbol{\tau}_{\mathrm{H}}(\boldsymbol{\nu}) = -\Phi(\boldsymbol{\nu})\Theta_{\mathrm{D}}^{*} + \boldsymbol{\omega}_{\mathrm{D}}(\boldsymbol{\nu}), \tag{3.3}$$

where $\boldsymbol{\omega}_{\mathrm{D}}(\boldsymbol{\nu}) \in R^3$ is a vector of minimum estimation error.

$$\begin{aligned} \Theta_{\mathrm{D}}^{*} &= (\boldsymbol{\theta}_1^{*\mathrm{T}}, \boldsymbol{\theta}_2^{*\mathrm{T}}, \boldsymbol{\theta}_3^{*\mathrm{T}})^{\mathrm{T}} \in R^{3M\times1} \\ &= \arg\min_{\Theta_{\mathrm{D}}\in R^{3M}}[\sup_{\nu\in U_\nu}|\boldsymbol{\tau}_{\mathrm{H}}(\boldsymbol{\nu}) + \Phi(\boldsymbol{\nu})\Theta_{\mathrm{D}}|] \end{aligned} \tag{3.4}$$

is the ideal weighting vector and

$$\Phi(\boldsymbol{\nu}) = \mathrm{diag}[\boldsymbol{\phi}_1^{\mathrm{T}}(\boldsymbol{\nu}), \boldsymbol{\phi}_2^{\mathrm{T}}(\boldsymbol{\nu}), \boldsymbol{\phi}_3^{\mathrm{T}}(\boldsymbol{\nu})] \in R^{3\times3M} \tag{3.5}$$

is the regressive matrix. The input signals of the FLSs, $\boldsymbol{\nu}$, is the velocity vector of the vessel because the hydrodynamic disturbances are directly related to the velocity vector of a vessel. As a multi-output FLS can generally be separated into several single-output FLSs, three sub-FLSs that have M rules each are used to approximate the three dimensional hydrodynamic disturbances in the surge, sway and yaw axes.

Equipping the linear proportional derivative (PD) controller with indirect adaptive IT2 estimation, the proposed control and adaptive law for plant (3.1), (3.2) are as follows.

$$\boldsymbol{\tau} = -\lambda_1 \boldsymbol{\nu} - \lambda_2 \mathbf{J}^{\mathrm{T}}(\boldsymbol{\eta})\boldsymbol{e} + \Phi(\boldsymbol{\nu})\hat{\Theta}_{\mathrm{D}} \tag{3.6}$$

$$\dot{\hat{\Theta}}_{\mathrm{D}} = \lambda_3 \Phi^{\mathrm{T}}(\boldsymbol{\nu})(\lambda_4 \boldsymbol{\nu} + \frac{2\mathbf{J}^{\mathrm{T}}(\boldsymbol{\eta})\boldsymbol{e}}{1 + 2\boldsymbol{e}^{\mathrm{T}}\boldsymbol{e}}) \tag{3.7}$$

where $\boldsymbol{e} = \boldsymbol{\eta} - \boldsymbol{\eta}_d \in R^3$ is the control error vector between vessel displacement vector $\boldsymbol{\eta}$ and the desired vessel placement vector $\boldsymbol{\eta}_d$. $\tilde{\Theta}_{\mathrm{D}} = \Theta_{\mathrm{D}} - \hat{\Theta}_{\mathrm{D}} \in R^{3M}$ is the error vector between ideal Θ_{D} in (3.4) and adapted $\hat{\Theta}_{\mathrm{D}}$, and λ_i $(i = 1, \ldots, 4)$ are positive constant.

Application of control and adaptive law (3.6), (3.7) to the plant (3.1), (3.2) yields the resultant closed-loop system

$$\mathbf{M}\dot{\boldsymbol{\nu}} + \bar{\mathbf{B}}\boldsymbol{\nu} = -\lambda_1 \boldsymbol{\nu} - \lambda_2 \mathbf{J}^{\mathrm{T}}(\boldsymbol{\eta})\boldsymbol{e} - \Phi(\boldsymbol{\nu})\tilde{\Theta}_{\mathrm{D}} + \boldsymbol{\omega}_{\mathrm{D}}(\boldsymbol{\nu}) \tag{3.8}$$

$$\dot{\tilde{\Theta}}_{\mathrm{D}} = \lambda_3 \Phi^{\mathrm{T}}(\boldsymbol{\nu})(\lambda_4 \boldsymbol{\nu} + \frac{2\mathbf{J}^{\mathrm{T}}(\boldsymbol{\eta})\boldsymbol{e}}{1 + 2\boldsymbol{e}^{\mathrm{T}}\boldsymbol{e}}) \tag{3.9}$$

$$\dot{\boldsymbol{e}} = \dot{\boldsymbol{\eta}} = \mathbf{J}(\boldsymbol{\eta})\boldsymbol{\nu}. \tag{3.10}$$

3.1.3 Stability Analysis

Theorem 3.1 *The regulation error* $\boldsymbol{e}$ *of the closed-loop system (3.8)-(3.10) semiglobally asymptotically converge to zero if* $\boldsymbol{\omega}_D$ *is squared integrable,*

$$4\lambda_M^2 - \lambda_4^2 \lambda_2 \lambda_m < 0, \tag{3.11}$$

and

$$(\lambda_d + 2\lambda_1)^2 - 8(\lambda_2 - 1)(\frac{\lambda_4 \lambda_d}{2} + \lambda_1 \lambda_4 - 2\lambda_M - \frac{\lambda_4^2}{4} - 1) < 0, \tag{3.12}$$

where λ_m and λ_M are the minimum and maximum eigenvalue of matrix $\mathbf{M}$ respectively, and λ_d is the minimum eigenvalue of matrix $\bar{\mathbf{B}} + \bar{\mathbf{B}}^{\mathrm{T}}$.

Proof: Consider the following Lyapunov function candidate.

$$V_{\mathrm{D}} = \frac{\lambda_2\lambda_4}{2}\boldsymbol{e}^{\mathrm{T}}\boldsymbol{e} + \frac{\lambda_4}{2}\boldsymbol{\nu}^{\mathrm{T}}\mathbf{M}\boldsymbol{\nu} + \frac{2\boldsymbol{\nu}^{\mathrm{T}}\mathbf{M}\mathbf{J}^{\mathrm{T}}\boldsymbol{e}}{1+2\boldsymbol{e}^{\mathrm{T}}\boldsymbol{e}} + \frac{1}{2\lambda_3}\tilde{\Theta}_{\mathrm{D}}^{\mathrm{T}}\tilde{\Theta}_{\mathrm{D}} \tag{3.13}$$

To make sure the Lyapunov function candidate V_{D} positive definite, due to the fact $\|\mathbf{J}\| = 1$ and $\lambda_m\mathbf{I} \leq \mathbf{M} \leq \lambda_M\mathbf{I}$, we have

$$\begin{aligned} V_{\mathrm{D1}} =& \frac{\lambda_2\lambda_4}{2}\boldsymbol{e}^{\mathrm{T}}\boldsymbol{e} + \frac{\lambda_4}{2}\boldsymbol{\nu}^{\mathrm{T}}\mathbf{M}\boldsymbol{\nu} + \frac{2\boldsymbol{\nu}^{\mathrm{T}}\mathbf{M}\mathbf{J}^{\mathrm{T}}\boldsymbol{e}}{1+2\boldsymbol{e}^{\mathrm{T}}\boldsymbol{e}} \\ \geq& \frac{\lambda_2\lambda_4}{2}\boldsymbol{e}^{\mathrm{T}}\boldsymbol{e} + \frac{\lambda_4\lambda_m}{2}\boldsymbol{\nu}^{\mathrm{T}}\boldsymbol{\nu} - \frac{2\lambda_M}{1+2\boldsymbol{e}^{\mathrm{T}}\boldsymbol{e}}\boldsymbol{\nu}^{\mathrm{T}}\boldsymbol{e}, \end{aligned}$$

If $4\lambda_M^2 - \lambda_4^2\lambda_2\lambda_m < 0$, then V_{D1} is positive definite, additionally,

$$V_{\mathrm{D2}} = \frac{1}{2\lambda_3}\tilde{\Theta}_{\mathrm{D}}^{\mathrm{T}}\tilde{\Theta}_{\mathrm{D}}$$

is positive definite, thus $V_{\mathrm{D}} = V_{\mathrm{D1}} + V_{\mathrm{D2}}$ is positive definite.

Differentiation of V_{D} along the trajectory of the closed-loop system (3.8)-(3.10) yields

$$\begin{aligned} \dot{V}_{\mathrm{D}} =& -\lambda_4\boldsymbol{\nu}^{\mathrm{T}}\bar{\mathbf{B}}\boldsymbol{\nu} - \lambda_1\lambda_4\boldsymbol{\nu}^{\mathrm{T}}\boldsymbol{\nu} + \frac{2\boldsymbol{\nu}^{\mathrm{T}}\mathbf{M}\boldsymbol{\nu}}{1+2\boldsymbol{e}^{\mathrm{T}}\boldsymbol{e}} - \frac{2\mathrm{e}^{\mathrm{T}}\mathbf{J}\bar{\mathbf{B}}\boldsymbol{\nu}}{1+2\boldsymbol{e}^{\mathrm{T}}\boldsymbol{e}} - \frac{2\lambda_1\mathrm{e}^{\mathrm{T}}\mathbf{J}\boldsymbol{\nu}}{1+2\boldsymbol{e}^{\mathrm{T}}\boldsymbol{e}} \\ & - \frac{2\lambda_2\boldsymbol{e}^{\mathrm{T}}\boldsymbol{e}}{1+2\boldsymbol{e}^{\mathrm{T}}\boldsymbol{e}} - \frac{8\boldsymbol{e}^{\mathrm{T}}\boldsymbol{\nu}\boldsymbol{\nu}^{\mathrm{T}}\mathbf{M}\boldsymbol{e}}{(1+2\boldsymbol{e}^{\mathrm{T}}\boldsymbol{e})^2} + \lambda_4\boldsymbol{\nu}^{\mathrm{T}}\boldsymbol{\omega}_{\mathrm{D}} + \frac{2\mathrm{e}^{\mathrm{T}}\mathbf{J}\boldsymbol{\omega}_{\mathrm{D}}}{1+2\boldsymbol{e}^{\mathrm{T}}\boldsymbol{e}}. \end{aligned}$$

Applying $\lambda_d\mathbf{I} \leq \bar{\mathbf{B}} + \bar{\mathbf{B}}^{\mathrm{T}}$, we have

$$\begin{aligned} \dot{V}_{\mathrm{D}} \leq& -(\frac{\lambda_4\lambda_d}{2} + \lambda_1\lambda_4 - 2\lambda_M)\boldsymbol{\nu}^{\mathrm{T}}\boldsymbol{\nu} - (\lambda_d + 2\lambda_1)\boldsymbol{e}^{\mathrm{T}}\boldsymbol{\nu} - 2\lambda_2\boldsymbol{e}^{\mathrm{T}}\boldsymbol{e} + \lambda_4\boldsymbol{\nu}^{\mathrm{T}}\boldsymbol{\omega}_{\mathrm{D}} + 2\mathrm{e}^{\mathrm{T}}\boldsymbol{\omega}_{\mathrm{D}} \\ \leq& -(\frac{\lambda_4\lambda_d}{2} + \lambda_1\lambda_4 - 2\lambda_M - \frac{\lambda_4^2}{4} - 1 + 1)\boldsymbol{\nu}^{\mathrm{T}}\boldsymbol{\nu} - (\lambda_d + 2\lambda_1)\boldsymbol{e}^{\mathrm{T}}\boldsymbol{\nu} - (2\lambda_2 - 2 + 1)\boldsymbol{e}^{\mathrm{T}}\boldsymbol{e} \\ & - (\frac{1}{2}\lambda_4\boldsymbol{\nu} + \boldsymbol{\omega}_{\mathrm{D}})^{\mathrm{T}}(\frac{1}{2}\lambda_4\boldsymbol{\nu} + \boldsymbol{\omega}_{\mathrm{D}}) - (\boldsymbol{e} + \boldsymbol{\omega}_{\mathrm{D}})^{\mathrm{T}}(\boldsymbol{e} + \boldsymbol{\omega}_{\mathrm{D}}) + 2\boldsymbol{\omega}_{\mathrm{D}}^{\mathrm{T}}\boldsymbol{\omega}_{\mathrm{D}}. \end{aligned}$$

If $(\lambda_d + 2\lambda_1)^2 - 8(\lambda_2 - 1)((\lambda_4\lambda_d)/2 + \lambda_1\lambda_4 - 2\lambda_M - \lambda_4^2/4 - 1) < 0$ then

$$\dot{V}_{\mathrm{D}} \leq -\boldsymbol{\nu}^{\mathrm{T}}\boldsymbol{\nu} - \boldsymbol{e}^{\mathrm{T}}\boldsymbol{e} + 2\boldsymbol{\omega}_{\mathrm{D}}^{\mathrm{T}}\boldsymbol{\omega}_{\mathrm{D}}.$$

Integrating both sides of the above equation yields

$$\int_0^t \boldsymbol{\nu}^{\mathrm{T}}\boldsymbol{\nu} dr + \int_0^t \boldsymbol{e}^{\mathrm{T}}\boldsymbol{e} dr \leq V_{\mathrm{D}}(0) + 2\int_0^t \boldsymbol{\omega}_{\mathrm{D}}^{\mathrm{T}}\boldsymbol{\omega}_{\mathrm{D}} dr.$$

This demonstrates that all the states and signals involved in the closed-loop system are bounded. Furthermore, if $\boldsymbol{\omega}_{\mathrm{D}}$ is squared integrable, that is $\int_0^\infty \boldsymbol{\omega}_{\mathrm{D}}^{\mathrm{T}}\boldsymbol{\omega}_{\mathrm{D}} dr < \infty$, we have $\boldsymbol{e} \in L_2$. As all the signals are bounded, we have $\dot{\boldsymbol{e}} \in L_\infty$. According to the Barbalat's Lemma, we have $\lim_{t\to\infty} |\boldsymbol{e}| = 0$. ∎

Remark 3.1 *For plant (3.1), (3.2), an intuitive adaptive law may be*

$$\dot{\hat{\Theta}}_D = \lambda_5 \Phi^{\mathrm{T}}(\boldsymbol{\nu})\boldsymbol{\nu}, \tag{3.14}$$

but rigorous analysis indicates that the regulation error using such adaptive law cannot asymptotically converge.

Remark 3.2 *Here, the theorem is developed for the case where the gains* λ_i $(i = 1, \ldots, 4)$ *are scalar, the proof for the case where the gains are matrices can be easily extended via a similar approach.*

Remark 3.3 *In this chapter the IT2 FLSs are used as estimates of the time-varying hydrodynamic disturbances. If other universal approximators, which can be expressed in the linear in the parameters form like (2.24), are used, the stability analysis will be same. Potential approximators could be type-1 FLSs, neural networks and polynomials etc.*

Remark 3.4 *From Theorem 3.1, it can be seen that in order for the regulation error* $\boldsymbol{e}$ *to converge to zero, the minimum approximation error* $\boldsymbol{\omega}_D$ *is required to be small (in the sense of squared integrable). Based on the universal approximation property discussed in Section 2.2.2, if a sufficient number of rules are used to construct* $\boldsymbol{\tau}_H$*, the* $\boldsymbol{\omega}_D$ *should be small.*

3.1.4 Passivity Interpretation

Passivity theory gives a framework for the design and analysis of control systems using an input-output description according to energy-related considerations. And the input-output description further allows for a modular approach to control systems design and analysis [105]. As illustrated in Fig. 3.1, the closed-loop system (3.8)-(3.10) can be interpreted as the negative feedback interconnection of two subsystems with respective inputs u_1, u_2 and outputs y_1 and y_2, with $y_1 = u_2$ and $u_1 = \boldsymbol{\omega}_{\mathrm{D}}(\boldsymbol{\nu}) - y_2$, and the two subsystems as follows.

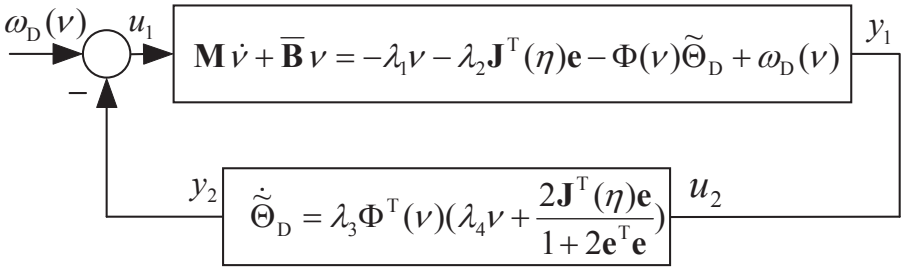

Figure 3.1: Closed-loop equivalent representation for DP.

Subsystem 1:

$$\begin{cases} \mathbf{M}\dot{\boldsymbol{\nu}} + \bar{\mathbf{B}}\boldsymbol{\nu} = -\lambda_1\boldsymbol{\nu} - \lambda_2\mathbf{J}^{\mathrm{T}}(\boldsymbol{\eta})\boldsymbol{e} + u_1 \\ y_1 = \lambda_4\boldsymbol{\nu} + \frac{2\mathbf{J}^{\mathrm{T}}(\boldsymbol{\eta})\boldsymbol{e}}{1+2\boldsymbol{e}^{\mathrm{T}}\boldsymbol{e}} \end{cases} \tag{3.15}$$

Subsystem 2:

$$\begin{cases} \dot{\tilde{\Theta}}_{\mathrm{D}} = \lambda_3\Phi^{\mathrm{T}}(\boldsymbol{\nu})u_2 \\ y_2 = \Phi(\boldsymbol{\nu})\tilde{\Theta}_{\mathrm{D}} \end{cases} \tag{3.16}$$

Theorem 3.2 *The closed-loop system (3.8)-(3.10) is passive if*

$$4\lambda_M^2 - \lambda_4^2\lambda_2\lambda_m < 0 \tag{3.17}$$

and

$$(\lambda_d + 2\lambda_1)^2 - 8(\lambda_2 - 1)(\frac{\lambda_4\lambda_d}{2} + \lambda_1\lambda_4 - 2\lambda_M - \frac{\lambda_4^2}{4} - 1) < 0. \tag{3.18}$$

Proof: For subsystem 1, its supply rate is

$$\begin{aligned} &\int_0^t u_1^{\mathrm{T}} y_1 ds \\ &= \int_0^t (\lambda_4\boldsymbol{\nu} + \frac{2\mathbf{J}^{\mathrm{T}}\boldsymbol{e}}{1+2\boldsymbol{e}^{\mathrm{T}}\boldsymbol{e}})^{\mathrm{T}}(\mathbf{M}\dot{\boldsymbol{\nu}} + \bar{\mathbf{B}}\boldsymbol{\nu} + \lambda_1\boldsymbol{\nu} + \lambda_2\mathbf{J}^{\mathrm{T}}\boldsymbol{e})ds \\ &= \int_0^t [\lambda_2\lambda_4\boldsymbol{\nu}^{\mathrm{T}}\mathbf{J}^{\mathrm{T}}\boldsymbol{e} + \frac{d}{ds}(\frac{\lambda_4}{2}\boldsymbol{\nu}^{\mathrm{T}}\mathbf{M}\boldsymbol{\nu} + \frac{2\boldsymbol{\nu}^{\mathrm{T}}\mathbf{M}\mathbf{J}^{\mathrm{T}}\boldsymbol{e}}{1+2\boldsymbol{e}^{\mathrm{T}}\boldsymbol{e}})]ds \\ &+ \int_0^t [\lambda_4\boldsymbol{\nu}^{\mathrm{T}}\bar{\mathbf{B}}\boldsymbol{\nu} + \lambda_1\lambda_4\boldsymbol{\nu}^{\mathrm{T}}\boldsymbol{\nu} - \frac{2\boldsymbol{\nu}^{\mathrm{T}}\mathbf{M}\boldsymbol{\nu}}{1+2\boldsymbol{e}^{\mathrm{T}}\boldsymbol{e}} + \frac{2\mathrm{e}^{\mathrm{T}}\mathbf{J}\bar{\mathbf{B}}\boldsymbol{\nu}}{1+2\boldsymbol{e}^{\mathrm{T}}\boldsymbol{e}} \\ &+ \frac{2\lambda_1\mathbf{e}^{\mathrm{T}}\mathbf{J}\boldsymbol{\nu}}{1+2\boldsymbol{e}^{\mathrm{T}}\boldsymbol{e}} + \frac{2\lambda_2\boldsymbol{e}^{\mathrm{T}}\boldsymbol{e}}{1+2\boldsymbol{e}^{\mathrm{T}}\boldsymbol{e}} + \frac{8\boldsymbol{e}^{\mathrm{T}}\boldsymbol{\nu}\boldsymbol{\nu}^{\mathrm{T}}\mathbf{M}\boldsymbol{e}}{(1+2\boldsymbol{e}^{\mathrm{T}}\boldsymbol{e})^2}]ds, \end{aligned}$$

if (3.17) and (3.18) are satisfied,

$$\int_0^t u_1^{\mathrm{T}} y_1 ds \geq V_{\mathrm{D1}}(t) - V_{\mathrm{D1}}(0),$$

which means the subsystem 1 is passive with supply rate $\int_0^t u_1^{\mathrm{T}} y_1 ds$ and storage function V_{D1}, which has been defined during the proof for Theorem 3.1.

For subsystem 2, its supply rate is

$$\begin{aligned}\int_0^t u_2^{\mathrm{T}} y_2 ds &= \int_0^t \tilde{\Theta}_{\mathrm{D}}^{\mathrm{T}} \Phi^{\mathrm{T}}(\boldsymbol{\nu}) u_2 ds \\ &= \int_0^t \tilde{\Theta}_{\mathrm{D}}^{\mathrm{T}} \frac{1}{\lambda_3} \dot{\tilde{\Theta}}_{\mathrm{D}} ds \\ &\geq V_{\mathrm{D2}}(t) - V_{\mathrm{D2}}(0)\end{aligned}$$

which means the subsystem 2 is passive with supply rate $\int_0^t u_2^{\mathrm{T}} y_2 ds$ and storage function V_{D2}.

According to the fact that the negative feedback interconnection of two passive systems is passive, the closed-loop system (3.8)-(3.10) is passive. ∎

3.2 Simulation Studies

The simulation studies are performed on the platform of MSS [98]. A container ship named as S-175 [37, 98], whose main particulars are shown in Table 3.1, is used as case study. The subsequent simulation results are obtained for following seas with the International Towing Tank Conference (ITTC) wave spectrum using significant wave height $H_s = 5$ m and peak frequency $\omega_0 = 0.56$ rad/s. The significant wave height H_s is used to classify the type of sea, $H_s = 5$ m corresponds to very rough sea with large waves. Even though ignored during Lyapunov analysis, the sea current is set with speed $V_c = 2$ m/s and direction $\beta_c = 30^\circ$ in the following simulations. The control objective is set to regulate the vessel to state $[\boldsymbol{\eta}_d^{\mathrm{T}}, \boldsymbol{\nu}_d^{\mathrm{T}}] = [\mathbf{0}, \mathbf{0}]$ from initial state $[\boldsymbol{\eta}_0^{\mathrm{T}}, \boldsymbol{\nu}_0^{\mathrm{T}}] = [2, 2, 5^\circ, 0, 0, 0]$.

Table 3.1: Main particulars of the S-175.

Ship	S-175
Length between perpendiculars	175 m
Beam	25 m
Draught	9.5 m
Mass	24610 ton

3.2.1 Closed-loop Performance

Although the controller (3.6), (3.7) is designed based on the control plant model (3.1), (3.2), it is tested with the process plant model (2.1), (2.2). As indicated in (3.4) and (3.5), three singleton IT2 sub-FLSs are used to approximate the complex hydrodynamic disturbances. In each sub-system, each of the input domain is partitioned by three fuzzy membership functions labeled as **N**, **Z**, and **P**, thus there are 27 rules. By doing this, the input domains are covered by a simple set of labels of **Negative**, **Zero**, and **Positive**. For the antecedent IT2 fuzzy sets, the primary membership functions are chosen to be Gaussian function with uncertain standard deviation, i.e.,

$$\mu_{\tilde{F}_i^j}(x_j) = \exp[-\frac{1}{2}(\frac{x_j - m_i}{\sigma})^2] \quad \sigma \in [\underline{\sigma}, \overline{\sigma}] \tag{3.19}$$

where $i = 1, 2, 3$ is the index of three fuzzy membership functions for jth input and $j = 1, 2, 3$ is the index of three inputs. The inputs to each sub-system is scaled properly so that the means for the Gaussian functions are fixed at $m_1 = -1$, $m_2 = 0$, and $m_3 = 1$ for each input, and the standard deviation for all of the lower membership function is fixed at $\underline{\sigma} = 0.6$, whereas the one for all of the upper membership function

is $\overline{\sigma} = 0.8$. The primary membership functions of the antecedent IT2 fuzzy sets are shown in Fig. 3.2. For the consequent IT2 fuzzy sets, singleton membership functions

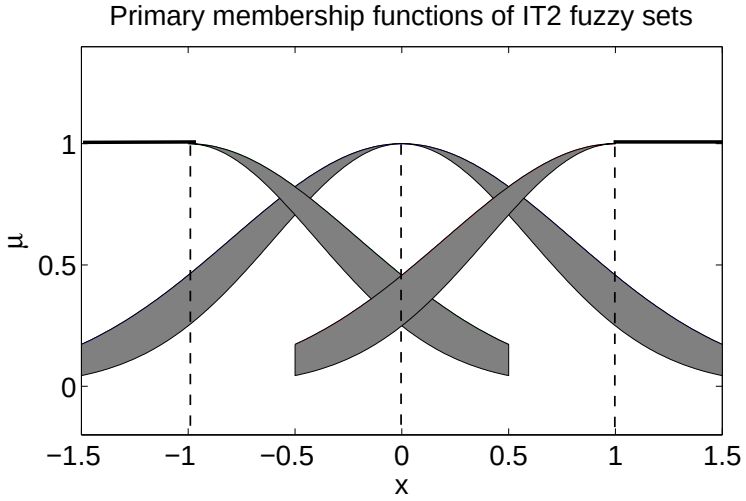

Figure 3.2: Primary membership functions of the antecedent IT2 fuzzy sets.

are chosen. So there are 27 adjustable consequent parameters, whose values are adapted according to adaptive law. There are four control gains λ_i $(i = 1, \ldots, 4)$ in the proposed controller (3.6) and (3.7). The control gain λ_4 determines the relative convergence speed of vessel displacement and velocity in the adaptive law (3.7) and should be chosen first. The choice of the value of λ_4 depends on the controlled plant. For container ship S-175 in the simulation studies, the value of λ_4 is set via trial and error as 5. The choices of λ_1 and λ_2 could refer to the procedure of determining the PD gains. The choice of λ_3 must satisfy the stability condition. When $\lambda_1 = 4.3 \times 10^6$, $\lambda_2 = 4.3 \times 10^5$, $\lambda_3 = 5 \times 10^8$, and $\lambda_4 = 5$ in (3.6) and (3.7), the controlled position and heading angle of the vessel are shown in Fig. 3.3. It can be observed that the closed-loop system is stable, the control performance is satisfactory despite the time-varying hydrodynamic disturbances, and the sub-FLSs efficiently approximate the

complex disturbances although universal approximation property for IT2 FLS has not been established yet. Fig. 3.4 shows the norms of the adapted weighting vectors $\|\hat{\boldsymbol{\theta}}_i\|$ $(i = 1, 2, 3)$, they verify the boundedness of $\hat{\boldsymbol{\Theta}}_{\mathrm{D}}$. Note that the norm of weighting vector $\hat{\boldsymbol{\theta}}_1$ shows fluctuation during the simulation, it is because the disturbances along the surge direction fluctuate heavily at the start of the simulation.

3.2.2 Impact of Control Gains

To investigate the impact of the control gains, simulations with the following three cases are conducted:

- Case 1: $\lambda_1 = 4.3 \times 10^5$, $\lambda_2 = 4.3 \times 10^4$, $\lambda_3 = 5 \times 10^7$;
- Case 2: $\lambda_1 = 4.3 \times 10^6$, $\lambda_2 = 4.3 \times 10^5$, $\lambda_3 = 5 \times 10^8$;
- Case 3: $\lambda_1 = 4.3 \times 10^7$, $\lambda_2 = 4.3 \times 10^6$, $\lambda_3 = 5 \times 10^9$.

The controlled positions and heading angles of the vessel are shown in Fig. 3.5. It can be observed that as the values of the control gains increase, the control performance becomes better. Conversely, the regulation errors would oscillate when the gains are reduced. In practice, large control gains are not recommended as they require larger actuators. Thus, the choice of control gains is a tradeoff between performance requirement and practical limitation.

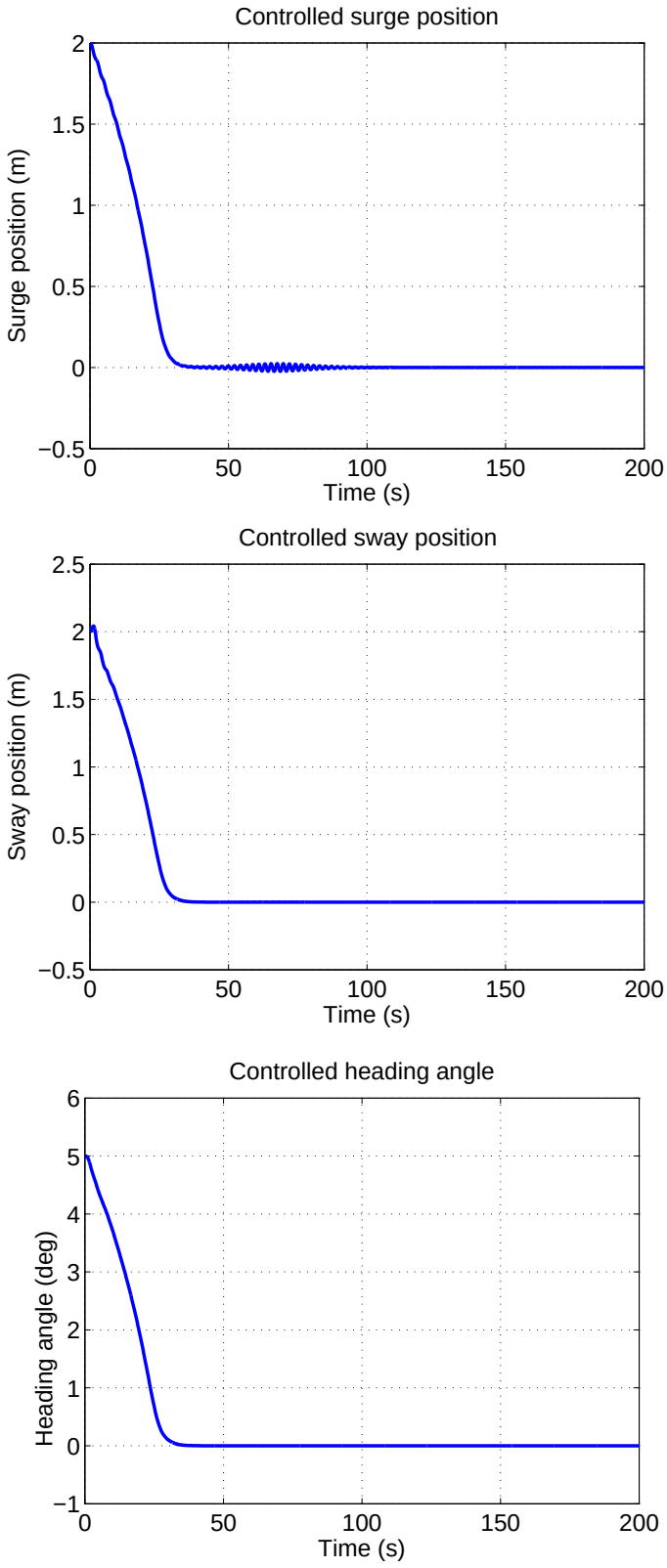

Figure 3.3: Regulation errors of indirect adaptive IT2 FLC for DP.

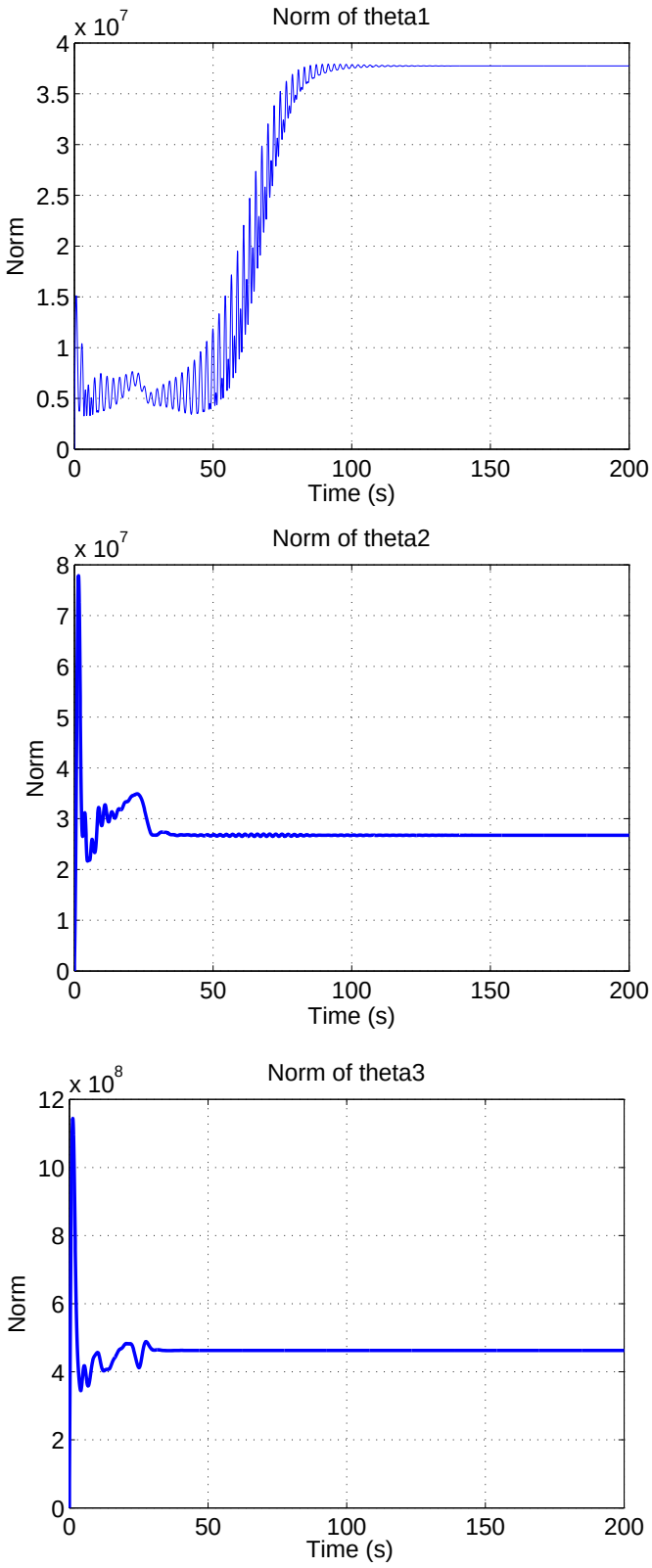

Figure 3.4: Norms of the adapted weighting vectors for indirect adaptive IT2 FLC.

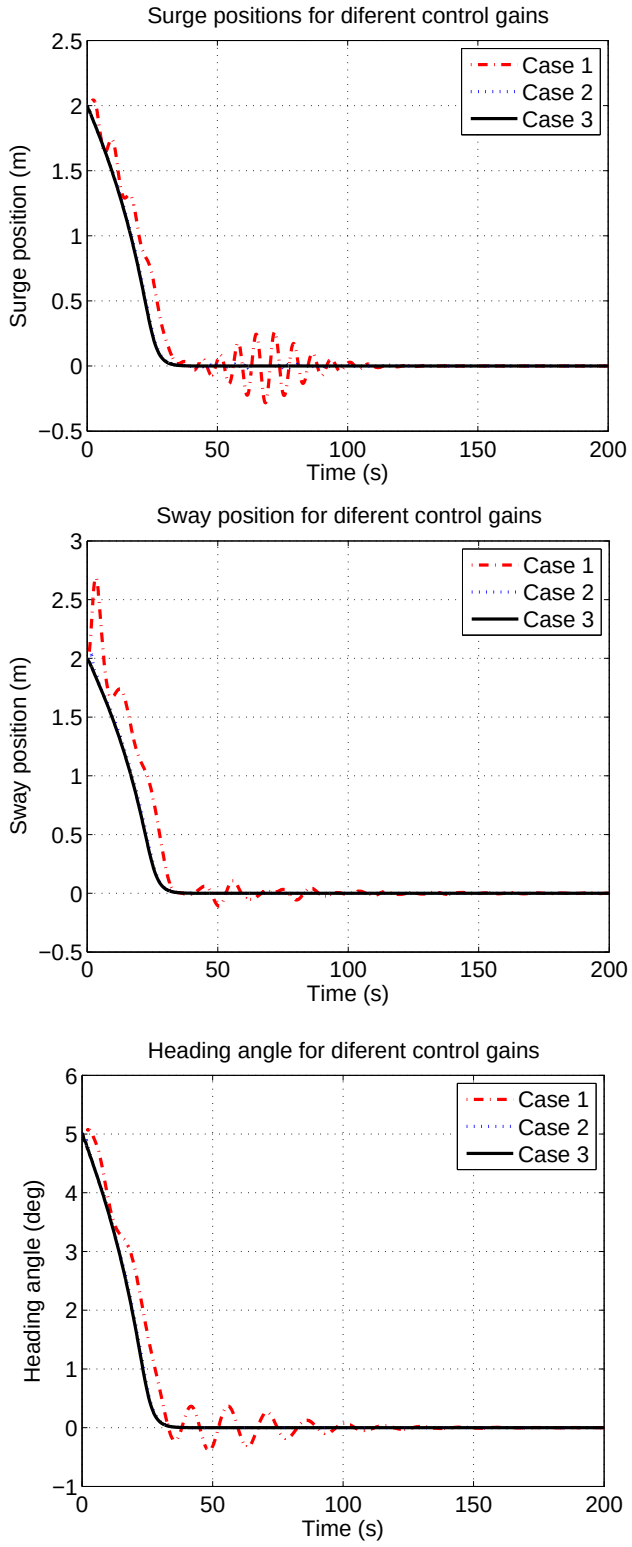

Figure 3.5: Regulation errors of indirect adaptive IT2 FLC with different control gains for DP.

3.2.3 Comparison with a PD Controller

Comparative study between the designed controller and a linear PD controller is presented. The PD controller is in the form of

$$\boldsymbol{\tau} = -\lambda_5 \boldsymbol{\nu} - \lambda_6 \mathbf{J}^{\mathrm{T}}(\boldsymbol{\eta}) \boldsymbol{e}. \tag{3.20}$$

Two sets of control gains are implemented for the PD controller, $\lambda_5^1 = 4.3 \times 10^6,\ \lambda_6^1 = 4.3 \times 10^5$ and $\lambda_5^2 = 4.3 \times 10^8,\ \lambda_6^2 = 4.3 \times 10^7$, meanwhile the parameter settings for the indirect adaptive IT2 FLC are kept same as the one in the subsection 3.2.1. The results are shown in Fig. 3.6, which demonstrates that with same proportion and derivative gains, the designed controller achieves satisfactory performance, whereas the PD controller is unstable as shown by the dot and dash line. By increasing its proportion and derivative gains, the PD controller can be stable as shown by the dot line, but still with large steady state error due to disturbances. Besides, large control gains are not recommended in practice as they reduce robustness and cause large overshoots. Hence, the designed controller performs much better than the PD controller and has better disturbance rejection property.

3.2.4 Comparison with an Adaptive Type-1 FLC

Replace the components in (3.5) and correspondingly in (3.6) and (3.7) with fuzzy basis function vector [41, 85],

$$\boldsymbol{\phi}^{\mathrm{T}} = (\phi^1(\mathbf{x}), \ldots, \phi^M(\mathbf{x})) \tag{3.21}$$

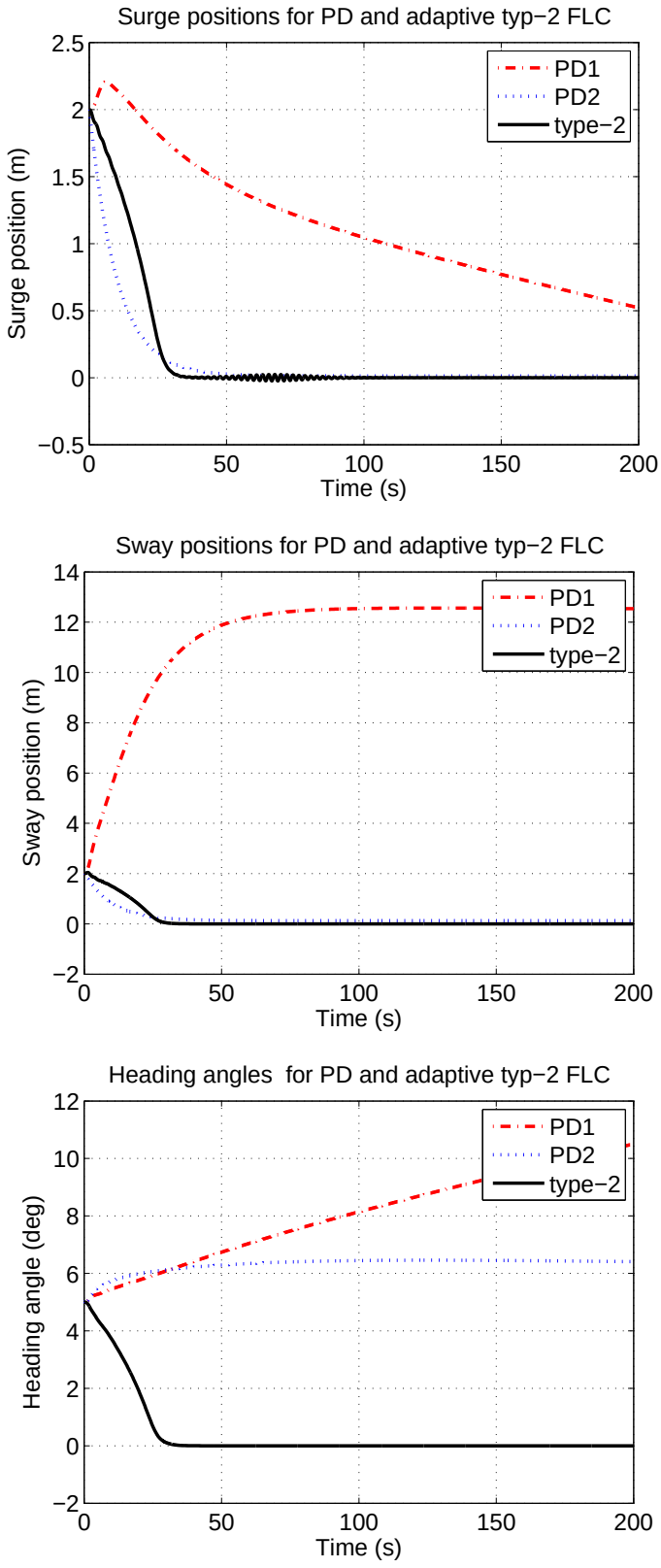

Figure 3.6: Regulation errors of indirect adaptive IT2 FLC and PD controller for DP.

where fuzzy basis function is defined as

$$\phi^l(\mathbf{x}) = \frac{\Pi_{i=1}^n \mu_{F_i^l}(x_i)}{\Sigma_{l=1}^M (\Pi_{i=1}^n \mu_{F_i^l}(x_i))}, \tag{3.22}$$

the controller (3.6), (3.7) becomes an adaptive type-1 FLC. In this subsection, the indirect adaptive IT2 FLC is compared with such an adaptive type-1 FLC. For each sub-system in the indirect adaptive IT2 FLC, the parameter settings are kept identical as the one in previous subsection, whereas for each sub-system in type-1 case, each of the input domain is partitioned by five fuzzy membership functions labeled as **NL**, **NS**, **Z**, **PS**, and **PL**, thus there are 125 rules and 125 adjustable consequent parameters accordingly in contrast to 27 rules and parameters for IT2 case. The membership functions of the antecedent sets for each input are chosen as Gaussian functions, i.e.,

$$\mu_{F_i^j}(x_j) = \exp[-\frac{1}{2}(\frac{x_j - m_i}{\sigma})^2]. \tag{3.23}$$

where $i = 1, \ldots, 5$ is the index of five fuzzy membership functions for jth input and $j = 1, 2, 3$ is the index of three inputs. While the means are set as $(m_1, \ldots, m_5) = (-1, -0.5, 0, 0.5, 1)$, the standard deviations for all the Gaussian functions are fixed at $\sigma = 0.4$. When $\lambda_1 = 4.3 \times 10^6$, $\lambda_2 = 4.3 \times 10^5$, $\lambda_3 = 1.5 \times 10^7$, and $\lambda_4 = 5$ in (3.6) and (3.7) for both adaptive type-1 and IT2 FLCs, the resultant positions and heading angles of the vessel are shown in Fig. 3.7. It can be observed that the rising and settling time for adaptive IT2 FLC is shorter than that for type-1 case, even though type-1 case uses more rules. To quantify the performance differences between adaptive type-1 and IT2 FLCs, the integral of time-weighted absolute errors (ITAE) for both cases in the following form are calculated.

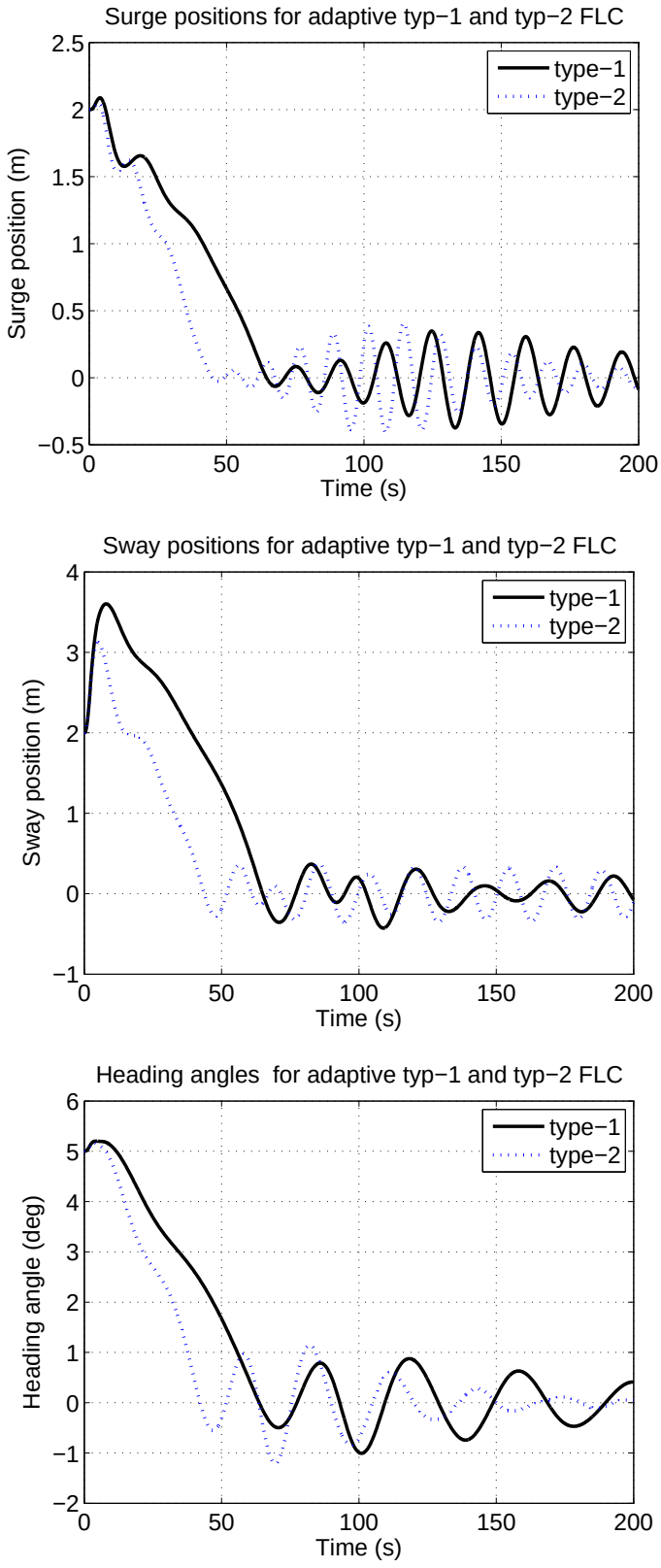

Figure 3.7: Regulation errors of indirect adaptive IT2 and type-1 FLC for DP.

Table 3.2: ITAE of adaptive type-1 and IT2 FLCs for DP.

ITAE	P_x	P_y	P_ψ
Type-1	4604	5960	210
IT2	3252	4951	121

$$P_x = \int_0^T t|x|dt \tag{3.24}$$

$$P_y = \int_0^T t|y|dt \tag{3.25}$$

$$P_\psi = \int_0^T t|\psi|dt \tag{3.26}$$

where T is the total simulation time. The results are shown in Table 3.2, and the ITAE for the IT2 case are smaller than those for type-1 case along all the three degrees of freedom. Regarding the computational burden, type-reduction for IT2 case does take some time, but the time is very little as only a few rules are fired simultaneously and it has been proved Karnik-Mendel algorithm is super-exponentially convergent [106]. In addition, the real-time application of the type-2 FLS has been reported [107]. Thus, type-reduction should not be an issue that causes any stability problem. In a word, it seems that the IT2 FLS has better approximation property with less rules than its type-1 counterpart.

3.3 Conclusions

In this chapter, an indirect adaptive IT2 FLC has been designed for DP vessels with attached thrusters in the presence of time-varying hydrodynamic disturbances. It has been proved that the regulation error under the proposed control semiglobally asymp-

totically converges to zero and the closed-loop system under the proposed control is passive. Simulation results have demonstrated that the indirect adaptive IT2 FLC is effective and robust. When compared against a PD controller, the proposed controller has better control performance and disturbance rejection property. Comparison with its type-1 counterpart suggests IT2 FLS has better approximation property.

Chapter 4

Passive Adaptive IT2 Fuzzy Observer for Dynamic Positioning

In Chapter 3, an indirect adaptive IT2 FLC is designed for DP. But the controller is proposed based on an assumption that the state variables of the vessel, i.e. displacements and velocities along surge, sway, and yaw, are measured by its own on-board devices (Assumption 3.2). In a DP system, filtering and state estimation are important features, as the position and heading measurements are corrupted by oscillatory motion due to first-order wave disturbances. Moreover, in most cases the measurements of the vessel velocities are not available. Thus, Assumption 3.2 restricts the practical application of the indirect adaptive IT2 FLC. To overcome the limitation, the work reported in this chapter assumes that only displacement measurements of the vessel are available. Some commercial position measurement systems are hydroacoustic positioning reference (HPR) systems and satellite navigation systems. The two famous satellite navigation systems are Navstar GPS and GLONASS. The accuracy of the GPS satellite navigation system is degraded for civilian users. Thus, a differential global positioning system (DGPS) is used to circumvent this problem. The main idea of the DGPS is to use a fixed receiver, which is on shore with known position, to calculate the GPS position errors. The position errors are then sent to

the GPS receiver on board the vessel to fine tune the measured position of the vessel. The attitude of the vessel is usually measured by a gyrocompass where the gyro drift could be compensated for by a magnetic compass. As a dynamically positioned vessel moves only with low speed, the influence of waves on the position and attitude of the vessel is significant. Ocean waves are often characterized by statistical analysis of the time history of the irregular waves. The statistical analysis leads to a "wave spectrum", which describes the distribution of wave energy (height) with frequency. Fig. 4.1 shows that the measured position and attitude of the vessel will be combination of the low frequency (LF) motion of the vessel and the wave frequency (WF) motion due to an ocean wave that has the fundamental frequency (first-order wave). The expression of the measured position and attitude is

$$\boldsymbol{y}' = \boldsymbol{\eta}' + \boldsymbol{\eta}'_w, \tag{4.1}$$

where $\boldsymbol{\eta}'_w$ is the vessel's WF motion due to first-order wave induced disturbances, and may be computed via a Motion Response Amplitude Operator explained in [92]. It is noted that the WF motion due to first-order wave is oscillatory.

The objective of this chapter is to design an observer to reconstruct the LF motion components $\boldsymbol{\eta}'$ from the measured position and attitude signals $\boldsymbol{y}' = \boldsymbol{\eta}' + \boldsymbol{\eta}'_w$. Moreover, an estimate of the LF velocity $\boldsymbol{\nu}'$ should also be produced from $\boldsymbol{y}'$. It is crucial to eliminate the high frequency disturbances induced by the first-order wave from the sensor signal before feeding to the feedback loop. Otherwise, the DP system will attempt to reject the oscillatory motion due to $\boldsymbol{\eta}'_w$ leading to an increase in fuel consumption and causing wear and tear to the actuators. To fulfill the objective,

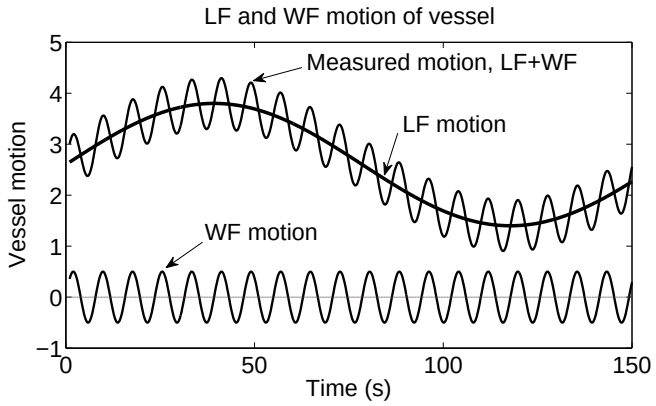

Figure 4.1: The measured vessel motion as the sum of the LF and WF motion.

a passive adaptive IT2 fuzzy observer for DP of floating vessels under time-varying hydrodynamic disturbances is proposed. The combination of approximation-based adaptive technique and IT2 FLS is used to handle the time-varying hydrodynamic disturbances and uncertainties. Besides, the observer for DP is treated as an engineering application to investigate the approximation property of IT2 FLS as well.

The remainder of this chapter is organized as follows. The design and stability analysis of the passive adaptive IT2 fuzzy observer for DP is delineated in Section 4.1. Section 4.2 describes the simulation results of the observer. Comparison with the passive nonlinear observer is also shown in this section. Finally, conclusions of this chapter are drawn in Section 4.3.

4.1 Adaptive Fuzzy Observer Design

In this section, the manner in which the process plant model is simplified to generate the control plant model that facilitates the observer design is described. In the control

plant model, a 2nd-order equation is used to estimate the Motion Response Amplitude Operator model of first-order wave. Thus, the 2nd-order equation is part of the control plant model. Then, based on the control plant model, the adaptive fuzzy observer is designed. The time-varying hydrodynamic disturbances are approximated by singleton IT2 FLSs in the observer. Using Lyapunov synthesis, the estimation errors of the observer error dynamics are proven to be semiglobally uniformly ultimately bounded. Rigorous analysis shows the observer error dynamics is passive.

4.1.1 Control Plant Model

The models of marine vessels may be classified into two categories [57], namely a process plant model and a control plant model. As in Section 3.1, the process plant model (2.1) and (2.2) for DP described in Section 2.1 is simplified to facilitate the observer design and analytical stability analysis. Applying Assumptions 3.1 and 3.3 to (2.1), (2.2) and (4.1), the following model is obtained.

$$\dot{\boldsymbol{\eta}} = \mathbf{J}(\boldsymbol{\eta})\boldsymbol{\nu} \tag{4.2}$$

$$\mathbf{M}\dot{\boldsymbol{\nu}} + \bar{\mathbf{B}}\boldsymbol{\nu} = \boldsymbol{\tau} + \boldsymbol{\tau}_{\mathrm{H}} \tag{4.3}$$

$$\boldsymbol{y} = \boldsymbol{\eta} + \boldsymbol{\eta}_w \tag{4.4}$$

where $\boldsymbol{\eta} = [x, y, \psi]^{\mathrm{T}}$ is the displacement vector along surge, sway, and yaw, whereas $\boldsymbol{\nu} = [u, v, r]^{\mathrm{T}}$ is the velocity vector. $\mathbf{J}(\boldsymbol{\eta}) \in R^{3\times3}$ is the rotation matrix. Note that $\mathbf{J}\mathbf{J}^{\mathrm{T}} = \mathbf{I}$ ($\mathbf{I}$ is the identity matrix). $\mathbf{M} \in R^{3\times3}$ is the system inertia matrix including added mass. $\bar{\mathbf{B}} \in R^{3\times3}$ is the three dimensional version of the damping matrix $\bar{\mathbf{B}}'$. $\boldsymbol{\tau} \in R^3$ and $\boldsymbol{\tau}_{\mathrm{H}} \in R^3$ are three dimensional versions of $\boldsymbol{\tau}'$ and $\boldsymbol{\tau}'_{\mathrm{H}}$ respectively.

$\boldsymbol{y} \in R^3$ is the position and heading measurement vector. $\boldsymbol{\eta}_w = [x_w, y_w, \psi_w]^{\mathrm{T}}$ is the WF motion vector. The difference between the control plant model presented here and the one presented in subsection 3.1.1 is that the measurement system is included in this model.

In order to approximate the vessel's WF motion due to first-order wave induced disturbances, a 2nd-order equation in frequency domain is first used to fit the shape of wave spectrum such as the Pierson-Moskovitz or the JONSWAP spectra. Then the 2nd-order equation in frequency domain is transformed to time domain to generate the vessel's WF motion. The 2nd-order equation was originally proposed by Balchen et al. in [10], which used three harmonic oscillators without damping. Later Sælid et al. introduced a damping term to better fit the shape of the wave spectrum [108]. The resultant model can be written as

$$h_i(s) = \frac{2\lambda_i \omega_{0i} \sigma_i s}{s^2 + 2\lambda_i \omega_{0i} s + \omega_{0i}^2} \tag{4.5}$$

where ω_{0i} $(i = 1, \ldots, 3)$ is the dominating wave frequency. λ_i $(i = 1, \ldots, 3)$ is a damping coefficient. And σ_i $(i = 1, \ldots, 3)$ is a constant describing the wave intensity. It is noted that there is one model for each degrees of freedom.

A linear state-space model can be obtained from (4.5) by transforming it to the time-domain. The state-space model is

$$\begin{bmatrix} \dot{\boldsymbol{\xi}}_1 \\ \dot{\boldsymbol{\xi}}_2 \end{bmatrix} = \begin{bmatrix} \mathbf{0} & \mathbf{I} \\ \mathbf{A}_{21} & \mathbf{A}_{22} \end{bmatrix} \begin{bmatrix} \boldsymbol{\xi}_1 \\ \boldsymbol{\xi}_2 \end{bmatrix} + \begin{bmatrix} \mathbf{0} \\ \mathbf{E}_2 \end{bmatrix} \boldsymbol{w} \tag{4.6}$$

$$\boldsymbol{\eta}_w = \begin{bmatrix} \mathbf{0} & \mathbf{I} \end{bmatrix} \begin{bmatrix} \boldsymbol{\xi}_1 \\ \boldsymbol{\xi}_2 \end{bmatrix} \tag{4.7}$$

where $\boldsymbol{\xi}_1 \in R^3$ and $\boldsymbol{\xi}_2 \in R^3$. $\boldsymbol{w} \in R^3$ is a vector of zero-mean Gaussian white noise, and

$$\mathbf{A}_{21} = -\operatorname{diag}\{\omega_{01}^2, \omega_{02}^2, \omega_{03}^2\}$$

$$\mathbf{A}_{22} = -\operatorname{diag}\{2\lambda_1\omega_{01}, 2\lambda_2\omega_{02}, 2\lambda_3\omega_{03}\}$$

$$\mathbf{E}_2 = \operatorname{diag}\{2\lambda_1\omega_{01}\sigma_1, 2\lambda_2\omega_{02}\sigma_2, 2\lambda_3\omega_{03}\sigma_3\}.$$

In the Lyapunov stability analysis, the following assumptions are made.

Assumption 4.1 $\mathbf{J}(\boldsymbol{\eta}) = \mathbf{J}(\boldsymbol{y})$. *This is an acceptable assumption since the magnitude of the wave-induced yaw disturbance ψ_w is small.*

Assumption 4.2 $\boldsymbol{w} = \mathbf{0}$. *The wave model (4.6) is driven by zero-mean Gaussian white noise $\boldsymbol{w}$. This term is omitted in the control plant model since the observer sates are driven by the state estimation errors.*

The applications of Assumption 4.1 and 4.2 to (4.2) and (4.6) yield the following control plant model.

$$\dot{\boldsymbol{\xi}} = \mathbf{A}_w\boldsymbol{\xi} \tag{4.8}$$

$$\dot{\boldsymbol{\eta}} = \mathbf{J}(\boldsymbol{y})\boldsymbol{\nu} \tag{4.9}$$

$$\mathbf{M}\dot{\boldsymbol{\nu}} = -\bar{\mathbf{B}}\boldsymbol{\nu} + \boldsymbol{\tau} + \boldsymbol{\tau}_{\mathrm{H}} \tag{4.10}$$

$$\boldsymbol{y} = \boldsymbol{\eta} + \mathbf{C}_w\boldsymbol{\xi} \tag{4.11}$$

where $\boldsymbol{\xi} = [\boldsymbol{\xi}_1^{\mathrm{T}}, \boldsymbol{\xi}_2^{\mathrm{T}}]^{\mathrm{T}} \in R^6$, $\mathbf{A}_w = \begin{bmatrix} \mathbf{0} & \mathbf{I} \\ \mathbf{A}_{21} & \mathbf{A}_{22} \end{bmatrix}$, and $\mathbf{C}_w = \begin{bmatrix} \mathbf{0} & \mathbf{I} \end{bmatrix}$. For notational

simplicity, (4.8), (4.9) and (4.11) are written in the state-space form

$$\dot{\boldsymbol{\eta}}_0 = \mathbf{A}_0\boldsymbol{\eta}_0 + \mathbf{B}_0\mathbf{J}(\boldsymbol{y})\boldsymbol{\nu} \tag{4.12}$$

$$\boldsymbol{y} = \mathbf{C}_0\boldsymbol{\eta}_0, \tag{4.13}$$

where $\boldsymbol{\eta}_0 = [\boldsymbol{\xi}^{\mathrm{T}}, \boldsymbol{\eta}^{\mathrm{T}}]^{\mathrm{T}}$ and $\mathbf{A}_0 = \begin{bmatrix} \mathbf{A}_w & \mathbf{0} \\ \mathbf{0} & \mathbf{0} \end{bmatrix}$, $\mathbf{B}_0 = \begin{bmatrix} \mathbf{0} \\ \mathbf{I} \end{bmatrix}$, $\mathbf{C}_0 = \begin{bmatrix} \mathbf{C}_w & \mathbf{I} \end{bmatrix}$.

4.1.2 Observer Equations

To handle the time-varying hydrodynamic disturbances $\boldsymbol{\tau}_{\mathrm{H}}$ in the plant model (4.10), the hydrodynamic disturbances are estimated by singleton IT2 FLSs (2.24). The hydrodynamic disturbances are estimated in earth-fixed frame and then transformed to body-fixed frame as

$$\boldsymbol{\tau}_{\mathrm{H}}(\boldsymbol{\nu}) = -\mathbf{J}^{\mathrm{T}}(\boldsymbol{y})\Phi(\boldsymbol{\nu})\Theta^* + \boldsymbol{\omega}_e(\boldsymbol{\nu}), \tag{4.14}$$

where $\boldsymbol{\omega}_e(\boldsymbol{\nu}) \in R^3$ is a vector of minimum estimation error.

$$\begin{aligned} \Theta^* &= (\boldsymbol{\theta}_1^{*\mathrm{T}}, \boldsymbol{\theta}_2^{*\mathrm{T}}, \boldsymbol{\theta}_3^{*\mathrm{T}})^{\mathrm{T}} \in R^{3M\times 1} \\ &= \arg\min_{\Theta\in R^{3M}}[\sup_{\nu\in U_\nu} |\boldsymbol{\tau}_{\mathrm{H}}(\boldsymbol{\nu}) + \mathbf{J}^{\mathrm{T}}(\boldsymbol{y})\Phi(\boldsymbol{\nu})\Theta|] \end{aligned} \tag{4.15}$$

is the ideal weighting vector and

$$\Phi(\boldsymbol{\nu}) = \mathrm{diag}\{\boldsymbol{\phi}_1^{\mathrm{T}}(\boldsymbol{\nu}), \boldsymbol{\phi}_2^{\mathrm{T}}(\boldsymbol{\nu}), \boldsymbol{\phi}_3^{\mathrm{T}}(\boldsymbol{\nu})\} \in \mathrm{R}^{3\times 3\mathrm{M}} \tag{4.16}$$

is the regressive matrix. The input signals to the FLSs, $\boldsymbol{\nu}$, is the velocity vector of the vessel because the hydrodynamic disturbances are directly related to the velocity vector of the vessel as shown in [92]. As a multi-output FLS can be divided into several single-output FLSs, three sub-FLSs that have M rules each are used to approximate

the three dimensional hydrodynamic disturbances $\boldsymbol{\tau}_{\mathrm{H}}$. As a result, by substituting (4.14) into (4.10), the plant model (4.10) may be expressed as

$$\mathbf{M}\dot{\boldsymbol{\nu}} = -\bar{\mathbf{B}}\boldsymbol{\nu} + \boldsymbol{\tau} - \mathbf{J}^{\mathrm{T}}(\boldsymbol{y})\Phi(\boldsymbol{\nu})\Theta^{*} + \boldsymbol{\omega}_{e}(\boldsymbol{\nu}). \tag{4.17}$$

Then, the observer is designed as

$$\dot{\hat{\boldsymbol{\xi}}} = \mathbf{A}_{w}\hat{\boldsymbol{\xi}} + \mathbf{K}_{1}\tilde{\boldsymbol{y}} \tag{4.18}$$

$$\dot{\hat{\boldsymbol{\eta}}} = \mathbf{J}(\boldsymbol{y})\hat{\boldsymbol{\nu}} + \mathbf{K}_{2}\tilde{\boldsymbol{y}} \tag{4.19}$$

$$\dot{\hat{\Theta}} = -\Phi^{\mathrm{T}}(\hat{\boldsymbol{\nu}})\mathbf{K}_{3}\tilde{\boldsymbol{y}} \tag{4.20}$$

$$\mathbf{M}\dot{\hat{\boldsymbol{\nu}}} = -\bar{\mathbf{B}}\hat{\boldsymbol{\nu}} + \boldsymbol{\tau} - \mathbf{J}^{\mathrm{T}}(\boldsymbol{y})\Phi(\hat{\boldsymbol{\nu}})\hat{\Theta} + \mathbf{J}^{\mathrm{T}}(\boldsymbol{y})\mathbf{K}_{4}\tilde{\boldsymbol{y}} \tag{4.21}$$

$$\hat{\boldsymbol{y}} = \hat{\boldsymbol{\eta}} + \mathbf{C}_{w}\hat{\boldsymbol{\xi}} \tag{4.22}$$

where $\tilde{\boldsymbol{y}} = \boldsymbol{y} - \hat{\boldsymbol{y}}$ is the estimation error vector. $\mathbf{K}_{1} \in R^{6\times 3}$ and $\mathbf{K}_{2,3,4} \in R^{3\times 3}$ are observer gain matrices. The block diagram of the observer is shown in Fig. 4.2, which demonstrates how the observer is implemented. The inputs to the observer are signals from sensors and actuators, whereas the outputs are estimated displacement and velocity signals of vessel. In order to facilitate the stability analysis, similar to (4.12) and (4.13), the observer equations (4.18), (4.19) and (4.22) are written in the state-space form

$$\dot{\hat{\boldsymbol{\eta}}}_{0} = \mathbf{A}_{0}\hat{\boldsymbol{\eta}}_{0} + \mathbf{B}_{0}\mathbf{J}(\boldsymbol{y})\hat{\boldsymbol{\nu}} + \mathbf{K}\tilde{\boldsymbol{y}} \tag{4.23}$$

$$\hat{\boldsymbol{y}} = \mathbf{C}_{0}\hat{\boldsymbol{\eta}}_{0}, \tag{4.24}$$

where $\hat{\boldsymbol{\eta}}_{0} = [\hat{\boldsymbol{\xi}}^{\mathrm{T}}, \hat{\boldsymbol{\eta}}^{\mathrm{T}}]^{\mathrm{T}}$ and $\mathbf{K} = \begin{bmatrix} \mathbf{K}_{1} \\ \mathbf{K}_{2} \end{bmatrix}$.

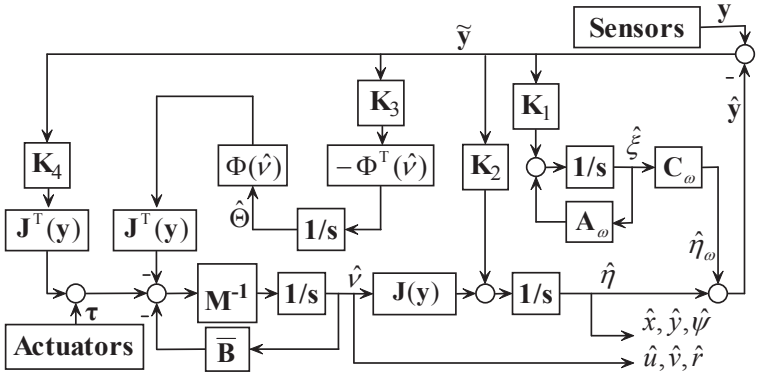

Figure 4.2: Block diagram of the adaptive IT2 fuzzy observer.

4.1.3 Observer Error Dynamics

Define the estimation errors as $\tilde{\boldsymbol{\eta}}_0 = \boldsymbol{\eta}_0 - \hat{\boldsymbol{\eta}}_0$, $\tilde{\Theta} = \Theta^* - \hat{\Theta}$ and $\tilde{\boldsymbol{\nu}} = \boldsymbol{\nu} - \hat{\boldsymbol{\nu}}$. By subtracting the observer equations from the control plant model, the observer error dynamics can be expressed as

$$\dot{\tilde{\boldsymbol{\eta}}}_0 = (\mathbf{A}_0 - \mathbf{K}\mathbf{C}_0)\tilde{\boldsymbol{\eta}}_0 + \mathbf{B}_0\mathbf{J}(\boldsymbol{y})\tilde{\boldsymbol{\nu}} \tag{4.25}$$

$$\dot{\tilde{\Theta}} = \Phi^{\mathrm{T}}(\hat{\boldsymbol{\nu}})\mathbf{K}_3\tilde{\boldsymbol{y}} \tag{4.26}$$

$$\mathbf{M}\dot{\tilde{\boldsymbol{\nu}}} = -\bar{\mathbf{B}}\tilde{\boldsymbol{\nu}} - \mathbf{J}^{\mathrm{T}}(\boldsymbol{y})\Phi(\hat{\boldsymbol{\nu}})\tilde{\Theta} - \mathbf{J}^{\mathrm{T}}(\boldsymbol{y})\mathbf{K}_4\tilde{\boldsymbol{y}} + \boldsymbol{\omega} \tag{4.27}$$

$$\tilde{\boldsymbol{y}} = \mathbf{C}_0\tilde{\boldsymbol{\eta}}_0, \tag{4.28}$$

where $\boldsymbol{\omega} = \boldsymbol{\omega}_e + \boldsymbol{\omega}_f$, and where $\boldsymbol{\omega}_f = \mathbf{J}^{\mathrm{T}}(\boldsymbol{y})\Phi(\hat{\boldsymbol{\nu}})\Theta^* - \mathbf{J}^{\mathrm{T}}(\boldsymbol{y})\Phi(\boldsymbol{\nu})\Theta^*$. Since the elements of the regressive matrices $\Phi(\boldsymbol{\nu})$ and $\Phi(\hat{\boldsymbol{\nu}})$ are fuzzy basis functions as defined in [74], $\|\Phi(\boldsymbol{\nu})\|^2 \leq 1$ and $\|\Phi(\hat{\boldsymbol{\nu}})\|^2 \leq 1$. Moreover, $\mathbf{J}^{\mathrm{T}}(\boldsymbol{y})$ is rotation matrix and $\|\mathbf{J}^{\mathrm{T}}(\boldsymbol{y})\|^2 \leq 1$. Thus, $\|\boldsymbol{\omega}_f\|^2 \leq \|\Theta^*\|^2$. Define $\tilde{\mathbf{Z}} = \Phi(\hat{\boldsymbol{\nu}})\tilde{\Theta} + \mathbf{K}_4\tilde{\boldsymbol{y}}$ and $\tilde{\mathbf{X}} = \begin{bmatrix} \tilde{\boldsymbol{\eta}}_0 \\ \tilde{\Theta} \end{bmatrix}$, the

observer error dynamics can be re-written in compact form as

$$\dot{\tilde{\mathbf{X}}} = \mathbf{A}\tilde{\mathbf{X}} + \mathbf{B}\mathbf{J}(\boldsymbol{y})\tilde{\boldsymbol{\nu}} \tag{4.29}$$

$$\tilde{\mathbf{Z}} = \mathbf{C}\tilde{\mathbf{X}} \tag{4.30}$$

$$\mathbf{M}\dot{\tilde{\boldsymbol{\nu}}} = -\bar{\mathbf{B}}\tilde{\boldsymbol{\nu}} - \mathbf{J}^{\mathrm{T}}(\boldsymbol{y})\tilde{\mathbf{Z}} + \boldsymbol{\omega}, \tag{4.31}$$

where $\mathbf{A} = \begin{bmatrix} \mathbf{A} - \mathbf{K}\mathbf{C}_0 & \mathbf{0} \\ \Phi^{\mathrm{T}}(\hat{\boldsymbol{\nu}})\mathbf{K}_3\mathbf{C}_0 & \mathbf{0} \end{bmatrix}$, $\mathbf{B} = \begin{bmatrix} \mathbf{B}_0 \\ \mathbf{0} \end{bmatrix}$ and $\mathbf{C} = \begin{bmatrix} \mathbf{K}_4\mathbf{C}_0 & \Phi(\hat{\boldsymbol{\nu}}) \end{bmatrix}$.
The block diagram of the observer error dynamics is shown in Fig. 4.3, where two new error terms $\boldsymbol{\varepsilon}_z = -\mathbf{J}^{\mathrm{T}}(\boldsymbol{y})\tilde{\mathbf{Z}} + \boldsymbol{\omega}$ and $\boldsymbol{\varepsilon}_v = \mathbf{J}(\boldsymbol{y})\tilde{\boldsymbol{\nu}}$ are defined.

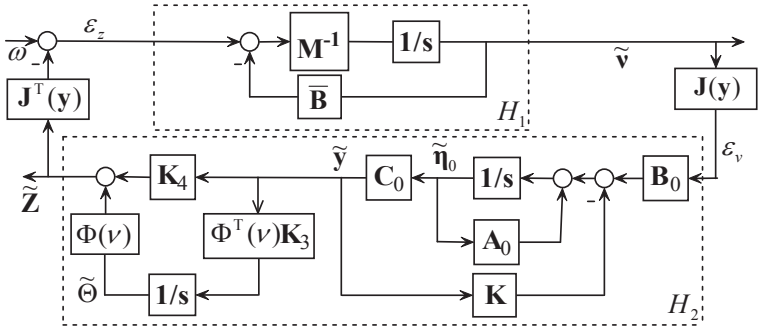

Figure 4.3: Block diagram of the observer error dynamics.

4.1.4 Stability Analysis

Lemma 4.1 *Kalman-Yakubovich-Popov (KYP) lemma as shown in [105]. Let* $G(s) = \mathbb{C}(s\mathbf{I} - \mathbb{A})^{-1}\mathbb{B}$ *be a* $n \times n$ *transfer function matrix, where* $\mathbb{A}$ *is Hurwitz,* $(\mathbb{A}, \mathbb{B})$ *is controllable, and* $(\mathbb{A}, \mathbb{C})$ *is observable. Then* $G(s)$ *is strictly positive real (SPR) if and only if there exist positive-definite matrices* $\mathbb{P} = \mathbb{P}^{\mathrm{T}}$ *and* $\mathbb{Q} = \mathbb{Q}^{\mathrm{T}}$ *such*

that

$$\mathbb{P}\mathbb{A} + \mathbb{A}^{\mathrm{T}}\mathbb{P} = -\mathbb{Q} \tag{4.32}$$

$$\mathbb{B}^{\mathrm{T}}\mathbb{P} = \mathbb{C}. \tag{4.33}$$

Proposition 4.1 *If the observer gain matrices have the following structure*

$$\mathbf{K}_1 = \begin{bmatrix} k_{11} & 0 & 0 \\ 0 & k_{12} & 0 \\ 0 & 0 & k_{13} \\ k_{14} & 0 & 0 \\ 0 & k_{15} & 0 \\ 0 & 0 & k_{16} \end{bmatrix}, \mathbf{K}_j = \begin{bmatrix} k_{j1} & 0 & 0 \\ 0 & k_{j2} & 0 \\ 0 & 0 & k_{j3} \end{bmatrix}$$

where $j = 2, 3, 4$, then the positive elements of the observer gain matrices can be chosen such that the system $(\mathbf{A}, \mathbf{B}, \mathbf{C})$ given by (4.29) and (4.30) satisfies the KYP lemma.

Proof: As shown in Fig. 4.3, the system $(\mathbf{A}, \mathbf{B}, \mathbf{C})$, which corresponds to the mapping $\boldsymbol{\varepsilon}_v \mapsto \tilde{\mathbf{Z}}$, can be described by transfer functions as

$$\tilde{\mathbf{Z}} = H(s)\boldsymbol{\varepsilon}_v = H_A(s)H_0(s)\boldsymbol{\varepsilon}_v \tag{4.34}$$

where

$$H_A(s) = \mathbf{K}_4 + \frac{1}{s}\Phi(\hat{\boldsymbol{\nu}})\Phi^{\mathrm{T}}(\hat{\boldsymbol{\nu}})\mathbf{K}_3$$

and

$$H_0(s) = \mathbf{C}_0(s\mathbf{I} - \mathbf{A}_0 + \mathbf{K}\mathbf{C}_0)^{-1}\mathbf{B}_0.$$

Since the elements of the regressive matrix $\Phi(\hat{\boldsymbol{\nu}})$ are fuzzy basis functions as defined in [74],

$$\Phi(\hat{\boldsymbol{\nu}})\Phi^{\mathrm{T}}(\hat{\boldsymbol{\nu}}) = \mathrm{diag}\{\phi_1, \phi_2, \phi_3\}$$

where $0 < \phi_i \leq 1$ $(i = 1, \ldots, 3)$. As the observer gain matrices are diagonal, the transfer function $H_A(s)$ and $H_0(s)$ are decoupled as

$$H_A(s) = \mathrm{diag}\{\mathrm{h}_\mathrm{A}^1(\mathrm{s}), \mathrm{h}_\mathrm{A}^2(\mathrm{s}), \mathrm{h}_\mathrm{A}^3(\mathrm{s})\}$$

and

$$H_0(s) = \mathrm{diag}\{\mathrm{h}_0^1(\mathrm{s}), \mathrm{h}_0^2(\mathrm{s}), \mathrm{h}_0^3(\mathrm{s})\}.$$

The elements of $H_A(s)$ and $H_0(s)$ are

$$h_A^i(s) = \frac{k_{4i}(s + \frac{\phi_i k_{3i}}{k_{4i}})}{s} \tag{4.35}$$

and

$$h_0^i(s) = \frac{s^2 + 2\lambda_i\omega_{0i}s + \omega_{0i}^2}{s^3 + as^2 + bs + \omega_{0i}^2 k_{2i}} \tag{4.36}$$

where $a = k_{1(i+3)} + k_{2i} + 2\lambda_i\omega_{0i}$, $b = \omega_{0i}^2 + 2\lambda_i\omega_{0i}k_{2i} - k_{1i}\omega_{0i}^2$ and $i = 1, \ldots, 3$. In order to obtain the desired notch effect and filter out the first-order WF motion, the desired shape of $h_0^i(s)$ is specified as

$$h_0^i(s) = \frac{s^2 + 2\lambda_i\omega_{0i}s + \omega_{0i}^2}{(s^2 + 2\lambda_{ni}\omega_{0i}s + \omega_{0i}^2)(s + \omega_{ci})} \tag{4.37}$$

where $\lambda_{ni} > \lambda_i$ determines the notch and $\omega_{ci} > \omega_{0i}$ is the filter cut-off frequency. Equating (4.36) and (4.37) yields the following formulas for the elements of the ob-

server gains $\mathbf{K}_1$ and $\mathbf{K}_2$.

$$K_{1i}(\omega_{0i}) = -2(\lambda_{ni} - \lambda_i)\frac{\omega_{ci}}{\omega_{0i}} \tag{4.38}$$

$$K_{1(i+3)}(\omega_{0i}) = 2\omega_{0i}(\lambda_{ni} - \lambda_i) \tag{4.39}$$

$$K_{2i} = \omega_{ci} \tag{4.40}$$

where $i = 1, \ldots, 3$. It is noted that the observer gains can be gain-scheduled with respect to dominating wave frequencies ω_{0i} if desired. In Fig. 4.4, the bode diagram of total transfer function $h^i(s) = h^i_A(s)h^i_0(s)$ is illustrated when all filter gains are properly selected. In order to meet the SPR requirement, the three decoupled transfer functions $h^i(s)$ in $H(s)$ should have phase greater than $-90°$. Hence, the system $(\mathbf{A}, \mathbf{B}, \mathbf{C})$ can satisfy the SPR requirement and thus the KYP lemma if the following tuning rules for k_{3i} and k_{4i} are applied.

$$\frac{\phi_i k_{3i}}{k_{4i}} < \omega_{0i} < \omega_{ci} \quad (i = 1, \ldots, 3) \tag{4.41}$$

∎

To investigate the stability property of observer error dynamics (4.29)-(4.31), a useful lemma from [109] as below is referred to.

Lemma 4.2 *For bounded initial conditions, if there exists a C^1 continuous and positive-definite Lyapunov function $V(x)$ satisfying $\kappa_1(\|x\|) \leq V(x) \leq \kappa_2(\|x\|)$, such that $\dot{V}(x) \leq -\rho V(x) + c$, where $\kappa_1, \kappa_2 : R^n \longrightarrow R$ are class $\mathcal{K}$ functions and c is positive, then the solution $x(t)$ is uniformly ultimately bounded.*

Theorem 4.1 *Consider the observer error dynamics (4.29)-(4.31). For each compact set Ω_0 where $(\tilde{\boldsymbol{\nu}}(0), \tilde{\mathbf{X}}(0)) \in \Omega_0$, the estimation errors of the observer error*

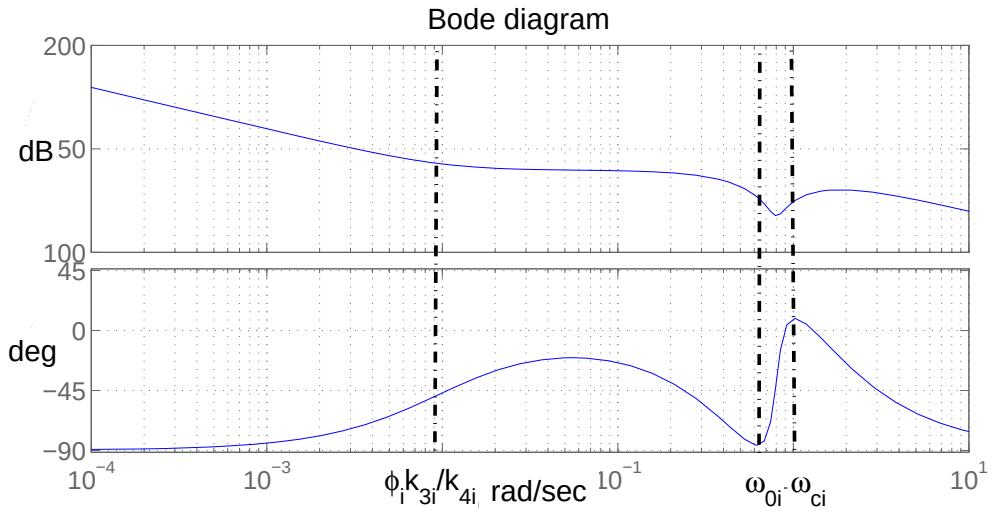

Figure 4.4: Bode diagram of the transfer function $h^i(s)$ when $\frac{\phi_i k_{3i}}{k_{4i}} < \omega_{0i} < \omega_{ci}$.

dynamics are semiglobally uniformly ultimately bounded. The estimation error signals, $\tilde{\boldsymbol{\nu}}$ and $\tilde{\mathbf{X}}$ will remain within the compact sets $\Omega_{\tilde{\nu}}$ and $\Omega_{\tilde{X}}$ respectively defined by

$$\Omega_{\tilde{\nu}} = \{\tilde{\boldsymbol{\nu}} \in R^3 | \ \|\tilde{\boldsymbol{\nu}}\| \leq \sqrt{\frac{D}{\lambda_{min}(\mathbf{M})}}\}, \tag{4.42}$$

$$\Omega_{\tilde{X}} = \{\tilde{\mathbf{X}} \in R^{(3M+9)\times 1} | \ \|\tilde{\mathbf{X}}\| \leq \sqrt{\frac{D}{\lambda_{min}(\mathbf{P})}}\}, \tag{4.43}$$

and eventually converge to the compact sets $\Omega_{\tilde{\nu}s}$ and $\Omega_{\tilde{X}s}$ respectively defined by

$$\Omega_{\tilde{\nu}s} = \{\tilde{\boldsymbol{\nu}} \in R^3 | \ \|\tilde{\boldsymbol{\nu}}\| \leq \sqrt{\frac{c}{\rho\lambda_{min}(\mathbf{M})}}\}, \tag{4.44}$$

$$\Omega_{\tilde{X}s} = \{\tilde{\mathbf{X}} \in R^{(3M+9)\times 1} | \ \|\tilde{\mathbf{X}}\| \leq \sqrt{\frac{c}{\rho\lambda_{min}(\mathbf{P})}}\}, \tag{4.45}$$

where $D = V(0) + c/\rho$ with ρ and c as defined in (4.49) and (4.50) respectively.

Proof: Consider the following Lyapunov function candidate.

$$V(t) = \tilde{\boldsymbol{\nu}}^{\mathrm{T}}\mathbf{M}\tilde{\boldsymbol{\nu}} + \tilde{\mathbf{X}}^{\mathrm{T}}\mathbf{P}\tilde{\mathbf{X}} \tag{4.46}$$

Differentiation of V along the trajectory of the observer error dynamics (4.29)-(4.31) yields

$$\begin{aligned}\dot{V} &= 2\tilde{\boldsymbol{\nu}}^{\mathrm{T}}\mathbf{M}\dot{\tilde{\boldsymbol{\nu}}} + \dot{\tilde{\mathbf{X}}}^{\mathrm{T}}\mathbf{P}\tilde{\mathbf{X}} + \tilde{\mathbf{X}}^{\mathrm{T}}\mathbf{P}\dot{\tilde{\mathbf{X}}} \\ &= 2\tilde{\boldsymbol{\nu}}^{\mathrm{T}}(-\bar{\mathbf{B}}\tilde{\boldsymbol{\nu}} - \mathbf{J}^{\mathrm{T}}\tilde{\mathbf{Z}} + \boldsymbol{\omega}) + \tilde{\mathbf{X}}^{\mathrm{T}}(\mathbf{A}^{\mathrm{T}}\mathbf{P} + \mathbf{P}\mathbf{A})\tilde{\mathbf{X}} \\ &\quad + 2\tilde{\mathbf{X}}^{\mathrm{T}}\mathbf{P}\mathbf{B}\mathbf{J}\tilde{\boldsymbol{\nu}}.\end{aligned}$$

According to Proposition 4.1, after properly choosing the observer gain matrices the system $(\mathbf{A}, \mathbf{B}, \mathbf{C})$ satisfies the KYP lemma, i.e., there exist positive-definite matrices $\mathbf{P} = \mathbf{P}^{\mathrm{T}}$ and $\mathbf{Q} = \mathbf{Q}^{\mathrm{T}}$ such that

$$\mathbf{P}\mathbf{A} + \mathbf{A}^{\mathrm{T}}\mathbf{P} = -\mathbf{Q} \tag{4.47}$$

$$\mathbf{B}^{\mathrm{T}}\mathbf{P} = \mathbf{C}. \tag{4.48}$$

Therefore,

$$\begin{aligned}\dot{V} &= -\tilde{\boldsymbol{\nu}}^{\mathrm{T}}(\bar{\mathbf{B}} + \bar{\mathbf{B}}^{\mathrm{T}})\tilde{\boldsymbol{\nu}} - \tilde{\mathbf{X}}^{\mathrm{T}}\mathbf{Q}\tilde{\mathbf{X}} + 2\tilde{\boldsymbol{\nu}}^{\mathrm{T}}\boldsymbol{\omega} \\ &\leq -\lambda_b\tilde{\boldsymbol{\nu}}^{\mathrm{T}}\tilde{\boldsymbol{\nu}} - \tilde{\mathbf{X}}^{\mathrm{T}}\mathbf{Q}\tilde{\mathbf{X}} + 2\tilde{\boldsymbol{\nu}}^{\mathrm{T}}\boldsymbol{\omega}\end{aligned}$$

where λ_b is the minimum eigenvalue of matrix $\bar{\mathbf{B}} + \bar{\mathbf{B}}^{\mathrm{T}}$. Choose λ_1, λ_2 and λ_3 such that $\lambda_1 + 1/\lambda_2^2 + 1/\lambda_3^2 = \lambda_b$, then

$$\begin{aligned}\dot{V} &\leq -\lambda_1\tilde{\boldsymbol{\nu}}^{\mathrm{T}}\tilde{\boldsymbol{\nu}} - \tilde{\mathbf{X}}^{\mathrm{T}}\mathbf{Q}\tilde{\mathbf{X}} - \frac{1}{\lambda_2^2}\tilde{\boldsymbol{\nu}}^{\mathrm{T}}\tilde{\boldsymbol{\nu}} - \frac{1}{\lambda_3^2}\tilde{\boldsymbol{\nu}}^{\mathrm{T}}\tilde{\boldsymbol{\nu}} + 2\tilde{\boldsymbol{\nu}}^{\mathrm{T}}\boldsymbol{\omega} \\ &\leq -\lambda_1\tilde{\boldsymbol{\nu}}^{\mathrm{T}}\tilde{\boldsymbol{\nu}} - \tilde{\mathbf{X}}^{\mathrm{T}}\mathbf{Q}\tilde{\mathbf{X}} - (\frac{1}{\lambda_2}\tilde{\boldsymbol{\nu}} - \lambda_2\boldsymbol{\omega}_e)^{\mathrm{T}}(\frac{1}{\lambda_2}\tilde{\boldsymbol{\nu}} - \lambda_2\boldsymbol{\omega}_e) \\ &\quad - (\frac{1}{\lambda_3}\tilde{\boldsymbol{\nu}} - \lambda_3\boldsymbol{\omega}_f)^{\mathrm{T}}(\frac{1}{\lambda_3}\tilde{\boldsymbol{\nu}} - \lambda_3\boldsymbol{\omega}_f) + \lambda_2^2\boldsymbol{\omega}_e^{\mathrm{T}}\boldsymbol{\omega}_e + \lambda_3^2\boldsymbol{\omega}_f^{\mathrm{T}}\boldsymbol{\omega}_f \\ &\leq -\lambda_1\tilde{\boldsymbol{\nu}}^{\mathrm{T}}\tilde{\boldsymbol{\nu}} - \tilde{\mathbf{X}}^{\mathrm{T}}\mathbf{Q}\tilde{\mathbf{X}} + \lambda_2^2\boldsymbol{\omega}_e^{\mathrm{T}}\boldsymbol{\omega}_e + \lambda_3^2\boldsymbol{\omega}_f^{\mathrm{T}}\boldsymbol{\omega}_f \\ &\leq -\rho V(t) + c.\end{aligned}$$

ρ and c are defined as

$$\rho = \min[\frac{\lambda_1}{\lambda_{max}(\mathbf{M})}, \frac{\lambda_{min}(\mathbf{Q})}{\lambda_{max}(\mathbf{P})}] \tag{4.49}$$

$$c = \lambda_2^2 \boldsymbol{\omega}_e^{\mathrm{T}} \boldsymbol{\omega}_e + \lambda_3^2 \|\Theta^*\|^2, \tag{4.50}$$

where $\lambda_{min}(\mathbf{A})$ and $\lambda_{max}(\mathbf{A})$ denote the minimum and maximum eigenvalues of matrix $\mathbf{A}$. According to lemma 4.2, it could be concluded that the estimation errors in the observer error dynamics (4.29)-(4.31) are semiglobally uniformly ultimately bounded. Multiplying $\dot{V}(t) \leq -\rho V(t) + c$ by $e^{\rho t}$ yields

$$\frac{d}{dt}(V(t)e^{\rho t}) \leq ce^{\rho t}.$$

Integrating the above inequality yields

$$V(t) \leq (V(0) - \frac{c}{\rho})e^{-\rho t} + \frac{c}{\rho} \leq V(0) + \frac{c}{\rho}. \tag{4.51}$$

Substituting $V(t)$ in (4.46) into the above inequality,

$$\tilde{\boldsymbol{\nu}}^{\mathrm{T}} \mathbf{M} \tilde{\boldsymbol{\nu}} \leq V(0) + \frac{c}{\rho}. \tag{4.52}$$

Hence, $\tilde{\boldsymbol{\nu}}$ is bounded by the compact set $\Omega_{\tilde{\nu}}$. From (4.51), we have

$$\|\tilde{\boldsymbol{\nu}}\| \leq \sqrt{\frac{(V(0) - \frac{c}{\rho})e^{-\rho t} + \frac{c}{\rho}}{\lambda_{min}(\mathbf{M})}}, \tag{4.53}$$

thus

$$\lim_{t \to \infty} \|\tilde{\boldsymbol{\nu}}\| \leq \sqrt{\frac{c}{\rho \lambda_{min}(\mathbf{M})}}. \tag{4.54}$$

Bound and convergence of $\tilde{\mathbf{X}}$ can be similarly shown and this concludes the proof.

∎

Remark 4.1 *In this chapter the IT2 FLSs are used as estimates of the time-varying hydrodynamic disturbances. If other universal approximators, which can be expressed in the linear in the parameters form like (2.24), are used, the stability analysis will be same. Potential approximators could be type-1 FLSs, neural networks and polynomials etc.*

4.1.5 Passivity Interpretation

As depicted in Fig. 4.3, the observer error dynamics (4.29)-(4.31) can be interpreted as the negative feedback interconnection of two subsystems with respective inputs u_1 and u_2 and outputs y_1 and y_2, with $u_1 = -\mathbf{J}^{\mathrm{T}}(\boldsymbol{y})y_2 + \boldsymbol{\omega}$, $u_2 = \mathbf{J}(\boldsymbol{y})y_1$ and the two subsystems as follows.

Subsystem H_1

$$\begin{cases} \mathbf{M}\dot{\tilde{\boldsymbol{\nu}}} + \bar{\mathbf{B}}\tilde{\boldsymbol{\nu}} = u_1 \\ y_1 = \tilde{\boldsymbol{\nu}} \end{cases} \tag{4.55}$$

Subsystem H_2

$$\begin{cases} \dot{\tilde{\mathbf{X}}} = \mathbf{A}\tilde{\mathbf{X}} + \mathbf{B}u_2 \\ y_2 = \tilde{\mathbf{Z}} \end{cases} \tag{4.56}$$

It is noted that the coordinate transformation is performed by a nonsingular and bounded matrix $\mathbf{J}(\boldsymbol{y})$.

Theorem 4.2 *The observer error dynamics comprising subsystems H_1 and H_2 is passive.*

Proof: For subsystem H_1, its supply rate is

$$\begin{aligned}
&\int_0^t u_1^{\mathrm{T}} y_1 dr \\
=&\int_0^t (\mathbf{M}\dot{\tilde{\boldsymbol{\nu}}} + \bar{\mathbf{B}}\tilde{\boldsymbol{\nu}})^{\mathrm{T}}\tilde{\boldsymbol{\nu}} dr \\
=&\int_0^t \tilde{\boldsymbol{\nu}}^{\mathrm{T}}\mathbf{M}\dot{\tilde{\boldsymbol{\nu}}} dr + \int_0^t \tilde{\boldsymbol{\nu}}^{\mathrm{T}}\bar{\mathbf{B}}\tilde{\boldsymbol{\nu}} dr \\
=&\frac{1}{2}\tilde{\boldsymbol{\nu}}^{\mathrm{T}}(t)\mathbf{M}\tilde{\boldsymbol{\nu}}(t) - \frac{1}{2}\tilde{\boldsymbol{\nu}}^{\mathrm{T}}(0)\mathbf{M}\tilde{\boldsymbol{\nu}}(0) + \int_0^t \tilde{\boldsymbol{\nu}}^{\mathrm{T}}\bar{\mathbf{B}}\tilde{\boldsymbol{\nu}} dr
\end{aligned}$$

Thus, the subsystem H_1 is output strictly passive with supply rate $\int_0^t u_1^{\mathrm{T}} y_1 dr$ and storage function $\tilde{\boldsymbol{\nu}}^{\mathrm{T}}\mathbf{M}\tilde{\boldsymbol{\nu}}/2$.

For subsystem H_2, according to Proposition 4.1 and the fact SPR systems are passive as explained in [105], the subsystem H_2 is passive. Since the negative feedback interconnection of two passive systems is passive, the observer error dynamics (4.29)-(4.31), which can be interpreted as negative feedback interconnection of subsystem H_1 and subsystem H_2, is passive. ∎

4.2 Simulation Studies

MSS as reviewed in [99] is employed as the platform for the simulation studies. This simulator provides necessary resources for rapid implementation of mathematical models of marine systems with focus on the control system design. Although the adaptive fuzzy observer (4.18)-(4.22) is designed based on the control plant model (4.8)-(4.11), it is evaluated with the process plant model (2.1), (2.2) and (4.1) in the simulations. The ITTC wave spectrum with significant wave height $H_s = 8$ m and dominating wave frequency $\omega_0 = 0.8$ rad/s is used to imitate high sea with high

waves. Sea current with speed $V_c = 0.2$ m/s and direction $\beta_c = 30^\circ$ is also included in the simulations, although ignored during the observer design. The container ship named as S-175 as shown in [37], whose main particulars are shown in Table 3.1, is employed as case study.

4.2.1 Performance of the Adaptive IT2 Fuzzy Observer

The IT2 FLSs in the adaptive fuzzy observer (4.18)-(4.22) are configured as follows. As there are three degrees of freedom considered for the motion of the vessel, three singleton IT2 sub-FLSs are employed one each for the surge, sway and yaw axis as defined in (4.15) and (4.16). For each sub-system, three fuzzy membership functions labeled as **N**, **Z**, and **P** are employed to partition each of the input domain. As there are three inputs, there are totally 27 rules and 27 adjustable consequent parameters for each sub-system. Gaussian function with uncertain standard deviation, as defined in (4.57), is chosen to be the primary membership functions of the antecedent IT2 fuzzy sets.

$$\mu_{\tilde{F}_i^j}(x_j) = \exp[-\frac{1}{2}(\frac{x_j - m_i}{\sigma})^2] \quad \sigma \in [\underline{\sigma}, \overline{\sigma}] \tag{4.57}$$

where $j = 1, \ldots, 3$ is the index of three inputs and $i = 1, \ldots, 3$ is the index of three fuzzy membership functions for jth input. For each input, the means of the Gaussian functions are $m_1 = -1$, $m_2 = 0$, and $m_3 = 1$, the standard deviations of the lower membership functions are $\underline{\sigma} = 0.6$, and the standard deviations of the upper membership functions are $\overline{\sigma} = 0.8$. The primary membership functions of the antecedent IT2 fuzzy sets are the same as those in the previous chapter, and shown

in Fig. 3.2. The consequent sets are chosen to be singletons. Their values are initially set as random numbers between 0 and 100, and then adapted online according to the adaptive law (4.20).

The observer parameters for first-order wave in (4.18) are chosen as $\lambda_i = 0.1$ and $\omega_{0i} = 0.8$ rad/s, whereas the observer parameters for notch filter effect are chosen as $\lambda_{ni} = 1$ and $\omega_{ci} = 1.04$ rad/s ($i = 1, \ldots, 3$). According to (4.38)-(4.40), the gain matrices $\mathbf{K}_1$ and $\mathbf{K}_2$ can be calculated. The gain matrices $\mathbf{K}_3$ and $\mathbf{K}_4$ are chosen as $\mathbf{K}_3 = \text{diag}\{10^6, 3\times10^6, 10^{10}\}$ and $\mathbf{K}_4 = \text{diag}\{10^7, 6\times10^6, 1.5\times10^{10}\}$. The vessel is driven by control inputs $\tau = [10^6 \sin(0.05t)\ \text{N}, 10^6 \sin(0.1\text{t})\ \text{N}, 10^8 \sin(0.07\text{t})\ \text{N}\cdot\text{m}]^{\text{T}}$. The initial states of the vessel are set as $[\boldsymbol{\eta}_0^{\text{T}}, \boldsymbol{\nu}_0^{\text{T}}] = [20\ \text{m}, 20\ \text{m}, -10^\circ, 0.8\ \text{m/s}, 0.8\ \text{m/s}, 0.3^\circ/\text{s}]$. The actual LF motion and the LF motion estimated by the adaptive fuzzy observer in surge, sway and yaw axes is shown in Fig. 4.5. It can be observed that excellent tracking of the LF motion is obtained and the first-order wave induced motion is filtered out. The actual velocities and the velocities estimated by the observer in surge, sway and yaw axes are shown in Fig. 4.6. The big errors at the start point are due to the differences between the initial states of actual and estimated velocities. As time passes by, the estimated velocities converge to their actual value. Although the velocity signals are not measured, they are efficiently reconstructed from the position measurement signals. The first-order wave induced motion in surge, sway and yaw axes and their estimates by the observer are shown in Fig. 4.7. It can be seen the oscillatory behavior of WF motion is estimated. Thus, the IT2 FLSs efficiently approximate the time-varying hydrodynamic disturbances and make the estimation errors of the observer error dynamics uniformly ultimately bounded. The combination

of approximation-based observer and IT2 FLS can effectively handles the hydrodynamic disturbances. The assumption such as the ignorance of sea current during algorithm design is appropriate.

4.2.2 Impact of Observer Gains

There are four observer gains $\mathbf{K}_i$ $(i = 1, \ldots, 4)$ in the adaptive IT2 fuzzy observer (4.18)-(4.22). According to (4.38)-(4.40), the observer gains $\mathbf{K}_1$ and $\mathbf{K}_2$ depend on the parameters of first-order wave and could be calculated based on those parameters. The choice of the observer gains $\mathbf{K}_3$ and $\mathbf{K}_4$ must satisfy the stability condition (4.41). To investigate the impact of the observer gains, simulations with the following three cases are conducted:

- Case 1: $\mathbf{K}_3 = \text{diag}\{10^5, 3 \times 10^5, 10^9\}$, $\mathbf{K}_4 = \text{diag}\{10^6, 6 \times 10^5, 1.5 \times 10^9\}$;
- Case 2: $\mathbf{K}_3 = \text{diag}\{10^6, 3 \times 10^6, 10^{10}\}$, $\mathbf{K}_4 = \text{diag}\{10^7, 6 \times 10^6, 1.5 \times 10^{10}\}$;
- Case 3: $\mathbf{K}_3 = \text{diag}\{10^7, 3 \times 10^7, 10^{11}\}$, $\mathbf{K}_4 = \text{diag}\{10^8, 6 \times 10^7, 1.5 \times 10^{11}\}$.

The estimation errors between actual LF motion and the LF motion estimated by the observers in surge, sway and yaw axes for different observer gains are shown in Fig. 4.8. It can be seen that among three cases, the observer gains in case 2 achieve best performance with smallest estimation errors of displacement in all three axes. The observer gains in case 1 achieve better performance than those in case 3. The estimation errors between actual velocities and the velocities estimated by the observers in surge, sway and yaw axes for different observer gains are depicted in Fig. 4.9. Similar conclusion to that for displacement estimation could be drawn. The

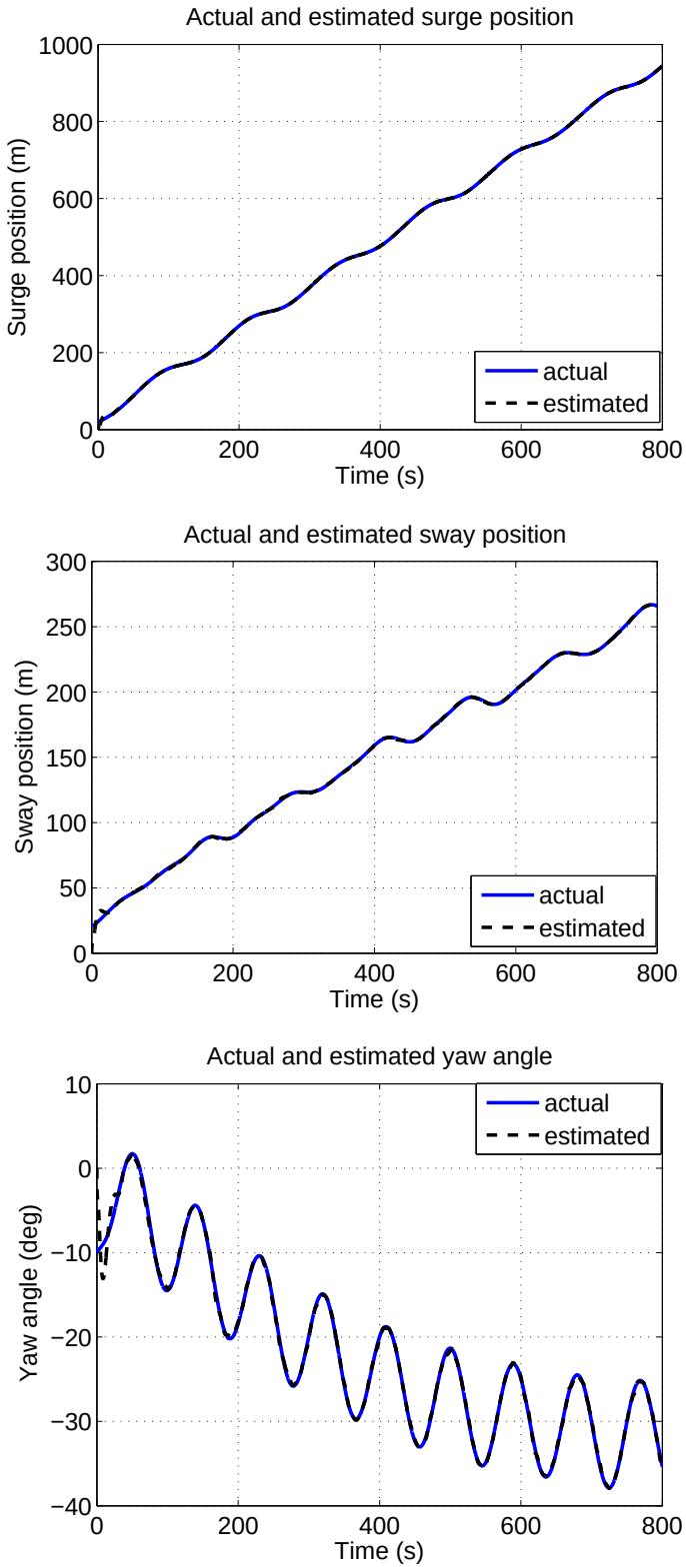

Figure 4.5: Actual and estimated LF motion of adaptive IT2 fuzzy observer.

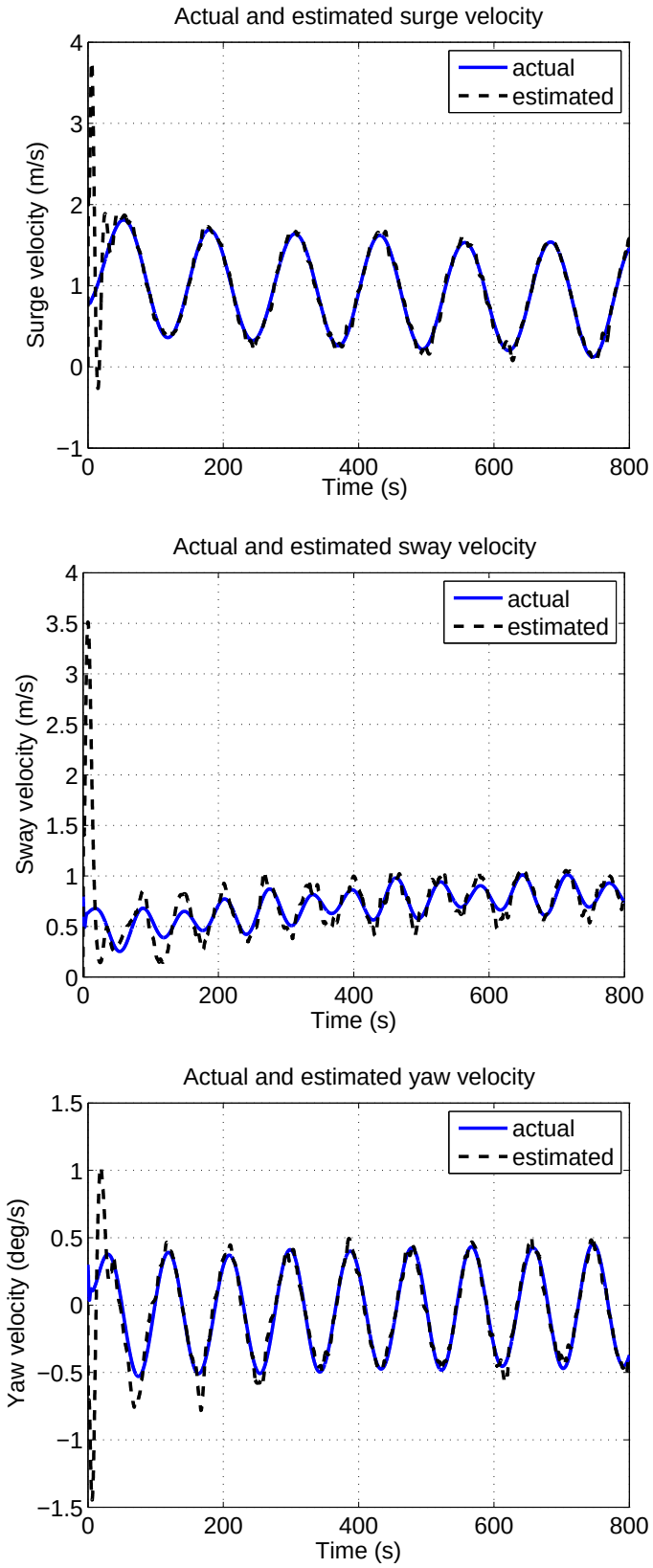

Figure 4.6: Actual and estimated velocities of adaptive IT2 fuzzy observer.

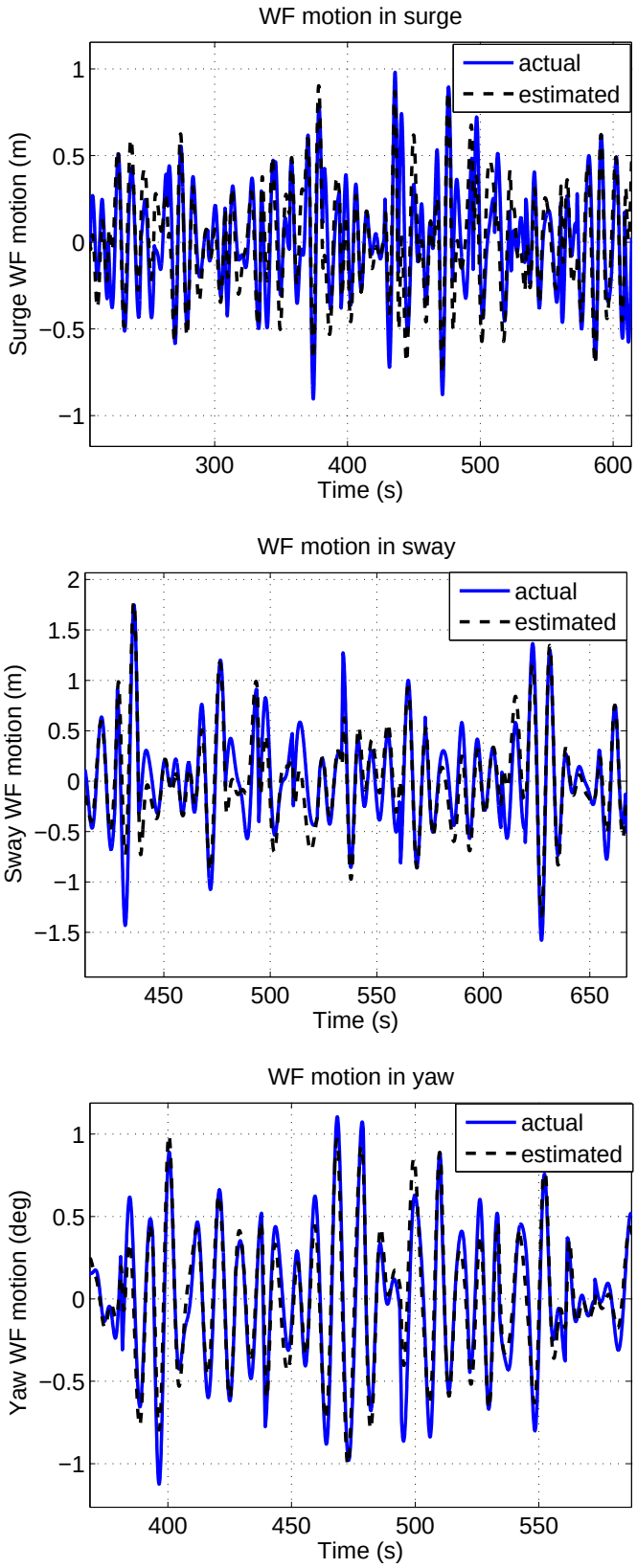

Figure 4.7: Actual and estimated WF motion of adaptive IT2 fuzzy observer.

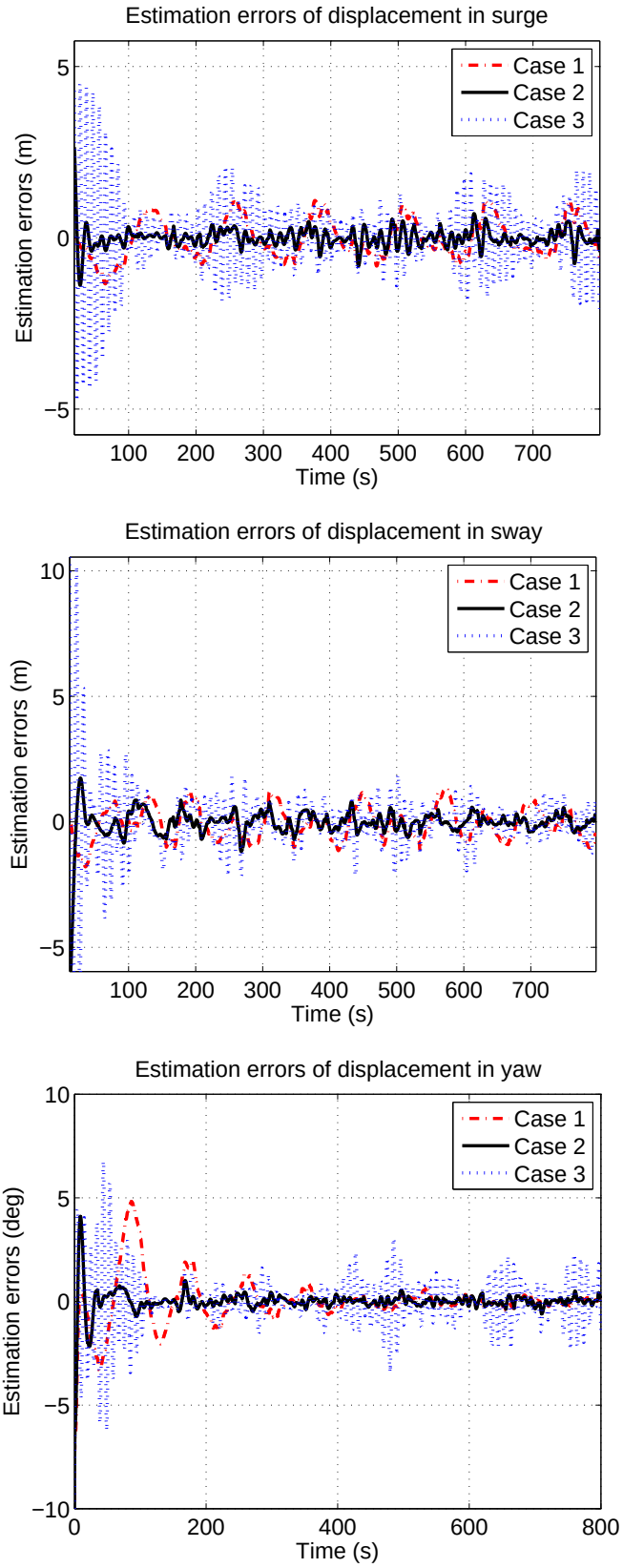

Figure 4.8: Estimation errors of LF motion for different observer gains.

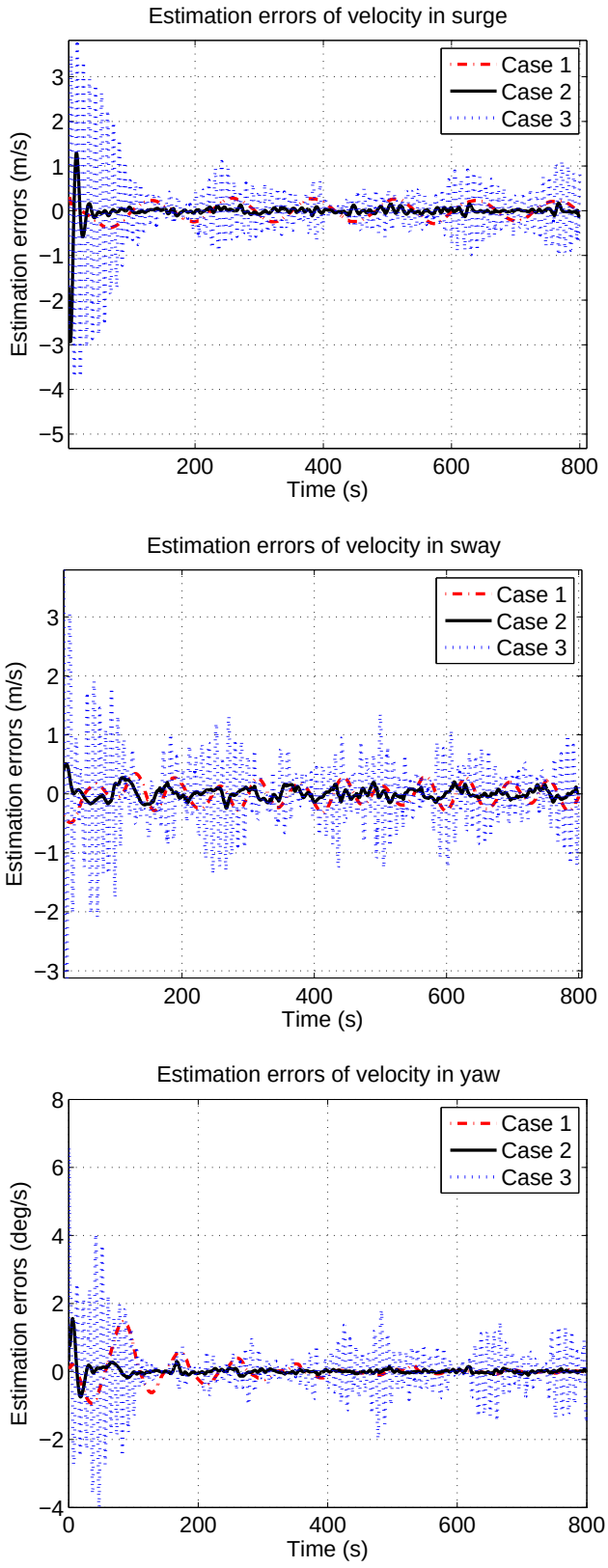

Figure 4.9: Estimation errors of velocity for different observer gains

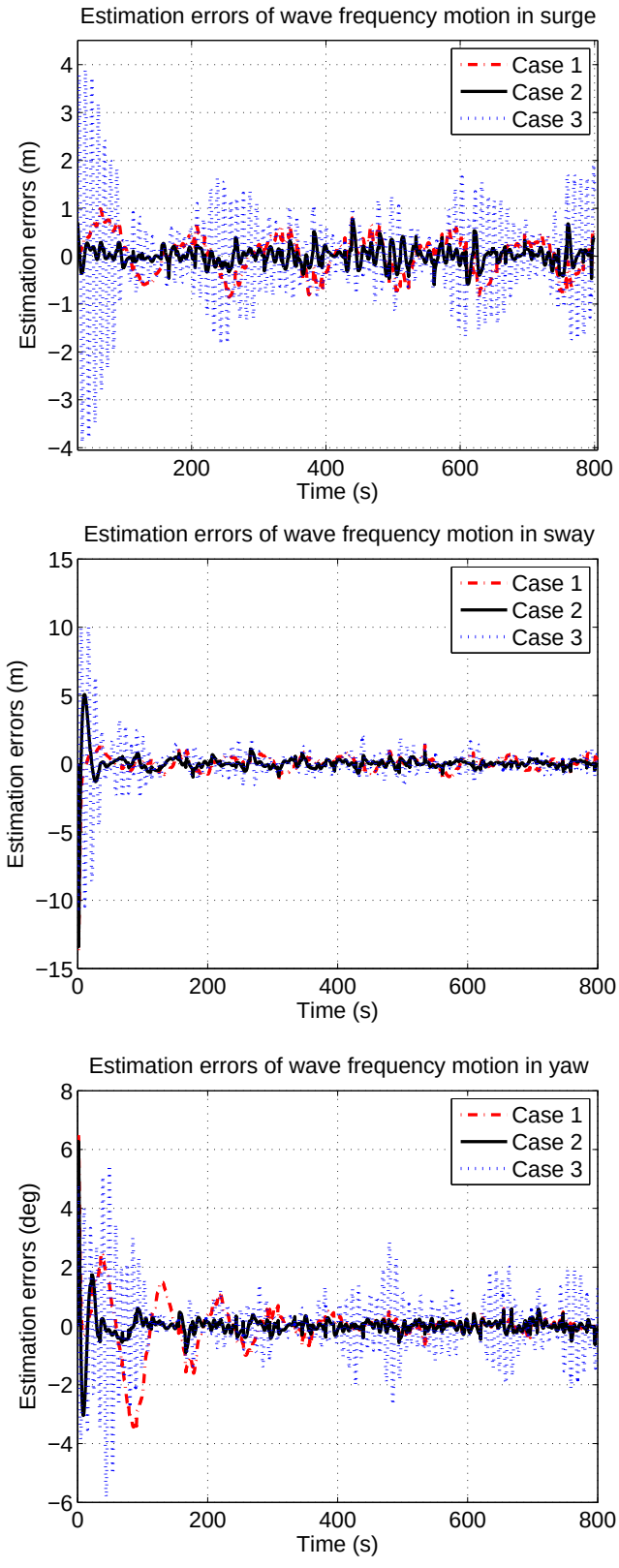

Figure 4.10: Estimation errors of WF motion for different observer gains.

observer gains in case 2 achieve best performance. The estimation errors between the first-order wave induced motion and their estimates by the observers for different observer gains are shown in Fig. 4.10. Similarly, the observer gains in case 2 obtain best performance followed by those in case 1. Thus, regarding the choice of the observer gains $\mathbf{K}_3$ and $\mathbf{K}_4$, too large or too small value of these gains would degrade the estimation performance.

4.2.3 Comparison with Passive Nonlinear Observer

In this subsection, the adaptive IT2 fuzzy observer is compared with the passive nonlinear observer proposed in [25], in which the time-varying hydrodynamic disturbances were modeled as a first order Markow process. To provide a common base for comparison, the parameter settings of the adaptive IT2 fuzzy observer are not changed as in subsection 4.2.1. The passive nonlinear observer is also tested on the MSS. The initial states and control forces of the ship and the environmental disturbances such as wave and current for the passive nonlinear observer are set same as those for the adaptive IT2 fuzzy observer. The bias time constants for the passive nonlinear observer are chosen as $\boldsymbol{T} = \text{diag}\{1000, 1000, 1000\}$. The gain matrices $\mathcal{K}$ and Λ for the passive nonlinear observer are chosen as $\mathcal{K} = \text{diag}\{10^6, 10^6, 6 \times 10^9\}$ and $\Lambda = 0.1\mathcal{K}$. The estimation errors between actual LF motion and the LF motion estimated by the observers in surge, sway and yaw axes for the two observers are shown in Fig. 4.11. It can be seen that the estimation errors of displacement for the adaptive IT2 fuzzy observer is smaller than those for the passive nonlinear observer,

especially in yaw axis. The estimation errors between actual velocities and the velocities estimated by the observers in surge, sway and yaw axes for the two observers are depicted in Fig. 4.12. It can be observed that the performance improvement by using adaptive IT2 fuzzy observer for velocity estimation is very obvious. The estimation errors between the first-order wave induced motion and their estimates by the observers for the two observers are shown in Fig. 4.13. Similarly, the adaptive IT2 fuzzy observer outperforms the passive nonlinear observer. The reason behind this is that the IT2 FLSs better model the time-varying hydrodynamic disturbances than the first order Markow process.

4.3 Conclusions

In this chapter, a passive adaptive IT2 fuzzy observer has been designed for dynamic positioning of floating vessels in the presence of time-varying hydrodynamic disturbances. The semiglobal uniform boundedness of the estimation errors of the observer error dynamics is guaranteed by means of Lyapunov synthesis. Besides, the observer error dynamics is proven to be passive. It has been shown that both the low frequency displacements and velocities of the vessel in surge, sway and yaw can be computed from noisy displacement measurements. In addition, filtering of wave frequency motion due to first-order wave induced disturbances has been done. The proposed observer has been simulated on a computer model of a container vessel. The simulation results show that all estimation errors are uniformly ultimately bounded in face of the hydrodynamic disturbances. In comparison with the passive nonlinear

observer by [25], the proposed observer has better performance.

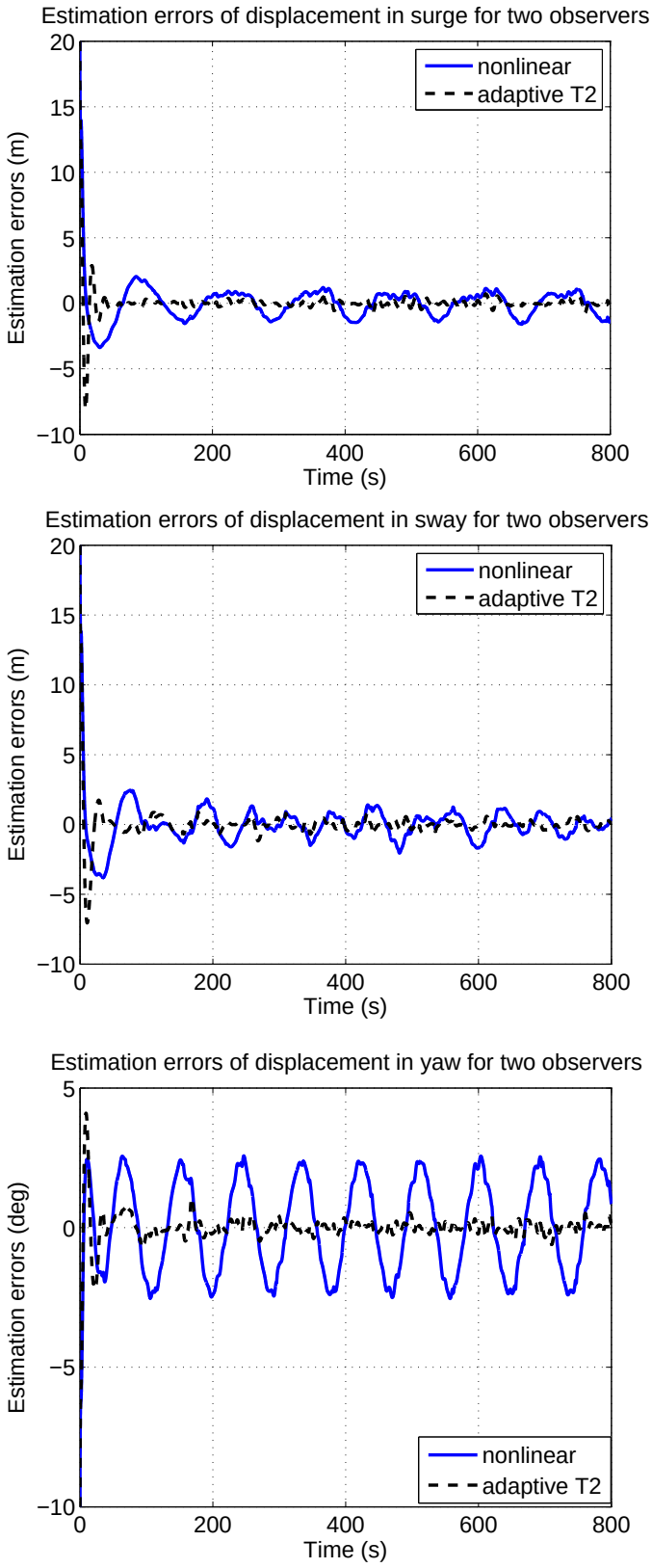

Figure 4.11: Estimation errors of LF motion for two observers.

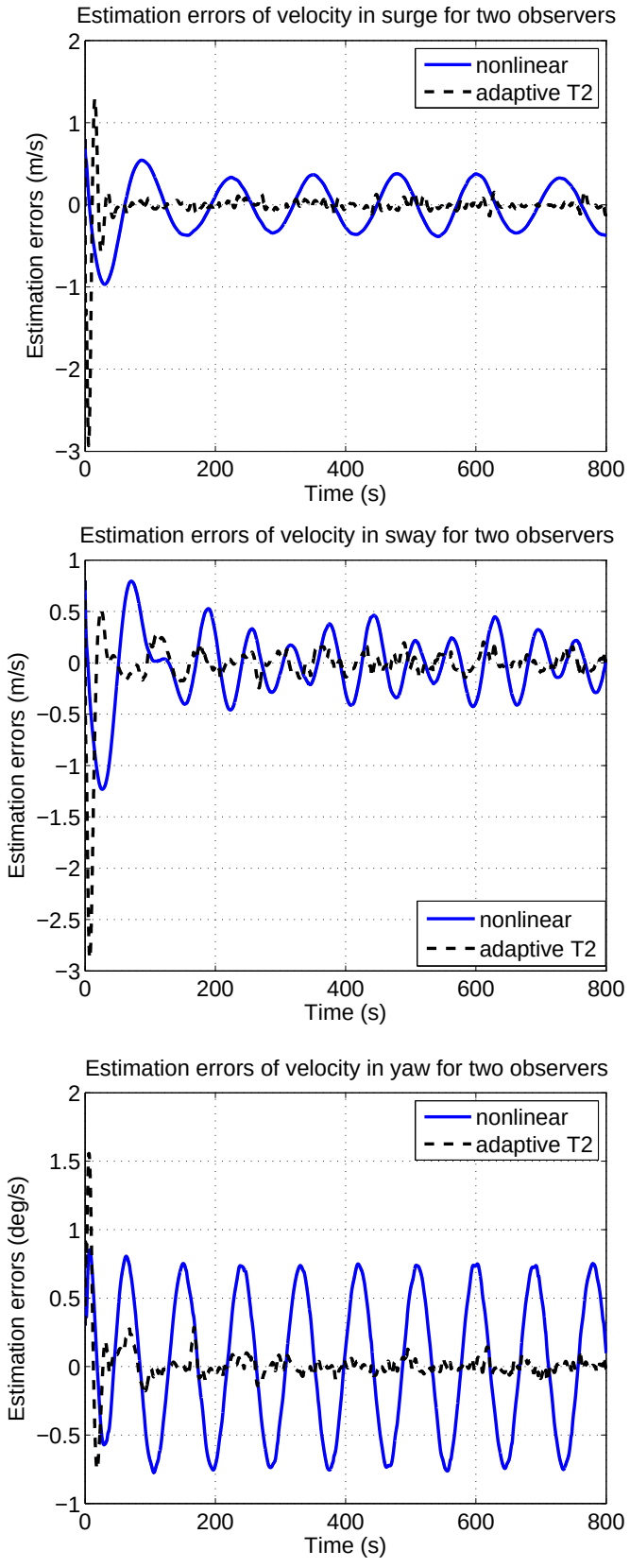

Figure 4.12: Estimation errors of velocity for two observers.

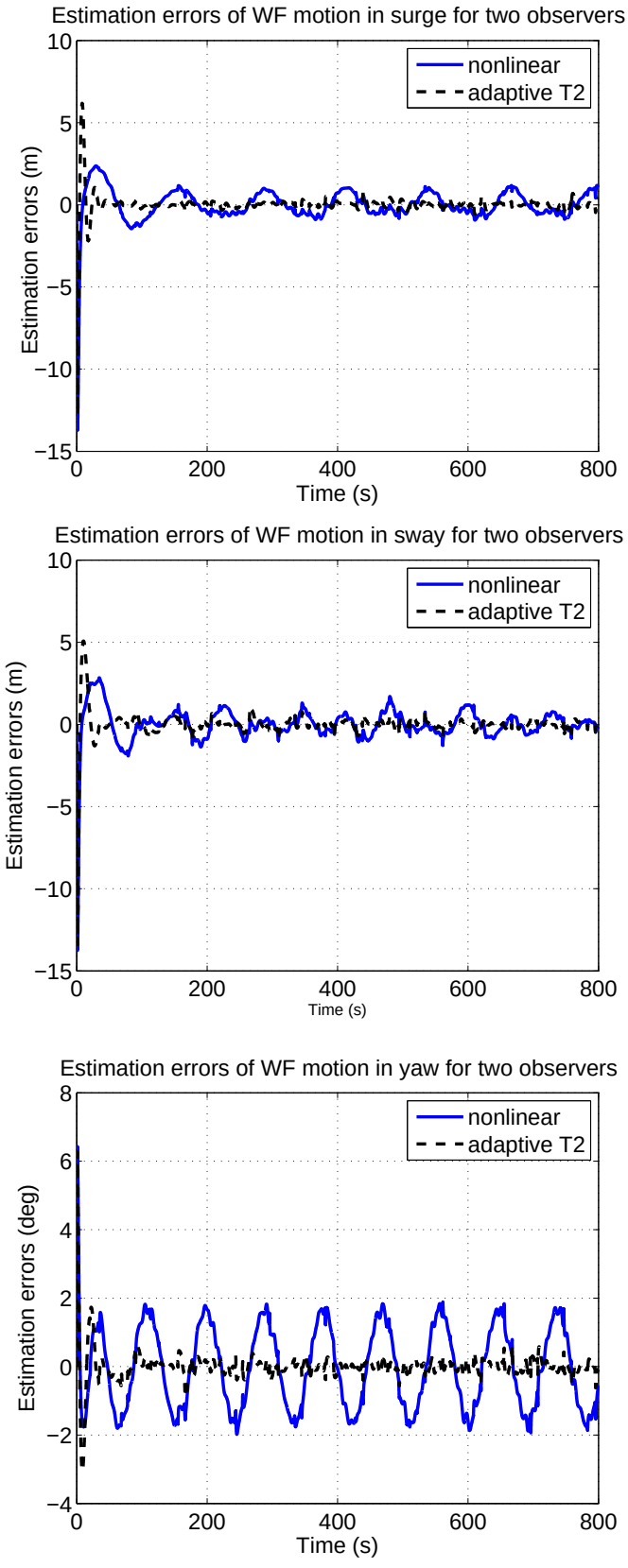

Figure 4.13: Estimation errors of WF motion for two observers.

Chapter 5

Tracking Control via Adaptive IT2 Fuzzy Control

Another major application of automatic control technique in the offshore and marine industry is trajectory tracking. When guiding a surface vessel through a busy water way or performing sea operations like dredging operations, towing operations, sea survey operations, cable/pipe laying operations, tracking control of surface vessels is necessary. The dynamics of surface vessels which have non-zero forward speed is characterized by large inertia, large damping and strong nonlinearity. Besides, the surface vessels are easily influenced by environment such as wind, waves and currents. As the time-varying hydrodynamic disturbances presented in the vessel model [37,38], trajectory tracking control of the model is very challenging. To alleviate the challenge, approximation-based adaptive control technique is combined with IT2 FLS to construct an indirect as well as a direct adaptive IT2 FLC for tracking control of marine vessels. The proposed control scheme aims at overcoming the limitation of model-based adaptive control technique and to reject the time-varying hydrodynamic disturbances. The ability of the proposed control scheme to yield a passive closed-loop system that ensures the tracking errors decay to zero asymptotically is studied. As asymptotical convergence of tracking errors occurs only when the IT2 FLS adequately

approximates the underlying function, another objective of this paper is to verify universal approximation property of IT2 FLS via an engineering application.

The rest of the chapter is organized as follows. The design and stability analysis of the two adaptive IT2 FLCs is delineated in Section 5.1. Section 5.2 describes the simulation results of the closed-loop system. Comparisons with their type-1 counterparts are also shown in this section. Finally, conclusions are drawn in Section 5.3.

5.1 Adaptive Fuzzy Logic Controller Design

The control objective of this chapter is to manipulate a surface vessel to track the desired trajectory $\boldsymbol{\eta}_d = [x_d, y_d, \psi_d]^{\mathrm{T}}$, whose second derivative is continuous, as closely as possible. In this section, the process plant model is first simplified to facilitate the controller design. Then, both indirect and direct adaptive fuzzy logic controller are designed for trajectory tracking control. However, the closed-loop systems under these two control schemes turn out to be similar. Using Lyapunov synthesis, the sufficient condition, under which the tracking errors of these two control techniques will semiglobally asymptotically converge to zero, is proposed. Rigorous analysis shows the closed-loop systems are passive.

5.1.1 Control Plant Model

Similar to the procedure in Section 3.1, the process plant model (2.1) and (2.3) for tracking control described in Section 2.1 is simplified to facilitate the tracking

controller design and analytical stability analysis. Applying Assumptions 3.1-3.3 to (2.1) and (2.3), the following control plant model is obtained.

$$\dot{\boldsymbol{\eta}} = \mathbf{J}(\boldsymbol{\eta})\boldsymbol{\nu} \tag{5.1}$$

$$\mathbf{M}\dot{\boldsymbol{\nu}} + \mathbf{D}\boldsymbol{\nu} = \boldsymbol{\tau} + \boldsymbol{\tau}_{\mathrm{H}} \tag{5.2}$$

where $\boldsymbol{\eta} = [x, y, \psi]^{\mathrm{T}}$ is the displacement vector along surge, sway, and yaw, whereas $\boldsymbol{\nu} = [u, v, r]^{\mathrm{T}}$ is the velocity vector. $\mathbf{J}(\boldsymbol{\eta}) \in R^{3\times3}$ is the rotation matrix. Note that $\mathbf{J}\mathbf{J}^{\mathrm{T}} = \mathbf{I}$ ($\mathbf{I}$ is the identity matrix). $\mathbf{M} \in R^{3\times3}$ is the system inertia matrix including added mass. $\mathbf{D} = \mathbf{C}_{RB} + \mathbf{C}_A + \bar{\mathbf{B}} \in R^{3\times3}$ is the damping matrix, and where $\mathbf{C}_{RB} \in R^{3\times3}$, $\mathbf{C}_A \in R^{3\times3}$, and $\bar{\mathbf{B}} \in R^{3\times3}$ are three dimensional versions of their corresponding matrices. $\boldsymbol{\tau} \in R^3$ and $\boldsymbol{\tau}_{\mathrm{H}} \in R^3$ are three dimensional versions of $\boldsymbol{\tau}'$ and $\boldsymbol{\tau}'_{\mathrm{H}}$ respectively. Compared to the control plant model used for DP in the previous two chapters, there are more hydrodynamic forces in the control plant model for tracking control. These hydrodynamic forces are related to velocity of vessel and generated due to non-zero forward speed of the vessel.

5.1.2 Indirect Adaptive Fuzzy Control

Indirect adaptive fuzzy control is an adaptive fuzzy controller that uses fuzzy logic systems to provide an estimation of the plant. The controller can incorporate fuzzy descriptions of some parts of the plant into itself. Here, the hydrodynamic disturbances $\boldsymbol{\tau}_{\mathrm{H}}$ in the plant model (5.2) are estimated by singleton IT2 FLSs (2.24) as

$$\boldsymbol{\tau}_{\mathrm{H}}(\boldsymbol{\nu}) = -\Phi(\boldsymbol{\nu})\Theta^*_{\mathrm{IA}} + \boldsymbol{\omega}_{\mathrm{IA}}(\boldsymbol{\nu}), \tag{5.3}$$

where $\boldsymbol{\omega}_{\mathrm{IA}}(\boldsymbol{\nu}) \in R^3$ is a vector of minimum estimation error.

$$\begin{aligned} \Theta_{\mathrm{IA}}^* &= (\boldsymbol{\theta}_1^{*\mathrm{T}}, \boldsymbol{\theta}_2^{*\mathrm{T}}, \boldsymbol{\theta}_3^{*\mathrm{T}})^{\mathrm{T}} \in R^{3M\times 1} \\ &= \arg\min_{\Theta_{\mathrm{IA}}\in R^{3M}} [\sup_{\nu\in U_\nu} |\boldsymbol{\tau}_{\mathrm{H}}(\boldsymbol{\nu}) + \Phi(\boldsymbol{\nu})\Theta_{\mathrm{IA}}|] \end{aligned} \tag{5.4}$$

is the ideal weighting vector and

$$\Phi(\boldsymbol{\nu}) = \mathrm{diag}[\boldsymbol{\phi}_1^{\mathrm{T}}(\boldsymbol{\nu}), \boldsymbol{\phi}_2^{\mathrm{T}}(\boldsymbol{\nu}), \boldsymbol{\phi}_3^{\mathrm{T}}(\boldsymbol{\nu})] \in R^{3\times 3M} \tag{5.5}$$

is the regressive matrix.

Define $\boldsymbol{e} = \boldsymbol{\eta} - \boldsymbol{\eta}_d \in R^3$ as the tracking error vector between the vessel actual displacement $\boldsymbol{\eta}$ and the desired displacement $\boldsymbol{\eta}_d$, $\boldsymbol{\nu}_d = \mathbf{J}^{\mathrm{T}}(\boldsymbol{\eta})\dot{\boldsymbol{\eta}}_d$ as the desired velocity vector, and $\boldsymbol{e}_\nu = \boldsymbol{\nu} - \boldsymbol{\nu}_d \in R^3$ as the velocity error vector. Note $\dot{\boldsymbol{e}} = \mathbf{J}(\boldsymbol{\eta})\boldsymbol{e}_\nu$ due to (2.1) and $\mathbf{J}\mathbf{J}^{\mathrm{T}} = \mathbf{I}$. Then the control and adaptive law of the indirect adaptive IT2 FLC for plant (5.1), (5.2) may be defined as

$$\boldsymbol{\tau} = \mathbf{M}\dot{\boldsymbol{\nu}}_t + \mathbf{D}\boldsymbol{\nu}_t - \lambda_1\boldsymbol{s} + \Phi(\boldsymbol{\nu})\hat{\Theta}_{\mathrm{IA}} + \boldsymbol{\tau}_a \tag{5.6}$$

$$\dot{\hat{\Theta}}_{\mathrm{IA}} = \lambda_2\Phi^{\mathrm{T}}(\boldsymbol{\nu})\boldsymbol{s} \tag{5.7}$$

where $\boldsymbol{\nu}_t = \boldsymbol{\nu}_d - \lambda_3\mathbf{J}^{\mathrm{T}}(\boldsymbol{\eta})\boldsymbol{e} = \mathbf{J}^{\mathrm{T}}(\boldsymbol{\eta})\dot{\boldsymbol{\eta}}_d - \lambda_3\mathbf{J}^{\mathrm{T}}(\boldsymbol{\eta})\boldsymbol{e} = \mathbf{J}^{\mathrm{T}}(\boldsymbol{\eta})(\dot{\boldsymbol{\eta}}_d - \lambda_3\boldsymbol{e})$, and $\boldsymbol{s} = \boldsymbol{\nu} - \boldsymbol{\nu}_t = \boldsymbol{e}_\nu + \lambda_3\mathbf{J}^{\mathrm{T}}(\boldsymbol{\eta})\boldsymbol{e} = \mathbf{J}^{\mathrm{T}}(\boldsymbol{\eta})\dot{\boldsymbol{e}} + \lambda_3\mathbf{J}^{\mathrm{T}}(\boldsymbol{\eta})\boldsymbol{e} = \mathbf{J}^{\mathrm{T}}(\boldsymbol{\eta})(\dot{\boldsymbol{e}} + \lambda_3\boldsymbol{e})$. $\tilde{\Theta}_{\mathrm{IA}} = \Theta_{\mathrm{IA}}^* - \hat{\Theta}_{\mathrm{IA}} \in R^{3M}$ is the error vector between the ideal weighting vector Θ_{IA}^* in (5.3) and the adapted weighting vector $\hat{\Theta}_{\mathrm{IA}}$. λ_i $(i = 1, 2, 3)$ are positive constants. $\boldsymbol{\tau}_a$ is designed in the following form as an adaptive robust term.

$$\boldsymbol{\tau}_a = -\frac{1}{2\lambda_4^2}\boldsymbol{s} \tag{5.8}$$

where λ_4 is a positive constant.

Application of the control and adaptive law of the indirect adaptive IT2 FLC (5.6) and (5.7) to the plant (5.1) and (5.2) yields the closed-loop system

$$\mathbf{M}\dot{\boldsymbol{s}} + \mathbf{D}\boldsymbol{s} = -(\lambda_1 + \frac{1}{2\lambda_4^2})\boldsymbol{s} - \Phi(\boldsymbol{\nu})\tilde{\Theta}_{\mathrm{IA}} + \boldsymbol{\omega}_{\mathrm{IA}}(\boldsymbol{\nu}) \tag{5.9}$$

$$\dot{\tilde{\Theta}}_{\mathrm{IA}} = \lambda_2 \Phi^{\mathrm{T}}(\boldsymbol{\nu})\boldsymbol{s} \tag{5.10}$$

$$\dot{\boldsymbol{e}} = -\lambda_3 \boldsymbol{e} + \mathbf{J}(\boldsymbol{\eta})\boldsymbol{s}. \tag{5.11}$$

The overall control scheme of this indirect adaptive IT2 FLC is shown in Fig. 5.1.

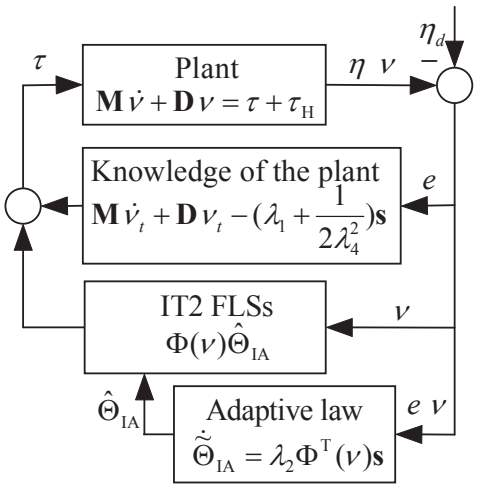

Figure 5.1: Overall scheme of indirect adaptive IT2 FLC for tracking control.

5.1.3 Direct Adaptive Fuzzy Control

Direct adaptive fuzzy control is an adaptive fuzzy controller that uses fuzzy logic systems as controllers. It can incorporate fuzzy control rules directly into itself. Thus, in direct adaptive fuzzy control, the parameters of the controller are directly adjusted to reduce the tracking error. Here, assume the singleton IT2 FLSs (2.24)

can estimate the function $\mathbf{M}\dot{\boldsymbol{\nu}}_t + \mathbf{D}\boldsymbol{\nu}_t - \boldsymbol{\tau}_{\mathrm{H}} - \lambda_1 \mathbf{s} + \boldsymbol{\tau}_a$ as follows.

$$\mathbf{M}\dot{\boldsymbol{\nu}}_t + \mathbf{D}\boldsymbol{\nu}_t - \boldsymbol{\tau}_{\mathrm{H}} - \lambda_1 \mathbf{s} + \boldsymbol{\tau}_a = \Phi(\boldsymbol{\nu})\Theta^*_{\mathrm{DA}} - \boldsymbol{\omega}_{\mathrm{DA}}(\boldsymbol{\nu}) \tag{5.12}$$

where $-\boldsymbol{\omega}_{\mathrm{DA}}(\boldsymbol{\nu}) \in R^3$ is the minimum estimation error vector. $\Theta^*_{\mathrm{DA}} \in R^{3M}$ which is similar to Θ^*_{IA} in (5.4) is the ideal weighting vector.

The control and adaptive law of the direct adaptive IT2 FLC for plant (5.1), (5.2) could be designed as follows.

$$\begin{aligned} \boldsymbol{\tau} &= \Phi(\boldsymbol{\nu})\hat{\Theta}_{\mathrm{DA}} \\ &= \mathbf{M}\dot{\boldsymbol{\nu}}_t + \mathbf{D}\boldsymbol{\nu}_t - \boldsymbol{\tau}_{\mathrm{H}} - \lambda_1 \mathbf{s} + \boldsymbol{\tau}_a + \boldsymbol{\omega}_{\mathrm{DA}}(\boldsymbol{\nu}) - \Phi(\boldsymbol{\nu})\tilde{\Theta}_{\mathrm{DA}} \qquad (5.13) \\ \dot{\hat{\Theta}}_{\mathrm{DA}} &= \lambda_2 \Phi^{\mathrm{T}}(\boldsymbol{\nu})\mathbf{s} \qquad (5.14) \end{aligned}$$

where $\tilde{\Theta}_{\mathrm{DA}} = \Theta^*_{\mathrm{DA}} - \hat{\Theta}_{\mathrm{DA}} \in R^{3M}$ is the error vector between the ideal weighting vector Θ^*_{DA} and the adapted weighting vector $\hat{\Theta}_{\mathrm{DA}}$. Thus, here three sub-FLSs (each one has M rules) are used to approximate the control actions.

Applying the control and adaptive law of the direct adaptive IT2 FLC (5.13) and (5.14) to the plant (5.1) and (5.2) results in the closed-loop system

$$\begin{aligned} \mathbf{M}\dot{\boldsymbol{s}} + \mathbf{D}\boldsymbol{s} &= -(\lambda_1 + \frac{1}{2\lambda_4^2})\boldsymbol{s} - \Phi(\boldsymbol{\nu})\tilde{\Theta}_{\mathrm{DA}} + \boldsymbol{\omega}_{\mathrm{DA}}(\boldsymbol{\nu}) \qquad (5.15) \\ \dot{\tilde{\Theta}}_{\mathrm{DA}} &= \lambda_2 \Phi^{\mathrm{T}}(\boldsymbol{\nu})\boldsymbol{s} \qquad (5.16) \\ \dot{\boldsymbol{e}} &= -\lambda_3 \boldsymbol{e} + \mathbf{J}(\boldsymbol{\eta})\boldsymbol{s}. \qquad (5.17) \end{aligned}$$

The overall control scheme of this direct adaptive IT2 FLC is shown in Fig. 5.2.

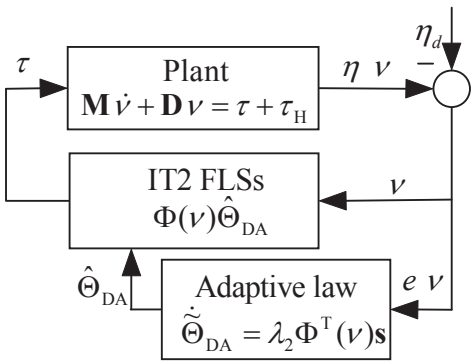

Figure 5.2: Overall scheme of direct adaptive IT2 FLC for tracking control.

5.1.4 Stability Analysis

Compare the closed-loop system for indirect adaptive control (5.9)-(5.11) with that for direct adaptive control (5.15)-(5.17), it can be observed they are identical except for the fuzzy weighting vectors $\tilde{\Theta}_{\mathrm{IA}}$ and $\tilde{\Theta}_{\mathrm{DA}}$. Thus, the stability and passivity analysis for these two control schemes are also analogous. For the sake of conciseness, the following set of equations will be used to represent (5.9)-(5.11) and (5.15)-(5.17) in the subsequent stability and passivity analysis.

$$\mathbf{M}\dot{\boldsymbol{s}}+\mathbf{D}\boldsymbol{s} = -(\lambda_1+\frac{1}{2\lambda_4^2})\boldsymbol{s}-\Phi(\boldsymbol{\nu})\tilde{\Theta}+\boldsymbol{\omega}(\boldsymbol{\nu}) \tag{5.18}$$

$$\dot{\tilde{\Theta}} = \lambda_2\Phi^{\mathrm{T}}(\boldsymbol{\nu})\boldsymbol{s} \tag{5.19}$$

$$\dot{\boldsymbol{e}} = -\lambda_3\boldsymbol{e}+\mathbf{J}(\boldsymbol{\eta})\boldsymbol{s} \tag{5.20}$$

Theorem 5.1 *Consider the plant (5.1) and (5.2) with the indirect adaptive fuzzy control (5.6) and (5.7) and direct adaptive fuzzy control (5.13) and (5.14). The tracking error* $\boldsymbol{e}$ *will semiglobally asymptotically converge to* $\mathbf{0}$*, if* $\boldsymbol{\omega}(\boldsymbol{\nu})$ *is squared integrable.*

Proof: Consider the following Lyapunov function candidate, which is positive definite.

$$V = \frac{1}{2}\boldsymbol{s}^{\mathrm{T}}\mathbf{M}\boldsymbol{s} + \lambda_1\lambda_3\boldsymbol{e}^{\mathrm{T}}\boldsymbol{e} + \frac{1}{2\lambda_2}\tilde{\Theta}^{\mathrm{T}}\tilde{\Theta} \tag{5.21}$$

Differentiation of V along the trajectory of the closed-loop system (5.18)-(5.20) yields

$$\begin{aligned}
\dot{V} &= \boldsymbol{s}^{\mathrm{T}}[-\mathbf{D}\boldsymbol{s} - (\lambda_1 + \frac{1}{2\lambda_4^2})\boldsymbol{s} - \Phi(\boldsymbol{\nu})\tilde{\Theta} + \boldsymbol{\omega}] + 2\lambda_1\lambda_3\boldsymbol{e}^{\mathrm{T}}\dot{\boldsymbol{e}} + \tilde{\Theta}^{\mathrm{T}}\Phi^{\mathrm{T}}(\boldsymbol{\nu})\boldsymbol{s} \\
&= -\boldsymbol{s}^{\mathrm{T}}\mathbf{D}\boldsymbol{s} - \lambda_1\dot{\boldsymbol{e}}^{\mathrm{T}}\dot{\boldsymbol{e}} - \lambda_1\lambda_3^2\boldsymbol{e}^{\mathrm{T}}\boldsymbol{e} - \frac{1}{2\lambda_4^2}\boldsymbol{s}^{\mathrm{T}}\boldsymbol{s} + \boldsymbol{s}^{\mathrm{T}}\boldsymbol{\omega} \\
&= -\boldsymbol{s}^{\mathrm{T}}\mathbf{D}\boldsymbol{s} - \lambda_1\dot{\boldsymbol{e}}^{\mathrm{T}}\dot{\boldsymbol{e}} - \lambda_1\lambda_3^2\boldsymbol{e}^{\mathrm{T}}\boldsymbol{e} - \frac{1}{2}[\frac{1}{\lambda_4}\boldsymbol{s} - \lambda_4\boldsymbol{\omega}]^{\mathrm{T}}[\frac{1}{\lambda_4}\boldsymbol{s} - \lambda_4\boldsymbol{\omega}] + \frac{1}{2}\lambda_4^2\boldsymbol{\omega}^{\mathrm{T}}\boldsymbol{\omega} \\
&\leq -\frac{1}{2}\boldsymbol{s}^{\mathrm{T}}(\mathbf{D} + \mathbf{D}^{\mathrm{T}})\boldsymbol{s} - \lambda_1\dot{\boldsymbol{e}}^{\mathrm{T}}\dot{\boldsymbol{e}} - \lambda_1\lambda_3^2\boldsymbol{e}^{\mathrm{T}}\boldsymbol{e} + \frac{1}{2}\lambda_4^2\boldsymbol{\omega}^{\mathrm{T}}\boldsymbol{\omega}.
\end{aligned}$$

If $\boldsymbol{\omega}(\boldsymbol{\nu}) = \mathbf{0}$, which is a special case of a squared integrable function, then $\dot{V} \leq 0$, which means the derivative of the Lyapunov function candidate is semi-negative definite. Moreover, the largest invariant set contained in the set $\dot{V} \equiv 0$ is contained in the set $(\boldsymbol{s}, \boldsymbol{e}) = (\mathbf{0}, \mathbf{0})$. According to Krasovskii-La Salle Invariant Set Theorem, we may conclude the point $(\boldsymbol{s}, \boldsymbol{e})$ semiglobally asymptotically converges to $(\mathbf{0}, \mathbf{0})$ as time tends to infinite, and $\dot{\hat{\Theta}} = \mathbf{0}$, which means $\hat{\Theta}$ is bounded.

If $\boldsymbol{\omega}(\boldsymbol{\nu}) \neq \mathbf{0}$, then

$$\dot{V} \leq -\lambda_1\dot{\boldsymbol{e}}^{\mathrm{T}}\dot{\boldsymbol{e}} - \lambda_1\lambda_3^2\boldsymbol{e}^{\mathrm{T}}\boldsymbol{e} + \frac{1}{2}\lambda_4^2\boldsymbol{\omega}^{\mathrm{T}}\boldsymbol{\omega}.$$

Integrating both sides of the above equation yields

$$\int_0^t \boldsymbol{e}^{\mathrm{T}}\boldsymbol{e}dr + \frac{1}{\lambda_3^2}\int_0^t \dot{\boldsymbol{e}}^{\mathrm{T}}\dot{\boldsymbol{e}}dr \leq \frac{1}{\lambda_1\lambda_3^2}V(0) + \frac{\lambda_4^2}{2\lambda_1\lambda_3^2}\int_0^t \boldsymbol{\omega}^{\mathrm{T}}\boldsymbol{\omega}dr.$$

This demonstrates that all the states and signals involved in the closed-loop system are bounded. Furthermore, if $\boldsymbol{\omega}$ is squared integrable, that is $\int_0^\infty \boldsymbol{\omega}^{\mathrm{T}}\boldsymbol{\omega}dr < \infty$, we

have $\boldsymbol{e} \in L_2$. As all the signals are bounded, we have $\dot{\boldsymbol{e}} \in L_\infty$. According to the Barbalat's Lemma, we have $\lim_{t\to\infty} |\boldsymbol{e}| = 0$. ∎

Remark 5.1 *Based on the above analysis, it can be observed that the accuracy of the singleton IT2 FLSs in estimating the nonlinear functions is essential to the stability of the adaptive fuzzy control. It has been proved in [85]– [88] that type-1 FLSs are universal approximators, i.e., for any given continuous nonlinear function, there exists a type-1 FLS that can uniformly approximate the function to any desired accuracy. Thus, type-1 FLSs may be used to achieve stable adaptive control. However, rigorous proofs that IT2 FLSs are universal approximators have not been developed. As IT2 FLSs have extra degree of freedoms compared to type-1 FLSs, it may be conjectured that the IT2 FLSs provide more modeling flexibility. Hence, an objective is to verify using a simulation example whether IT2 FLSs are able to model nonlinearities sufficiently accurately for indirect and direct adaptive controllers.*

Remark 5.2 *The theorem developed in this paper is for the case where the gains* λ_i $(i = 1, 2, \ldots, 4)$ *are scalar. The case where the gains are matrices could be extended to in a similar approach, and the matrix gains will not cause any stability problem.*

5.1.5 Passivity Interpretation

According to energy-related considerations, the passivity theory provides a framework for the design and analysis of control systems. The input-output description further allows for a modular method of control systems design and analysis [105]. As shown in Fig. 5.3, the closed-loop system (5.18)-(5.20) can be interpreted as the negative

feedback interconnection of three subsystems with respective inputs u_1, u_2, u_3 and outputs y_1, y_2, and y_3, with $y_1 = u_2 = u_3$ and $u_1 = -y_2 - y_3 + \boldsymbol{\omega}(\boldsymbol{\nu})$, and the three subsystems as follows.

Subsystem 1:

$$\begin{cases} \mathbf{M}\dot{\boldsymbol{s}} + \mathbf{D}\boldsymbol{s} = u_1 \\ y_1 = \boldsymbol{s} \end{cases} \tag{5.22}$$

Subsystem 2:

$$\begin{cases} \dot{\tilde{\Theta}} = \lambda_2 \Phi^{\mathrm{T}}(\boldsymbol{\nu}) u_2 \\ y_2 = \Phi(\boldsymbol{\nu})\tilde{\Theta} \end{cases} \tag{5.23}$$

Subsystem 3:

$$\begin{cases} \dot{\boldsymbol{e}} = -\lambda_3 \boldsymbol{e} + \mathbf{J}(\boldsymbol{\eta}) u_3 \\ y_3 = (\lambda_1 + \frac{1}{2\lambda_4^2}) u_3 \end{cases} \tag{5.24}$$

Theorem 5.2 *The closed-loop system comprising subsystems 1, 2 and 3 is passive.*

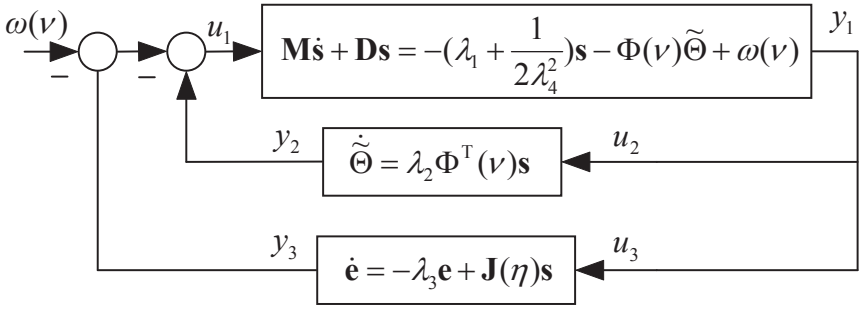

Figure 5.3: Closed-loop equivalent representation for tracking control.

Proof: For subsystem 1, its supply rate is

$$\begin{aligned}
&\int_0^t u_1^{\mathrm{T}} y_1 dr \\
=&\int_0^t (\mathbf{M}\dot{\boldsymbol{s}} + \mathbf{D}\boldsymbol{s})^{\mathrm{T}} \boldsymbol{s} dr \\
=&\int_0^t \boldsymbol{s}^{\mathrm{T}} \mathbf{M}\dot{\boldsymbol{s}} dr + \int_0^t \boldsymbol{s}^{\mathrm{T}} \mathbf{D}\boldsymbol{s} dr \\
=&\frac{1}{2}\boldsymbol{s}^{\mathrm{T}}(t)\mathbf{M}\boldsymbol{s}(t) - \frac{1}{2}\boldsymbol{s}^{\mathrm{T}}(0)\mathbf{M}\boldsymbol{s}(0) + \int_0^t \boldsymbol{s}^{\mathrm{T}} \mathbf{D}\boldsymbol{s} dr
\end{aligned}$$

Thus, the subsystem 1 is output strictly passive with supply rate $\int_0^t u_1^{\mathrm{T}} y_1 dr$ and storage function $\boldsymbol{s}^{\mathrm{T}}\mathbf{M}\boldsymbol{s}/2$.

For subsystem 2 its supply rate is

$$\begin{aligned}
\int_0^t u_2^{\mathrm{T}} y_2 dr =& \int_0^t \tilde{\Theta}^{\mathrm{T}} \Phi^{\mathrm{T}}(\boldsymbol{\nu}) u_2 dr \\
=& \int_0^t \tilde{\Theta}^{\mathrm{T}} \frac{1}{\lambda_2} \dot{\tilde{\Theta}} dr \\
=& \frac{1}{2\lambda_2}\tilde{\Theta}^{\mathrm{T}}(t)\tilde{\Theta}(t) - \frac{1}{2\lambda_2}\tilde{\Theta}^{\mathrm{T}}(0)\tilde{\Theta}(0)
\end{aligned}$$

which means the subsystem 2 is passive with supply rate $\int_0^t u_2^{\mathrm{T}} y_2 dr$ and storage function $\tilde{\Theta}^{\mathrm{T}}\tilde{\Theta}/(2\lambda_2)$.

For subsystem 3, its supply rate is

$$\begin{aligned}
\int_0^t u_3^{\mathrm{T}} y_3 dr =& \int_0^t u_3^{\mathrm{T}} (\lambda_1 + \frac{1}{2\lambda_4^2}) u_3 dr \\
=& \int_0^t \frac{2\lambda_4^2}{2\lambda_1\lambda_4^2 + 1} y_3^{\mathrm{T}} y_3 dr \\
=& \frac{2\lambda_1\lambda_4^2 + 1}{4\lambda_4^2} \int_0^t u_3^{\mathrm{T}} u_3 dr + \frac{\lambda_4^2}{2\lambda_1\lambda_4^2 + 1} \int_0^t y_3^{\mathrm{T}} y_3 dr
\end{aligned}$$

which means the subsystem 3 is very strictly passive with supply rate $\int_0^t u_3^{\mathrm{T}} y_3 dr$.

According to the fact that the negative feedback interconnection of two passive systems is passive, the closed-loop system (5.18)-(5.20), which can be interpreted as

negative feedback interconnection of subsystem 1 and subsystem 2, then together with subsystem 3, is passive. ∎

5.2 Simulation Studies

As in the previous chapters, MSS [98] is employed as the platform for the simulation studies. The container ship S-175 [37, 98], whose main particulars are shown in Table 3.1, is used as case study. Ship collisions and groundings frequently happen in restricted water way, threaten staff safety, result in financial loss, and affect the marine environment. To enhance safety, the International Maritime Organization has advocated the e-navigation concept in 2005 [110]. Under this concept, the vessels traveling in restricted water way may automatically track a pre-set trajectory to avoid collision. As a preliminary work towards e-navigation, the control objective in this chapter is to control the vessel to track a sinusoidal trajectory. In this way, the frequent turning behaviors of a vessel when it is traveling in restricted water way are mimicked. The sinusoidal trajectory is chosen as $\boldsymbol{\eta}_d = [x_d, y_d, \psi_d]^{\mathrm{T}}$, where $x_d = 8t$, $y_d = 200\cos(0.005\pi t)$, and $\psi_d = \arctan(y_d/x_d)$. The initial states are set as $[\boldsymbol{\eta}_0^{\mathrm{T}}, \boldsymbol{\nu}_0^{\mathrm{T}}] = [10, 210, 0, 0, 0, 0]$. The ITTC wave spectrum with significant wave height $H_s = 3$ m and peak frequency $\omega_0 = 0.56$ rad/s is used to imitate rough sea with large waves. Sea current with speed $V_c = 0.2$ m/s and direction $\beta_c = 30^\circ$ is also included in the simulations, although ignored during the controller design. All the IT2 FLSs in indirect adaptive fuzzy controller (5.6), (5.7) and direct adaptive fuzzy controller (5.13), (5.14) are configured as follows. As there are three degrees of freedom con-

sidered for the motion of the vessel, three singleton IT2 sub-FLSs are employed for each controller, which is defined in (5.4) and (5.5). For each sub-system, three fuzzy membership functions labeled as **N**, **Z**, and **P** are employed to partition each of the input domain. As there are three inputs, there are totally 27 rules and 27 adjustable consequent parameters for each sub-system. Gaussian function with uncertain standard deviation, as defined in (5.25), is chosen to be the primary membership functions of the antecedent IT2 fuzzy sets.

$$\mu_{\tilde{F}_i^j}(x_j) = \exp[-\frac{1}{2}(\frac{x_j - m_i}{\sigma})^2] \quad \sigma \in [\underline{\sigma}, \overline{\sigma}] \tag{5.25}$$

where $j = 1, 2, 3$ is the index of three inputs and $i = 1, 2, 3$ is the index of three fuzzy membership functions for jth input. For each input, the means of the Gaussian functions are $m_1 = -1$, $m_2 = 0$, and $m_3 = 1$, the standard deviations of the lower membership functions are $\underline{\sigma} = 0.6$, and the standard deviations of the upper membership functions are $\overline{\sigma} = 0.8$. The primary membership functions of the antecedent IT2 fuzzy sets are shown in Fig. 3.2. The consequent sets are chosen to be singletons. Their values are initially set as random numbers between 0 and 100, and then adapted online according to the adaptive law.

5.2.1 Closed-loop Performance

5.2.1.1 Indirect Adaptive Fuzzy Control

The desired and actual trajectory of the vessel under the indirect adaptive IT2 FLC, when $\lambda_1 = 4.3 \times 10^8$, $\lambda_2 = 1 \times 10^8$, $\lambda_3 = 0.02$, and $\lambda_4 = 1$ in (5.6) and (5.7), is shown in Fig. 5.4. The tracking errors of the vessel's actual trajectories to the

desired trajectories are shown in Fig. 5.6. It can be observed that the tracking errors asymptotically converge to zero despite the time-varying hydrodynamic disturbances and the sub-FLSs effectively approximate the complex disturbances $\boldsymbol{\tau}_H$.

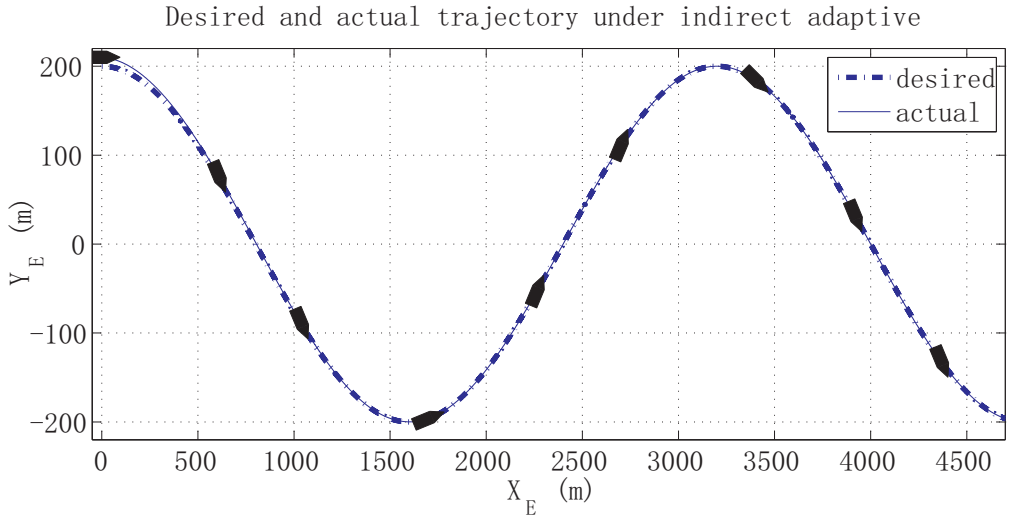

Figure 5.4: The desired and actual trajectory of the container ship under indirect adaptive IT2 FLC.

5.2.1.2 Direct Adaptive Fuzzy Control

The desired and actual trajectory of the vessel under the direct adaptive IT2 FLC, when $\lambda_2 = 1 \times 10^8$ and $\lambda_3 = 0.02$ in (5.13) and (5.14), is shown in Fig. 5.5. The tracking errors are shown in Fig. 5.7. The tracking performance is satisfactory in the presence of the time-varying disturbances, and the sub-FLSs effectively generate the control forces and moment. Small fluctuations in the tracking error of surge direction are observed, that is because the inputs to the sub-FLSs are insufficient to make the sub-FLSs accurately approximate the function in (5.12). Specifically, the function on

the left side of (5.12) is a function of displacement, velocity and acceleration signals. But the inputs to the sub-FLSs are just velocity signals.

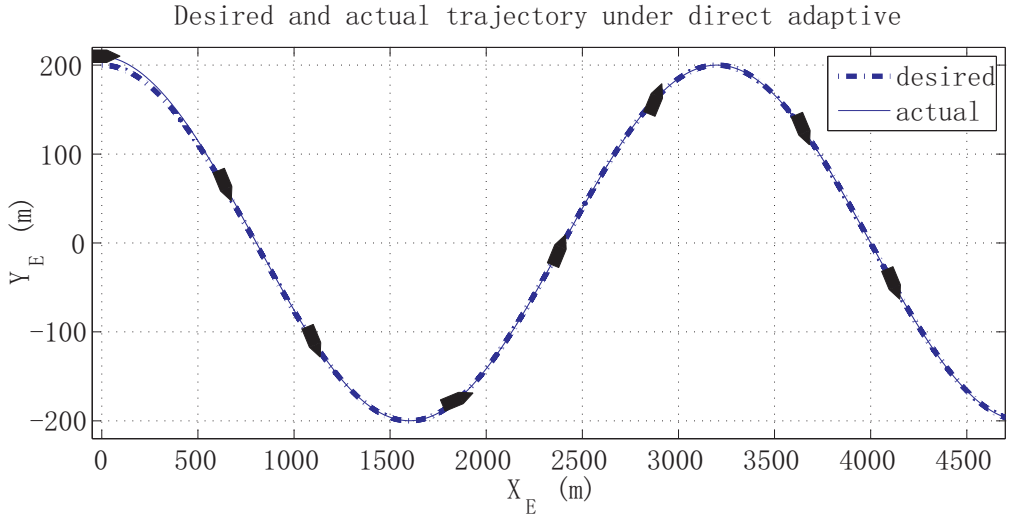

Figure 5.5: The desired and actual trajectory of the container ship under direct adaptive IT2 FLC.

The control performance under indirect adaptive fuzzy control is noted to be better than that under direct adaptive fuzzy control. However, the direct adaptive fuzzy controller has an advantage over the indirect one, i.e., the direct adaptive fuzzy controller does not need the knowledge of inertial matrix $\mathbf{M}$ and damping matrix $\mathbf{D}$. The direct adaptive controller can, therefore, be used under the situation where such knowledge is not available.

5.2.2 Impact of Control Gains

There are four control gains λ_i $(i = 1, \ldots, 4)$ in the indirect adaptive IT2 FLC (5.6) and (5.7) and two control gains λ_2 and λ_3 in the direct adaptive IT2 FLC (5.13) and

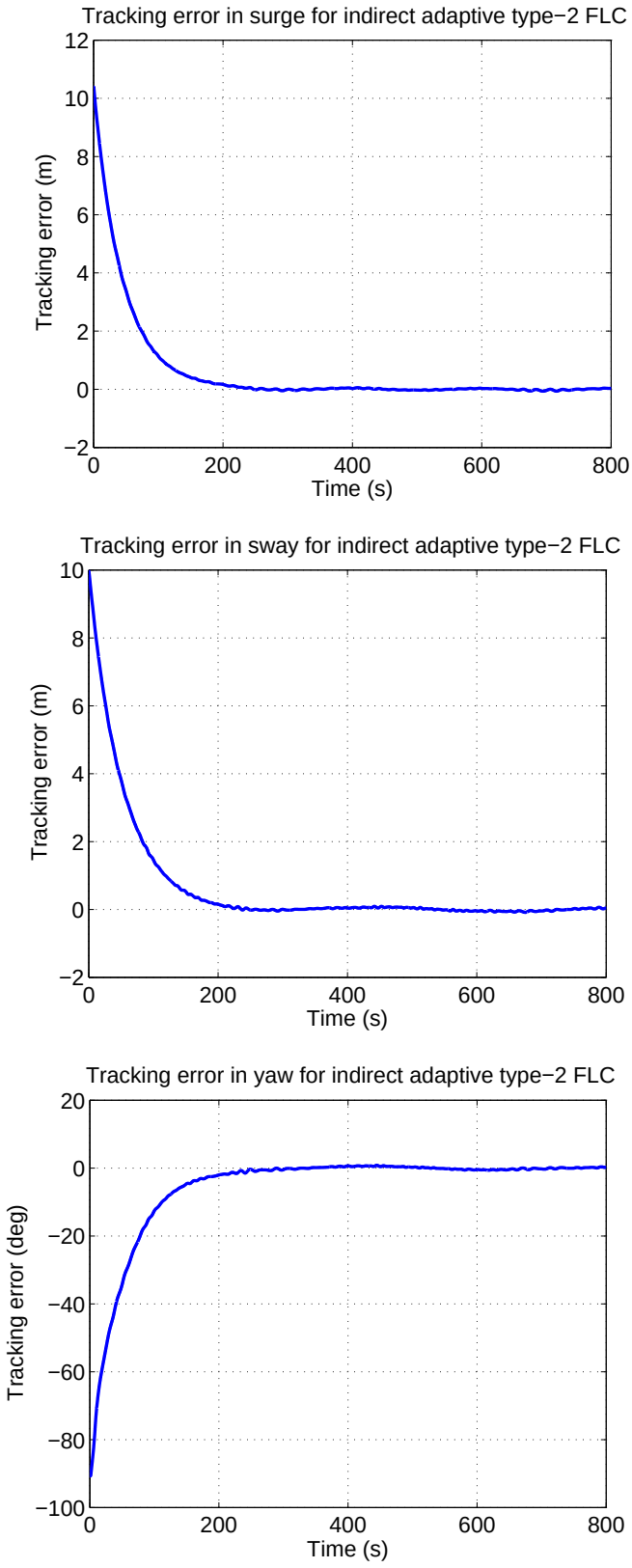

Figure 5.6: Tracking errors of indirect adaptive IT2 FLC for tracking control.

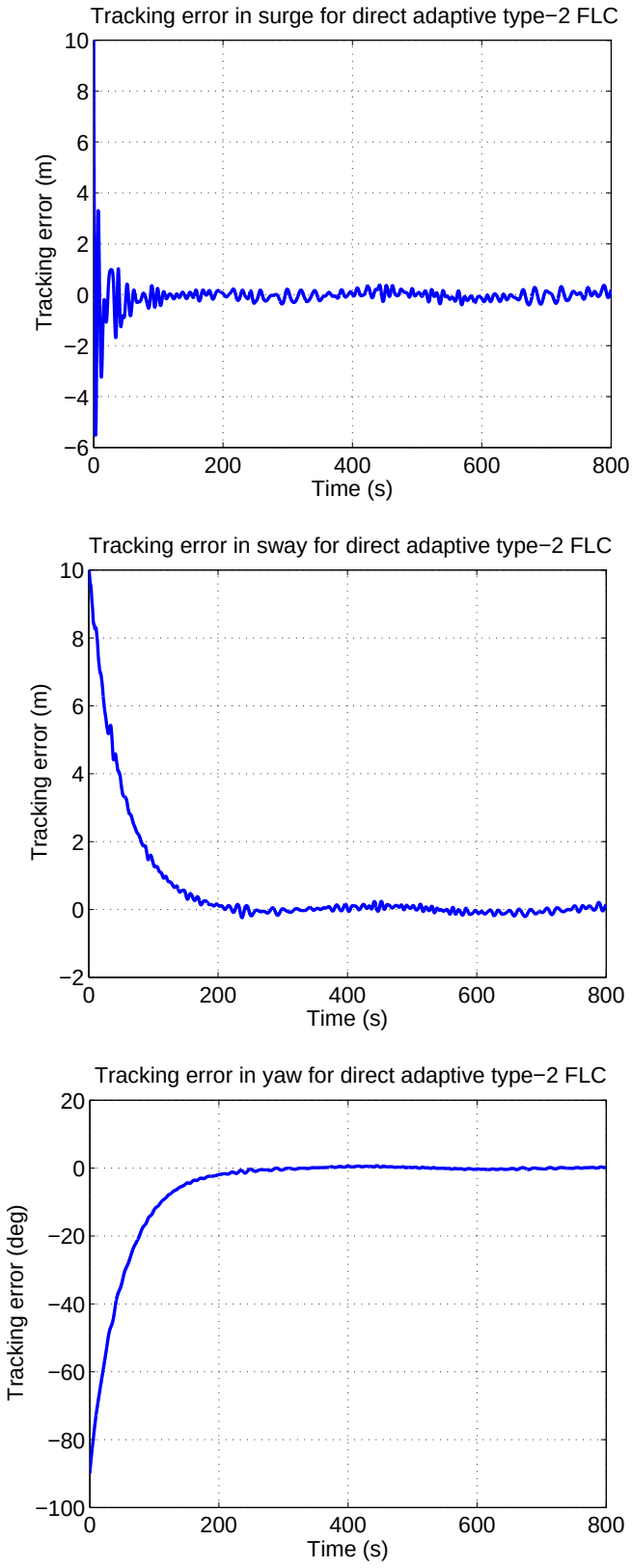

Figure 5.7: Tracking errors of direct adaptive IT2 FLC for tracking control.

(5.14). Since the functions of control gains λ_2 and λ_3 in indirect and direct adaptive IT2 FLCs are similar, same notations are used. The control gain λ_3 determines the relative convergence speed of vessel displacement and velocity and should be chosen first based on trial and error. The choice of the value of λ_3 depends on the controlled plant. For container ship S-175 in the simulation studies, the value of λ_3 is set as 0.02. The control gain λ_4 in (5.8) is used to handle estimation error $\boldsymbol{\omega}(\boldsymbol{\nu})$ and is set as 1. Besides, the control gain λ_1 is similar to PD gain in PD controller and could be chosen accordingly. The control gain λ_2 determines the convergent speed of adaptive law and could be chosen according to experience. To investigate the impact of the control gains in the indirect adaptive IT2 FLC, simulations with the following three cases are conducted:

- Case 1: $\lambda_1 = 4.3 \times 10^7$, $\lambda_2 = 1 \times 10^7$;
- Case 2: $\lambda_1 = 4.3 \times 10^8$, $\lambda_2 = 1 \times 10^8$;
- Case 3: $\lambda_1 = 4.3 \times 10^9$, $\lambda_2 = 1 \times 10^9$.

The tracking errors of the vessel's actual trajectories to the desired trajectories under the indirect adaptive IT2 FLC (5.6) and (5.7) for different control gains are shown in Fig. 5.8. It could be seen that as the values of control gains increase, the steady state errors decrease, but the rising time increases. Thus, the choice of control gains of the indirect adaptive IT2 FLC is a tradeoff between steady state errors and rising time.

To investigate the impact of the control gains in the direct adaptive IT2 FLC, simulations with the following three cases are conducted:

- Case 1: $\lambda_2 = 1 \times 10^7$;

- Case 2: $\lambda_2 = 1 \times 10^8$;
- Case 3: $\lambda_2 = 1 \times 10^9$.

The tracking errors of the vessel's actual trajectories to the desired trajectories under the direct adaptive IT2 FLC (5.13) and (5.14) for different control gains are shown in Fig. 5.9. It could be observed that among three cases, the control gains in case 2 achieve best performance with smallest estimation errors in all three axes. Thus, regarding the choice of the control gain λ_2 for the direct adaptive IT2 FLC, too large or too small value would degrade the performance.

5.2.3 Comparison with Adaptive Type-1 Fuzzy Controllers

In this subsection, the adaptive IT2 FLCs are compared with their type-1 counterparts. Replace the regressive vector (2.25) in the indirect adaptive fuzzy controller (5.6), (5.7) and the direct adaptive fuzzy controller (5.13), (5.14) with the fuzzy basis function vector [41, 85],

$$\boldsymbol{\phi}^{\mathrm{T}} = (\phi^1(\mathbf{x}), \ldots, \phi^M(\mathbf{x})) \tag{5.26}$$

where the fuzzy basis function is defined as

$$\phi^l(\mathbf{x}) = \frac{\Pi_{i=1}^n \mu_{F_i^l}(x_i)}{\Sigma_{l=1}^M (\Pi_{i=1}^n \mu_{F_i^l}(x_i))}. \tag{5.27}$$

The controllers (5.6), (5.7) and (5.13), (5.14) become adaptive type-1 FLCs. For each sub-FLS in the type-1 cases, five fuzzy membership functions labeled as **NL**, **NS**, **Z**, **PS**, and **PL** are employed to partition each of the input domain. As there are three inputs, there are 125 rules compared to 27 rules for type-2 cases. Gaussian functions

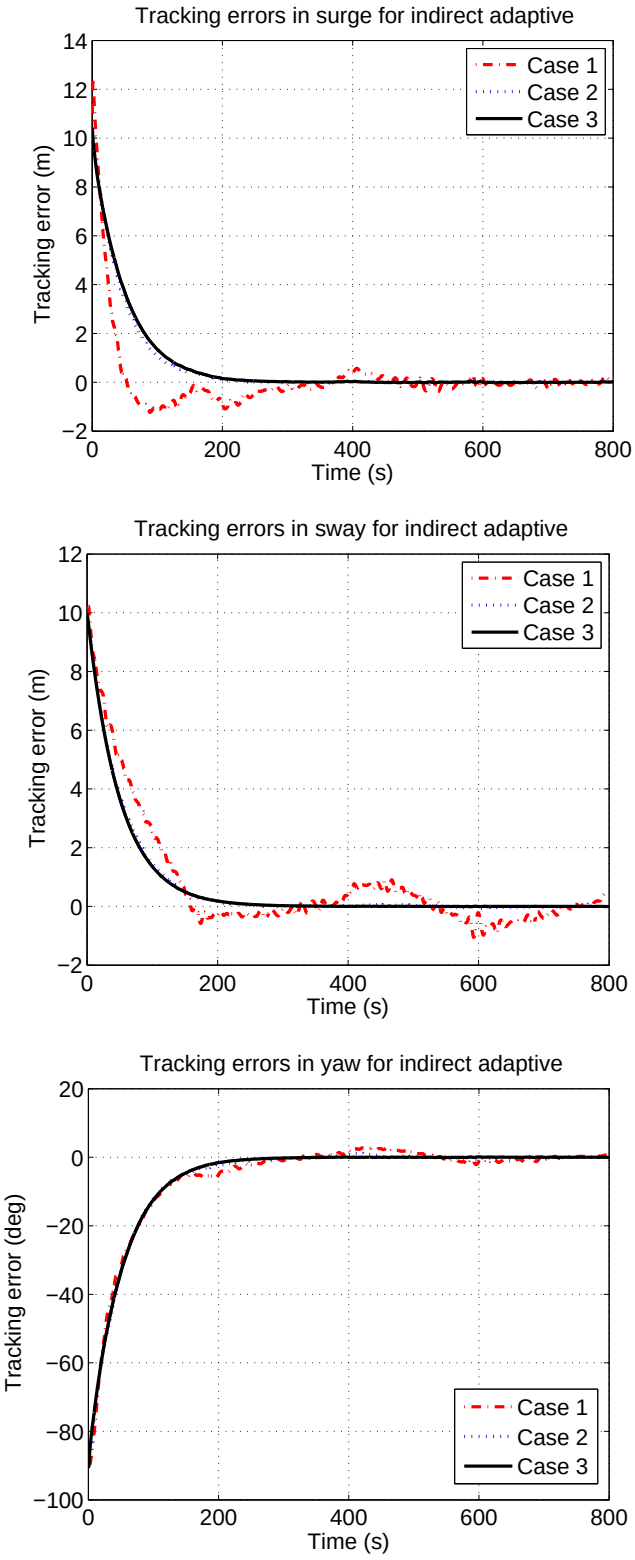

Figure 5.8: Tracking errors of indirect adaptive IT2 FLCs with different control gains for tracking control.

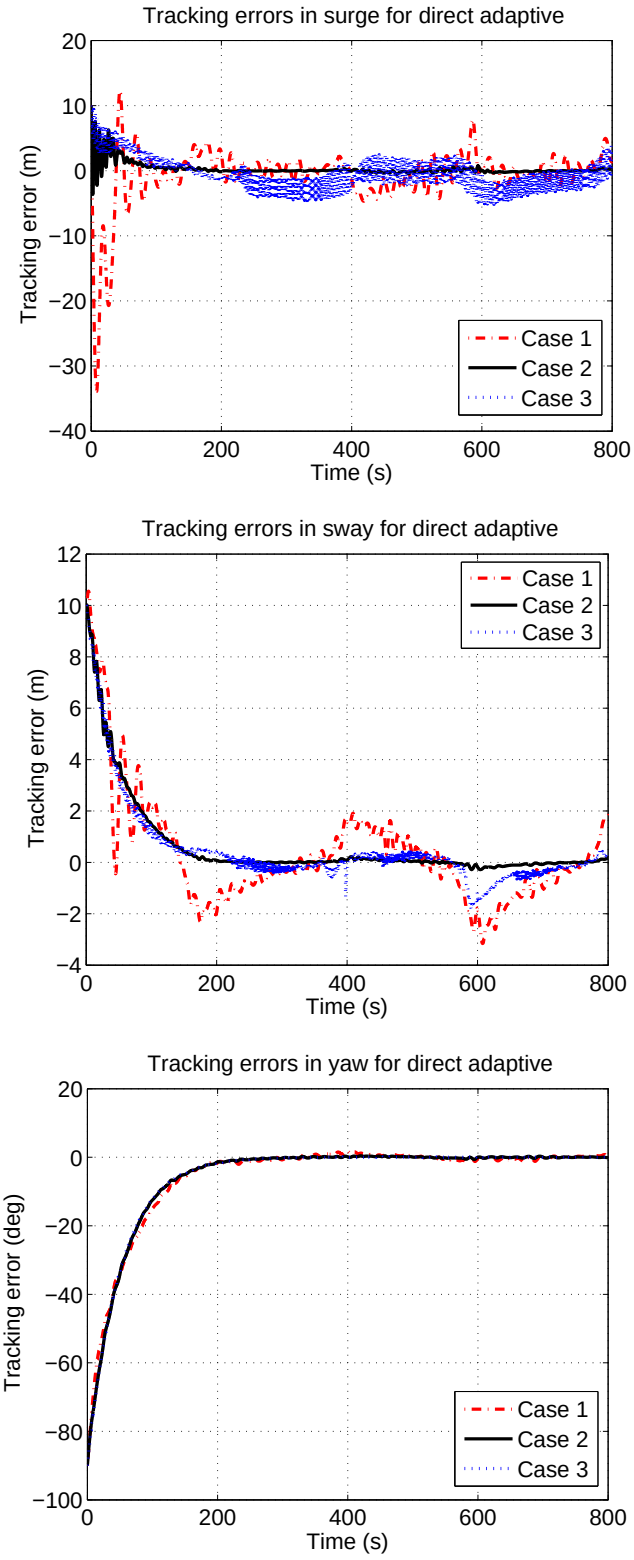

Figure 5.9: Tracking errors of direct adaptive IT2 FLCs with different control gains for tracking control.

are chosen to be the membership functions of the antecedent sets for each input, they can be written as

$$\mu_{F_i^j}(x_j) = \exp[-\frac{1}{2}(\frac{x_j - m_i}{\sigma})^2], \tag{5.28}$$

where $j = 1, 2, 3$ is the index of three inputs and $i = 1, \ldots, 5$ is the index of five fuzzy membership functions for jth input. The means are fixed as $(m_1, \ldots, m_5) = (-1, -0.5, 0, 0.5, 1)$, whereas the standard deviations for all the Gaussian functions are set as $\sigma = 0.4$. The consequent sets for the type-1 cases are also chosen to be singletons. So, there are 125 adjustable consequent parameters compared to 27 parameters for type-2 cases. Their values are randomly generated to be between 0 and 100, and then adapted online according to the adaptive law (5.7) and (5.14). Other conditions such as wave, current, and other hydrodynamic forces are same as the ones for IT2 cases.

When $\lambda_1 = 4.3 \times 10^8$, $\lambda_2 = 1 \times 10^7$, $\lambda_3 = 0.02$, and $\lambda_4 = 1$ in (5.6) and (5.7) for both indirect adaptive type-1 and IT2 FLCs, the tracking errors are shown in Fig. 5.10. When $\lambda_2 = 1 \times 10^8$ and $\lambda_3 = 0.02$ in (5.13) and (5.14) for both direct adaptive type-1 and IT2 FLCs, the tracking errors are depicted in Fig. 5.11.

It can be observed from Fig. 5.10 and Fig. 5.11 that the adaptive IT2 FLCs perform comparably with, if not better than, their type-1 counterparts, even though type-1 cases use more than four times the number of the rules. In order to quantify the performance differences between adaptive type-1 and IT2 FLCs, the ITAE for all

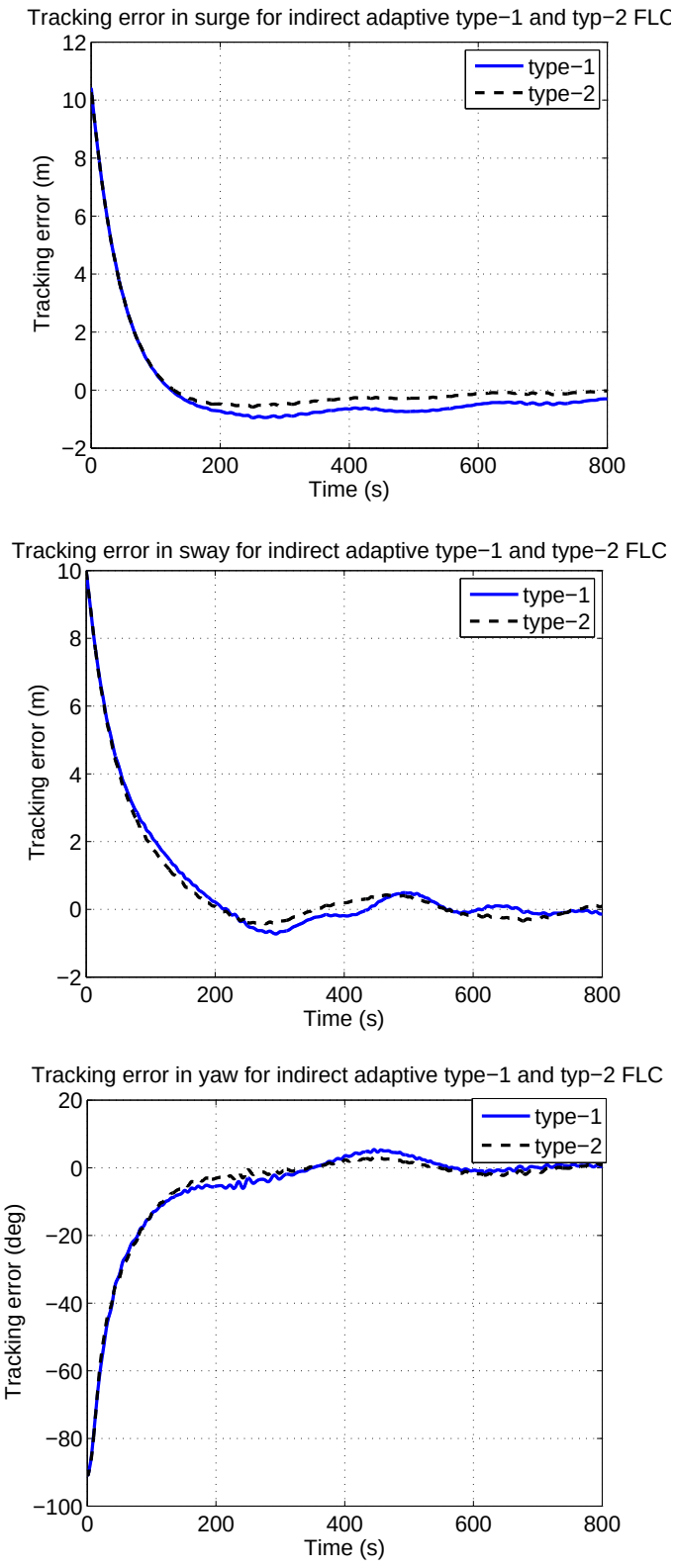

Figure 5.10: Tracking errors of indirect adaptive type-1 and IT2 FLCs for tracking control.

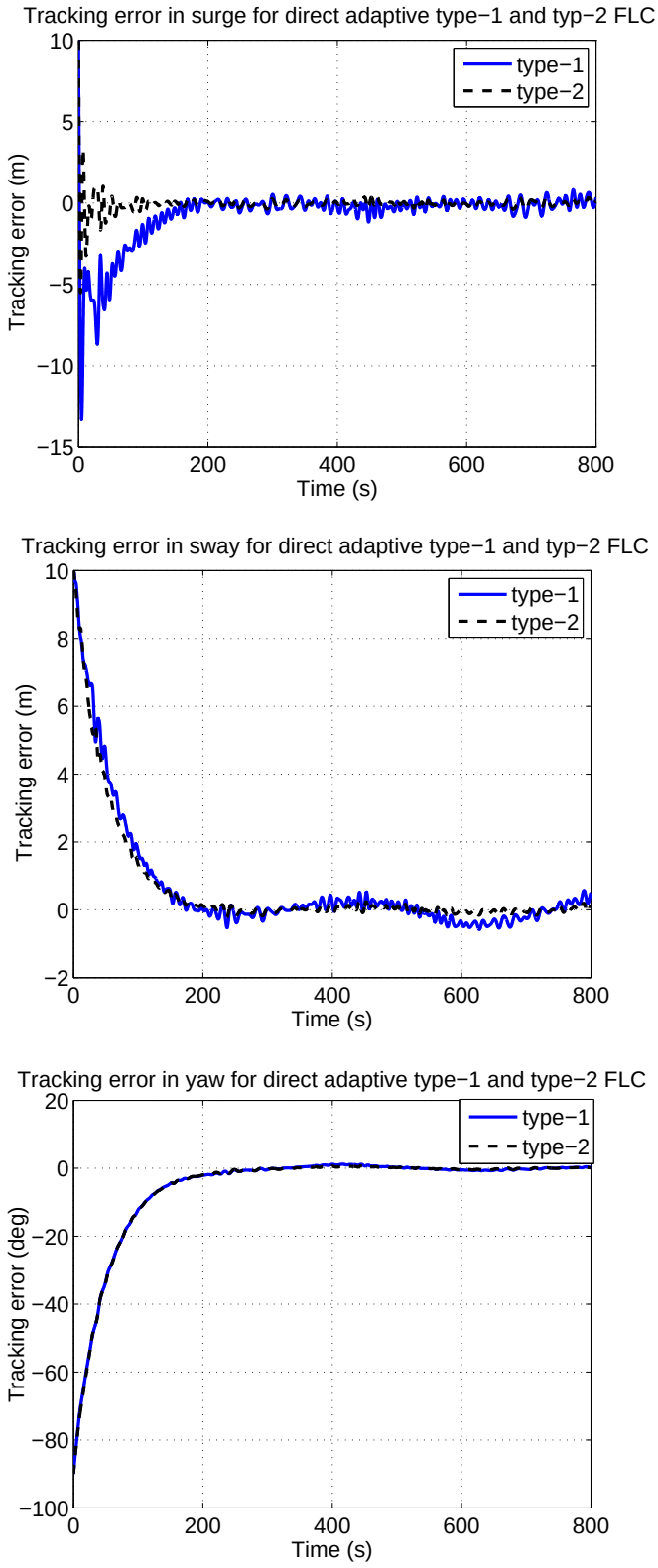

Figure 5.11: Tracking errors of direct adaptive type-1 and IT2 FLCs for tracking control.

the above four cases in the following form are calculated.

$$P_x = \int_0^T t|e_x|dt \tag{5.29}$$

$$P_y = \int_0^T t|e_y|dt \tag{5.30}$$

$$P_\psi = \int_0^T t|e_\psi|dt \tag{5.31}$$

where T is the total simulation time and e_x, e_y, and e_ψ are three components of the tracking error vector $\boldsymbol{e}$. Moreover, an improvement index defined as following is also calculated to quantify the performance improvement.

$$I = \frac{P_{T1} - P_{T2}}{P_{T1}} \tag{5.32}$$

where P_{T1} corresponds to P_x, P_y and P_ψ for adaptive type-1 FLCs. P_{T2} corresponds to P_x, P_y and P_ψ for adaptive IT2 cases. According to the results shown in Table 5.1, the values of the ITAE for the adaptive IT2 FLCs are smaller than those for type-1 cases along all the three degrees of freedom. The performance improvement of the indirect adaptive FLC using IT2 FLSs over the one using type-1 FLSs could be as high as 57.6%, and at least is 21.9%. In contrast, the performance improvement of the direct adaptive FLC could be as high as 66.9%, and at least is 18.0%. As regards the computational burden, type-reductions for IT2 cases do take some time, but the time is very little as only a few rules are fired at the same time and Karnik-Mendel algorithm has been proved to be super-exponentially convergent [106]. Furthermore, it has been reported the type-2 FLS can be implemented in real-time applications [107]. Thus, type-reduction should not be an issue and will not cause any stability problem. In conclusion, the simulation results indicate that the IT2 FLS has better

approximation property with fewer fuzzy rules than its type-1 counterpart in this application.

Table 5.1: ITAE of adaptive type-1 and IT2 FLCs for tracking control.

ITAE	P_x	P_y	P_ψ
Indirect T1	192746	85064	14154
Indirect IT2	81796	66428	9592
Improvement index I	57.6%	21.9%	32.2%
Direct T1	162892	78648	5680
Direct IT2	53917	43013	4660
Improvement index I	66.9%	45.3%	18.0%

5.3 Conclusions

In this chapter, indirect and direct adaptive IT2 FLCs have been designed for tracking control of surface vessels in the presence of time-varying hydrodynamic disturbances. The sufficient condition, under which the tracking errors of both of the proposed controls will semiglobally asymptotically converge to zero, is proposed by means of Lyapunov synthesis. Although designed through different approaches, the closed-loop systems for both indirect and direct IT2 FLCs are similar and passive. Simulation results have demonstrated that the two controllers are effective and robust. Comparison with their type-1 counterpart suggests the IT2 FLS has comparable approximation property even with fewer fuzzy rules. The indirect adaptive IT2 FLC can achieve at

least 21.9% performance improvement, whereas the improvement for direct adaptive IT2 FLC is 18.0%.

Chapter 6

Tracking Control via Fault-tolerant Adaptive Backstepping

In Chapter 5, an indirect as well as a direct adaptive IT2 FLC are proposed for tracking control of marine vessels. The main limitation of this work is that the control scheme is proposed based on the assumption that the state variables of the vessel, i.e. displacements and velocities along surge, sway, and yaw, are measured by its own on-board devices (Assumption 3.2). This limitation prevents the indirect and direct adaptive IT2 FLCs from applying in situations where the measurements of vessel velocities are not available. Since the influence of first-order wave on the measurements of vessel displacements is not very significant for vessels traveling with non-zero forward speed, a high-gain observer [111] is used to construct velocities from displacement measurements in this chapter. With the high-gain observer, the stability of the output feedback closed-loop system could be theoretically proved. But if the influence of first-order wave on the measurements of vessel displacements is very significant, i.e. the WF motion has to be filtered out, the passive adaptive IT2 fuzzy observer introduced in Chapter 4 could be used. Moreover, in order to improve the reliability of marine control systems, fault-tolerant control technique is explored in this chapter. Through backstepping control and Lyapunov synthesis, a sate feedback fault-tolerant

adaptive backstepping IT2 FLC for tracking control of marine vessels is constructed, with the option of high-gain observer for output feedback control. The combination of backstepping control and approximation-based adaptive technique allows the proposed control scheme to be able to accommodate certain faults in the plant and the controller itself, and to handle time-varying hydrodynamic disturbances without explicit knowledge about the disturbance model. The ability of the proposed control schemes to yield stable closed-loop systems that ensure the tracking errors decay to zero asymptotically is studied. For the sate feedback case, the asymptotic convergence of tracking errors occurs only when the IT2 FLS adequately approximates the underlying function. For the output feedback case, the tracking errors are uniformly bounded by a parameter proportional to the approximation error between the IT2 FLS and the underlying function.

The rest of the chapter is organized as follows. The design and stability analysis of the state feedback fault tolerant adaptive backstepping IT2 FLC are delineated in Section 6.1. The fault accommodation mechanism is also explained in this section. Section 6.2 describes the high-gain observer. The stability property of the output feedback fault tolerant adaptive backstepping IT2 FLC is analyzed in this section as well. Section 6.3 illustrates the simulation results of the state and output feedback closed-loop systems with a container ship. Finally, conclusions are drawn in Section 6.4.

6.1 Adaptive Backstepping Fuzzy Controller Design

The control objective in this chapter is to manipulate a surface vessel to track the desired trajectory $\boldsymbol{\eta}_d = [x_d, y_d, \psi_d]^{\mathrm{T}}$, whose second derivative is continuous, as closely as possible. In this section, the process plant model is first simplified to facilitate the controller design. Then, through the combination of approximation-based adaptive technique and backstepping control a fault-tolerant adaptive backstepping IT2 FLC is designed. Using Lyapunov synthesis, the sufficient condition, under which the tracking errors of the controller will semiglobally asymptotically converge to zero, is proposed. At last, the fault accommodation mechanism of the controller for certain faults in the plant and the controller itself is explained.

6.1.1 Control Plant Model

Analogous with the procedure in previous chapters, the process plant model (2.1) and (2.3) for tracking control described in Section 2.1 is simplified to facilitate the tracking controller design. Applying Assumptions 3.1 and 3.3 to (2.1) and (2.3), the same control plant model as in section 5.1.1 is obtained.

$$\dot{\boldsymbol{\eta}} = \mathbf{J}(\boldsymbol{\eta})\boldsymbol{\nu} \tag{6.1}$$

$$\mathbf{M}\dot{\boldsymbol{\nu}} + \mathbf{D}\boldsymbol{\nu} = \boldsymbol{\tau} + \boldsymbol{\tau}_{\mathrm{H}} \tag{6.2}$$

6.1.2 Fault-tolerant Control

Through following the conventional backstepping procedure in [24], the generalized tracking error as $\boldsymbol{z}_1 = \boldsymbol{\eta} - \boldsymbol{\eta}_d$ such that $\dot{\boldsymbol{z}}_1 = \mathbf{J}(\boldsymbol{\eta})\boldsymbol{\nu} - \dot{\boldsymbol{\eta}}_d$ is defined. Introduce a virtual control signal $\boldsymbol{\alpha}_1$ and define a second error variable as $\boldsymbol{z}_2 = \boldsymbol{\nu} - \boldsymbol{\alpha}_1$. The derivative of $\boldsymbol{z}_1$ with respect to time can be expressed as

$$\dot{\boldsymbol{z}}_1 = \mathbf{J}(\boldsymbol{\eta})(\boldsymbol{z}_2 + \boldsymbol{\alpha}_1) - \dot{\boldsymbol{\eta}}_d. \tag{6.3}$$

Consider a Lyapunov function candidate with quadratic $\boldsymbol{z}_1$

$$V_1 = \frac{1}{2}\boldsymbol{z}_1^{\mathrm{T}}\boldsymbol{z}_1 \tag{6.4}$$

and taking its derivative along (6.3) results in

$$\dot{V}_1 = \boldsymbol{z}_1^{\mathrm{T}}\mathbf{J}(\boldsymbol{\eta})\boldsymbol{z}_2 + \boldsymbol{z}_1^{\mathrm{T}}[\mathbf{J}(\boldsymbol{\eta})\boldsymbol{\alpha}_1 - \dot{\boldsymbol{\eta}}_d]. \tag{6.5}$$

Note the property $\mathbf{J}(\boldsymbol{\eta})\mathbf{J}^{\mathrm{T}}(\boldsymbol{\eta}) = \mathbf{I}$ and choose

$$\boldsymbol{\alpha}_1 = \mathbf{J}^{\mathrm{T}}(\boldsymbol{\eta})(\dot{\boldsymbol{\eta}}_d - \mathbf{K}_1\boldsymbol{z}_1), \tag{6.6}$$

where the gain matrix $\mathbf{K}_1 > 0$ is diagonal. Then, (6.5) becomes

$$\dot{V}_1 = -\boldsymbol{z}_1^{\mathrm{T}}\mathbf{K}_1\boldsymbol{z}_1 + \boldsymbol{z}_1^{\mathrm{T}}\mathbf{J}(\boldsymbol{\eta})\boldsymbol{z}_2. \tag{6.7}$$

Differentiating $\boldsymbol{z}_2$ with respect to time yields

$$\dot{\boldsymbol{z}}_2 = \mathbf{M}^{-1}(-\mathbf{D}\boldsymbol{\nu} + \boldsymbol{\tau} + \boldsymbol{\tau}_{\mathrm{H}}) - \dot{\boldsymbol{\alpha}}_1 \tag{6.8}$$

where

$$\dot{\boldsymbol{\alpha}}_1 = \frac{\partial \boldsymbol{\alpha}_1}{\partial \boldsymbol{\eta}}\dot{\boldsymbol{\eta}} + \frac{\partial \boldsymbol{\alpha}_1}{\partial \dot{\boldsymbol{\eta}}_d}\ddot{\boldsymbol{\eta}}_d + \frac{\partial \boldsymbol{\alpha}_1}{\partial \boldsymbol{z}_1}\dot{\boldsymbol{z}}_1. \tag{6.9}$$

Next, consider the following Lyapunov function candidate

$$V_2 = V_1 + \frac{1}{2}\boldsymbol{z}_2^{\mathrm{T}}\mathbf{M}\boldsymbol{z}_2. \tag{6.10}$$

Its time derivative is

$$\begin{aligned}\dot{V}_2 = &- \boldsymbol{z}_1^{\mathrm{T}}\mathbf{K}_1\boldsymbol{z}_1 + \boldsymbol{z}_1^{\mathrm{T}}\mathbf{J}(\boldsymbol{\eta})\boldsymbol{z}_2 \\ &+ \boldsymbol{z}_2^{\mathrm{T}}(-\mathbf{D}\boldsymbol{\nu} + \boldsymbol{\tau} + \boldsymbol{\tau}_{\mathrm{H}} - \mathbf{M}\dot{\boldsymbol{\alpha}}_1).\end{aligned} \tag{6.11}$$

Suppose the time-varying hydrodynamic disturbance vector $\boldsymbol{\tau}_{\mathrm{H}}$ is known, the following model based control law could be designed.

$$\boldsymbol{\tau} = -\mathbf{J}^{\mathrm{T}}(\boldsymbol{\eta})\boldsymbol{z}_1 - \mathbf{K}_2\boldsymbol{z}_2 + \mathbf{D}\boldsymbol{\nu} - \boldsymbol{\tau}_{\mathrm{H}} + \mathbf{M}\dot{\boldsymbol{\alpha}}_1 \tag{6.12}$$

where the gain matrix $\mathbf{K}_2 > 0$ is diagonal. Substituting (6.12) into (6.11) yields

$$\dot{V}_2 = -\boldsymbol{z}_1^{\mathrm{T}}\mathbf{K}_1\boldsymbol{z}_1 - \boldsymbol{z}_2^{\mathrm{T}}\mathbf{K}_2\boldsymbol{z}_2 \tag{6.13}$$

which is negative semidefinite. Since the time-varying hydrodynamic disturbances are very complex and unknown, the model based control law (6.12) obtained through backstepping may not be realizable. To overcome this challenge, the approximation-based adaptive technique is combined with the backstepping control. Subsequently, a fault-tolerant adaptive backstepping fuzzy controller is designed.

To handle the time-varying hydrodynamic disturbances and equip the designed controller with fault-tolerant ability, a compensator $\Phi(\boldsymbol{\nu})\hat{\Theta}_{\mathrm{H}}$ which is composed of singleton IT2 FLSs (2.24) is introduced. The structure of the singleton IT2 FLSs will be adapted according to hydrodynamic disturbances and fault natures. Apply the compensator to estimate $\Phi(\boldsymbol{\nu})\Theta_{\mathrm{H}}^*$ defined via the following expression

$$\boldsymbol{\tau}_{\mathrm{H}}(\boldsymbol{\nu}) = -\Phi(\boldsymbol{\nu})\Theta_{\mathrm{H}}^* + \boldsymbol{\omega}_{\mathrm{H}}(\boldsymbol{\nu}), \tag{6.14}$$

where $\boldsymbol{\omega}_{\mathrm{H}}(\boldsymbol{\nu}) \in R^3$ is a vector of minimum estimation error.

$$\begin{aligned} \Theta_{\mathrm{H}}^* &= (\boldsymbol{\theta}_1^{*\mathrm{T}}, \boldsymbol{\theta}_2^{*\mathrm{T}}, \boldsymbol{\theta}_3^{*\mathrm{T}})^{\mathrm{T}} \in R^{3M\times 1} \\ &= \arg\min_{\Theta_{\mathrm{H}}\in R^{3M}} [\sup_{\nu\in U_\nu} |\boldsymbol{\tau}_{\mathrm{H}}(\boldsymbol{\nu}) + \Phi(\boldsymbol{\nu})\Theta_{\mathrm{H}}|] \end{aligned} \tag{6.15}$$

is the ideal weighting vector and

$$\Phi(\boldsymbol{\nu}) = \mathrm{diag}[\boldsymbol{\phi}_1^{\mathrm{T}}(\boldsymbol{\nu}), \boldsymbol{\phi}_2^{\mathrm{T}}(\boldsymbol{\nu}), \boldsymbol{\phi}_3^{\mathrm{T}}(\boldsymbol{\nu})] \in R^{3\times 3M} \tag{6.16}$$

is the regressive matrix.

Referring to the model based control law (6.12), the control and adaptive law of the fault-tolerant adaptive backstepping IT2 FLC for plant (6.1), (6.2) may be defined as

$$\boldsymbol{\tau} = -\mathbf{J}^{\mathrm{T}}(\boldsymbol{\eta})\boldsymbol{z}_1 - \mathbf{K}_2\boldsymbol{z}_2 + \mathbf{D}\boldsymbol{\nu} + \Phi(\boldsymbol{\nu})\hat{\Theta}_{\mathrm{H}} + \mathbf{M}\dot{\boldsymbol{\alpha}}_1 \tag{6.17}$$

$$\dot{\hat{\Theta}}_{\mathrm{H}} = \mathbf{K}_3\Phi^{\mathrm{T}}(\boldsymbol{\nu})\boldsymbol{z}_2 \tag{6.18}$$

where the gain matrix

$$\mathbf{K}_3 = \mathrm{diag}[\underbrace{k_{31}, \ldots, k_{31}}_{\mathrm{M}}, \underbrace{k_{32}, \ldots, k_{32}}_{\mathrm{M}}, \underbrace{k_{33}, \ldots, k_{33}}_{\mathrm{M}}] > 0.$$

$\tilde{\Theta}_{\mathrm{H}} = \Theta_{\mathrm{H}}^* - \hat{\Theta}_{\mathrm{H}} \in R^{3M}$ is the error vector between the ideal weighting vector Θ_{H}^* in (6.14) and the adapted weighting vector $\hat{\Theta}_{\mathrm{H}}$. From the control law (6.17), it can be observed that the control law could be divided into two parts. One part is the model based control law $-\mathbf{J}^{\mathrm{T}}(\boldsymbol{\eta})\boldsymbol{z}_1 - \mathbf{K}_2\boldsymbol{z}_2 + \mathbf{D}\boldsymbol{\nu} + \mathbf{M}\dot{\boldsymbol{\alpha}}_1$ derived through backstepping. The other part is the compensator $\Phi(\boldsymbol{\nu})\hat{\Theta}_{\mathrm{H}}$. The stability problem of the closed-loop system will be addressed by the following theorem.

Theorem 6.1 *Consider the plant (6.1) and (6.2) with the adaptive backstepping fuzzy control (6.17) and (6.18). The tracking error* $\boldsymbol{z}_1$ *will semiglobally asymptotically converge to zero, if* $\boldsymbol{\omega}_H(\boldsymbol{\nu})$ *is squared integrable.*

Proof: Consider the augmented Lyapunov function candidate, which is positive definite.

$$V_{\mathrm{H}} = V_2 + \frac{1}{2}\tilde{\Theta}_{\mathrm{H}}^{\mathrm{T}}\mathbf{K}_3^{-1}\tilde{\Theta}_{\mathrm{H}} \tag{6.19}$$

Differentiating (6.19) along closed-loop trajectory with (6.17) and (6.18) yields

$$\begin{aligned}
\dot{V}_{\mathrm{H}} =& -\boldsymbol{z}_1^{\mathrm{T}}\mathbf{K}_1\boldsymbol{z}_1 - \boldsymbol{z}_2^{\mathrm{T}}\mathbf{K}_2\boldsymbol{z}_2 - \boldsymbol{z}_2^{\mathrm{T}}\Phi(\boldsymbol{\nu})\tilde{\Theta}_{\mathrm{H}} + \boldsymbol{z}_2^{\mathrm{T}}\boldsymbol{\omega}_{\mathrm{H}} \\
&+ \tilde{\Theta}_{\mathrm{H}}^{\mathrm{T}}\mathbf{K}_3^{-1}\dot{\tilde{\Theta}}_{\mathrm{H}} \\
=& -\boldsymbol{z}_1^{\mathrm{T}}\mathbf{K}_1\boldsymbol{z}_1 - \boldsymbol{z}_2^{\mathrm{T}}\mathbf{K}_2\boldsymbol{z}_2 + \boldsymbol{z}_2^{\mathrm{T}}\boldsymbol{\omega}_{\mathrm{H}} \\
=& -\boldsymbol{z}_1^{\mathrm{T}}\mathbf{K}_1\boldsymbol{z}_1 - \boldsymbol{z}_2^{\mathrm{T}}(\mathbf{K}_2 - \frac{1}{2}\mathbf{I})\boldsymbol{z}_2 \\
&- \frac{1}{2}(\boldsymbol{z}_2 - \boldsymbol{\omega}_{\mathrm{H}})^{\mathrm{T}}(\boldsymbol{z}_2 - \boldsymbol{\omega}_{\mathrm{H}}) + \frac{1}{2}\boldsymbol{\omega}_{\mathrm{H}}^{\mathrm{T}}\boldsymbol{\omega}_{\mathrm{H}} \\
\leq& -\boldsymbol{z}_1^{\mathrm{T}}\mathbf{K}_1\boldsymbol{z}_1 - \boldsymbol{z}_2^{\mathrm{T}}(\mathbf{K}_2 - \frac{1}{2}\mathbf{I})\boldsymbol{z}_2 + \frac{1}{2}\boldsymbol{\omega}_{\mathrm{H}}^{\mathrm{T}}\boldsymbol{\omega}_{\mathrm{H}}
\end{aligned}$$

Choose the gain matrix $\mathbf{K}_1$ and $\mathbf{K}_2$ such that $\mathbf{K}_1 > 0$ and $\mathbf{K}_2 - \mathbf{I}/2 > 0$, and integrate both sides of the above equation. Then,

$$\begin{aligned}
&\int_0^t \boldsymbol{z}_1^{\mathrm{T}}\mathbf{K}_1\boldsymbol{z}_1 dr + \int_0^t \boldsymbol{z}_2^{\mathrm{T}}(\mathbf{K}_2 - \frac{1}{2}\mathbf{I})\boldsymbol{z}_2 dr + V_{\mathrm{H}}(t) \\
&\leq V_{\mathrm{H}}(0) + \frac{1}{2}\int_0^t \boldsymbol{\omega}_{\mathrm{H}}^{\mathrm{T}}\boldsymbol{\omega}_{\mathrm{H}} dr,
\end{aligned}$$

which demonstrates that $\boldsymbol{z}_1$, $\boldsymbol{z}_2$, $\tilde{\Theta}_{\mathrm{H}}$ and other signals involved are bounded. Furthermore, if $\boldsymbol{\omega}_{\mathrm{H}}$ is squared integrable, that is $\int_0^\infty \boldsymbol{\omega}_{\mathrm{H}}^{\mathrm{T}}\boldsymbol{\omega}_{\mathrm{H}} dr < \infty$, we have $\boldsymbol{z}_1 \in L_2$. As all the signals are bounded, we have $\dot{\boldsymbol{z}}_1 \in L_\infty$. According to Barbalat's Lemma, we have $\lim_{t\to\infty} |\boldsymbol{z}_1| = 0$. ∎

Remark 6.1 *According to the above analysis, the accuracy of the singleton IT2 FLSs estimating the time-varying hydrodynamic disturbances is essential to the stability of the adaptive backstepping fuzzy control. The quality of the estimation will be checked in the subsequent simulations.*

6.1.3 Fault Accommodation Mechanism

Automated systems are vulnerable to faults. Defects in sensors, actuators, the plant itself or within the controller can be amplified by the closed-loop system, and faults can develop into malfunction of the loop. Research into fault-tolerant control concerns wide fault natures. The faults that the adaptive backstepping fuzzy controller can accommodate are discussed in the following.

6.1.3.1 Faults in the Plant

Although advanced modeling techniques are used, the modeling error is inevitable in the modeling of surface vessels. Moreover, supposing the modeling is very accurate, the parameters of the mathematical model will change according to various loading conditions and trimming of the vessels. Here, suppose the system parameters $\mathbf{M}$ and $\mathbf{D}$ are changed to $\mathbf{M}+\Delta\mathbf{M}$ and $\mathbf{D}+\Delta\mathbf{D}$ due to loading conditions or trimming, i.e., the system parameters $\mathbf{M}$ and $\mathbf{D}$ are unknown in control law (6.17), the compensator $\Phi(\boldsymbol{\nu})\hat{\Theta}_{\mathrm{H}}$ in (6.17) will compensate for the fault without significant degradation of the control performance. That is because in this situation, the modeling errors and the errors due to loading conditions or trimming can be lumped together with the

hydrodynamic disturbances to be represented by a new vector of hydrodynamic disturbances $\boldsymbol{\tau}_{\mathrm{H1}} = \boldsymbol{\tau}_{\mathrm{H}} - \Delta\mathbf{M}\dot{\boldsymbol{\nu}} - \Delta\mathbf{D}\boldsymbol{\nu}$. Now the compensator is adapted from $\Phi(\boldsymbol{\nu})\hat{\Theta}_{\mathrm{H}}$ to $\Phi(\boldsymbol{\nu})\hat{\Theta}_{\mathrm{H1}}$ to estimate $\Phi(\boldsymbol{\nu})\Theta^*_{\mathrm{H1}}$ defined as follows.

$$\begin{aligned} &\mathbf{D}\boldsymbol{\nu} - \boldsymbol{\tau}_{\mathrm{H1}} + \mathbf{M}\dot{\boldsymbol{\alpha}}_1 \\ &= \Phi(\boldsymbol{\nu})\Theta^*_{\mathrm{H1}} - \boldsymbol{\omega}_{\mathrm{H1}}(\boldsymbol{\nu}) \end{aligned} \tag{6.20}$$

where $-\boldsymbol{\omega}_{\mathrm{H1}}(\boldsymbol{\nu}) \in R^3$ is the minimum estimation error vector. $\Theta^*_{\mathrm{H1}} \in R^{3M}$ which is similar to Θ^*_{H} in (6.15) is the ideal weighting vector. The control and adaptive law now may be considered as follows.

$$\begin{aligned} \boldsymbol{\tau}_1 =& -\mathbf{J}^{\mathrm{T}}(\boldsymbol{\eta})\boldsymbol{z}_1 - \mathbf{K}_2\boldsymbol{z}_2 + \Phi(\boldsymbol{\nu})\hat{\Theta}_{\mathrm{H1}} \\ =& -\mathbf{J}^{\mathrm{T}}(\boldsymbol{\eta})\boldsymbol{z}_1 - \mathbf{K}_2\boldsymbol{z}_2 + \mathbf{D}\boldsymbol{\nu} - \boldsymbol{\tau}_{\mathrm{H1}} + \mathbf{M}\dot{\boldsymbol{\alpha}}_1 \\ &- \Phi(\boldsymbol{\nu})\tilde{\Theta}_{\mathrm{H1}} + \boldsymbol{\omega}_{\mathrm{H1}}(\boldsymbol{\nu}) \end{aligned} \tag{6.21}$$

$$\dot{\tilde{\Theta}}_{\mathrm{H1}} = \mathbf{K}_3\Phi^{\mathrm{T}}(\boldsymbol{\nu})\boldsymbol{z}_2 \tag{6.22}$$

where $\tilde{\Theta}_{\mathrm{H1}} = \Theta^*_{\mathrm{H1}} - \hat{\Theta}_{\mathrm{H1}} \in R^{3M}$ is the error vector between the ideal weighting vector Θ^*_{H1} and the adapted weighting vector $\hat{\Theta}_{\mathrm{H1}}$. Compared to the proposed control law (6.17), the control law (6.21) do not contain information of the parameters $\mathbf{M}$ and $\mathbf{D}$. Regarding the stability property of the control and adaptive law (6.21) and (6.22), consider the Lyapunov function candidate

$$V_{\mathrm{H1}} = V_2 + \frac{1}{2}\tilde{\Theta}^{\mathrm{T}}_{\mathrm{H1}}\mathbf{K}_3^{-1}\tilde{\Theta}_{\mathrm{H1}}, \tag{6.23}$$

similar conclusion as Theorem 6.1 could be drawn. Thus, the proposed control law (6.17) could stabilize the closed-loop system even if the parameters $\mathbf{M}$ and $\mathbf{D}$ are set as $\mathbf{M} = \mathbf{0}$ and $\mathbf{D} = \mathbf{0}$ in the control law.

6.1.3.2 Faults in the Controller

As explained, the control law of the fault-tolerant adaptive backstepping IT2 FLC (6.17) can be viewed as a combination of two parts, a model based control law $-\mathbf{J}^{\mathrm{T}}(\boldsymbol{\eta})\boldsymbol{z}_1 - \mathbf{K}_2\boldsymbol{z}_2 + \mathbf{D}\boldsymbol{\nu} + \mathbf{M}\dot{\boldsymbol{\alpha}}_1$ and a compensator $\Phi(\boldsymbol{\nu})\hat{\Theta}_{\mathrm{H}}$.

Imagine the model based control law and the compensator are implemented on two separate computers. If the fault occurs in the computer that implements the model based control law, the errors due to the fault can be lumped together with the hydrodynamic disturbances to be represented by a new vector of hydrodynamic disturbances $\boldsymbol{\tau}_{\mathrm{H2}}$. In this case the compensator is adapted from $\Phi(\boldsymbol{\nu})\hat{\Theta}_{\mathrm{H}}$ to $\Phi(\boldsymbol{\nu})\hat{\Theta}_{\mathrm{H2}}$ to estimate $\Phi(\boldsymbol{\nu})\Theta^*_{\mathrm{H2}}$ defined as follows.

$$\begin{aligned} &-\mathbf{J}^{\mathrm{T}}(\boldsymbol{\eta})\boldsymbol{z}_1 - \mathbf{K}_2\boldsymbol{z}_2 + \mathbf{D}\boldsymbol{\nu} - \boldsymbol{\tau}_{\mathrm{H2}} + \mathbf{M}\dot{\boldsymbol{\alpha}}_1 \\ &= \Phi(\boldsymbol{\nu})\Theta^*_{\mathrm{H2}} - \boldsymbol{\omega}_{\mathrm{H2}}(\boldsymbol{\nu}) \end{aligned} \tag{6.24}$$

where $-\boldsymbol{\omega}_{\mathrm{H2}}(\boldsymbol{\nu}) \in R^3$ is the minimum estimation error vector. $\Theta^*_{\mathrm{H2}} \in R^{3M}$ which is similar to Θ^*_{H} in (6.15) is the ideal weighting vector. The control and adaptive law now could be viewed as follows.

$$\begin{aligned} \boldsymbol{\tau}_2 &= \Phi(\boldsymbol{\nu})\hat{\Theta}_{\mathrm{H2}} \\ &= -\mathbf{J}^{\mathrm{T}}(\boldsymbol{\eta})\boldsymbol{z}_1 - \mathbf{K}_2\boldsymbol{z}_2 + \mathbf{D}\boldsymbol{\nu} - \boldsymbol{\tau}_{\mathrm{H2}} + \mathbf{M}\dot{\boldsymbol{\alpha}}_1 \\ &\quad - \Phi(\boldsymbol{\nu})\tilde{\Theta}_{\mathrm{H2}} + \boldsymbol{\omega}_{\mathrm{H2}}(\boldsymbol{\nu}) \end{aligned} \tag{6.25}$$

$$\dot{\hat{\Theta}}_{\mathrm{H2}} = \mathbf{K}_3\Phi^{\mathrm{T}}(\boldsymbol{\nu})\boldsymbol{z}_2 \tag{6.26}$$

where $\tilde{\Theta}_{\mathrm{H2}} = \Theta^*_{\mathrm{H2}} - \hat{\Theta}_{\mathrm{H2}} \in R^{3M}$ is the error vector between the ideal weighting vector Θ^*_{H2} and the adapted weighting vector $\hat{\Theta}_{\mathrm{H2}}$. It is noticed that in this case the control

forces are directly generated by the compensator. The parameters of the conpensator are directly adjusted to reduce the tracking errors. As regards the stability property of the control and adaptive law (6.25) and (6.26), similar Theorem as Theorem 6.1 could be derived. Thus, the compensator $\Phi(\boldsymbol{\nu})\hat{\Theta}_{\mathrm{H}}$ alone could stabilize the closed-loop system.

If the fault is in the compensator, the system will rely on the robustness of the model based control law $\boldsymbol{\tau}_3 = -\mathbf{J}^{\mathrm{T}}(\boldsymbol{\eta})\boldsymbol{z}_1 - \mathbf{K}_2\boldsymbol{z}_2 + \mathbf{D}\boldsymbol{\nu} + \mathbf{M}\dot{\boldsymbol{\alpha}}_1$ derived through backstepping.

6.2 Output Feedback Control

The proposed controller (6.17) and (6.18) requires the states $\boldsymbol{\eta}$ and $\boldsymbol{\nu}$ are measurable. In the absence of velocity sensors such as the doppler velocity log, a high-gain observer introduced by [111] is designed to estimate $\boldsymbol{\nu}$. With the high-gain observer, the stability of the output feedback closed-loop system could be theoretically derived.

Lemma 6.1 *Suppose a system output $y(t)$ and its first n derivatives are bounded such that $|y^{(k)}| < Y_k$ with positive constants Y_k, consider the following linear system:*

$$\varepsilon\dot{\pi}_i = \pi_{i+1}, \qquad i = 1, \ldots, n-1 \tag{6.27}$$

$$\varepsilon\dot{\pi}_n = -\lambda_1\pi_n - \lambda_2\pi_{n-1} - \cdots - \lambda_{n-1}\pi_2 - \pi_1 + y(t) \tag{6.28}$$

where ε is any small positive constant and the parameters λ_1 to λ_{n-1} are chosen such that the polynomial $s^n + \lambda_1 s^{n-1} + \cdots + \lambda_{n-1}s + 1$ is Hurwitz. Then, the following

property holds:

$$\xi_k = y^{(k-1)} - \frac{\pi_k}{\varepsilon^{k-1}} = \varepsilon\zeta^{(k)}, \quad k = 1, \ldots, n \tag{6.29}$$

where $\zeta = \pi_n + \lambda_1\pi_{n-1} + \cdots + \lambda_{n-1}\pi_1$ *with* $\zeta^{(k)}$ *denoting the* k*th derivative of* ζ*. Furthermore, there exist positive constants* h_k *(independent of* ε*) and* t^* *such that* $|\xi_k| \leq \varepsilon h_k$ *for* $t > t^*$*.*

The proof of Lemma 6.1 could be found in [111]. Note that π_{k+1}/ε^k asymptotically converges to $y^{(k)}$ with a small time constant, provided that y and its k derivatives are bounded. Hence, π_{k+1}/ε^k for $k = 1, 2, \ldots, n$ is a suitable observer to estimate the output derivatives up to the nth order. In this chapter the high-gain observer is designed as follows.

$$\varepsilon\dot{\boldsymbol{\pi}}_1 = \boldsymbol{\pi}_2 \tag{6.30}$$

$$\varepsilon\dot{\boldsymbol{\pi}}_2 = -\lambda_1\boldsymbol{\pi}_2 - \boldsymbol{\pi}_1 + \boldsymbol{\eta} \tag{6.31}$$

According to Lemma 6.1, $\hat{\boldsymbol{\nu}} = \mathbf{J}^{\mathrm{T}}(\boldsymbol{\eta})(\boldsymbol{\pi}_2/\varepsilon)$ asymptotically converges to $\boldsymbol{\nu}$. Define $\tilde{\boldsymbol{\nu}} = \boldsymbol{\nu} - \hat{\boldsymbol{\nu}}$, note that $\tilde{\boldsymbol{\nu}} = \mathbf{J}^{\mathrm{T}}(\boldsymbol{\eta})\boldsymbol{\xi}_2$ and $\tilde{\boldsymbol{\nu}}^{\mathrm{T}}\tilde{\boldsymbol{\nu}} \leq \varepsilon^2 h_2^2$ for $t > t^*$. Modifying the control and adaptive law (6.17) and (6.18) from full state feedback case, the control and adaptive law for output feedback control are obtained as

$$\boldsymbol{\tau}_o = -\mathbf{J}^{\mathrm{T}}(\boldsymbol{\eta})\boldsymbol{z}_1 - \mathbf{K}_2\hat{\boldsymbol{z}}_2 + \mathbf{D}\hat{\boldsymbol{\nu}} + \Phi(\hat{\boldsymbol{\nu}})\hat{\Theta}_{\mathrm{H}} + \mathbf{M}\dot{\boldsymbol{\alpha}}_1 \tag{6.32}$$

$$\dot{\hat{\Theta}}_{\mathrm{H}} = \mathbf{K}_3\Phi^{\mathrm{T}}(\hat{\boldsymbol{\nu}})\hat{\boldsymbol{z}}_2, \tag{6.33}$$

where $\hat{\boldsymbol{z}}_2 = \hat{\boldsymbol{\nu}} - \boldsymbol{\alpha}_1$. Define $\tilde{\boldsymbol{z}}_2 = \boldsymbol{z}_2 - \hat{\boldsymbol{z}}_2$, note that $\tilde{\boldsymbol{z}}_2 = \tilde{\boldsymbol{\nu}}$.

Theorem 6.2 *Consider the plant (6.1) and (6.2) with the output feedback adaptive backstepping fuzzy control (6.32) and (6.33). For each compact set* Ω_0 *where*

$(\boldsymbol{\eta}(0), \boldsymbol{\nu}(0), \hat{\Theta}_H(0)) \in \Omega_0$, *the trajectories of the closed-loop system are semiglobally uniformly bounded. The closed-loop error signals,* $\boldsymbol{z}_1$, $\boldsymbol{z}_2$ *and* $\tilde{\Theta}_{\mathrm{H}}$ *will remain within the compact sets* Ω_{z_1}, Ω_{z_2} *and* $\Omega_{\Theta_{\mathrm{H}}}$ *respectively defined by*

$$\Omega_{z_1} = \{\boldsymbol{z}_1 \in R^3 | \ \|\boldsymbol{z}_1\| \leq \sqrt{D}\}, \tag{6.34}$$

$$\Omega_{z_2} = \{\boldsymbol{z}_2 \in R^3 | \ \|\boldsymbol{z}_2\| \leq \sqrt{\frac{D}{\lambda_{min}(\mathbf{M})}}\}, \tag{6.35}$$

$$\Omega_{\Theta_{\mathrm{H}}} = \{\tilde{\Theta}_{\mathrm{H}} \in R^{3M\times 1} | \ \|\tilde{\Theta}_{\mathrm{H}}\| \leq \sqrt{\frac{D}{\lambda_{min}(\mathbf{K}_3^{-1})}}\}, \tag{6.36}$$

where $D = 2(V_{\mathrm{H}}(0) + C/\rho)$ *with* ρ *and* C *as defined in (6.37) and (6.38) respectively.*

Proof: Assuming $\Phi^{\mathrm{T}}(\boldsymbol{\nu}) = \Phi^{\mathrm{T}}(\hat{\boldsymbol{\nu}})$, the time derivative of the Lyapunov function candidate V_{H} in (6.19) along the closed-loop trajectory with (6.32) and (6.33) yields

$$\begin{aligned}
\dot{V}_{\mathrm{H}} =& -\boldsymbol{z}_1^{\mathrm{T}}\mathbf{K}_1\boldsymbol{z}_1 + \boldsymbol{z}_2^{\mathrm{T}}[-\mathbf{K}_2\hat{\boldsymbol{z}}_2 - \mathbf{D}\tilde{\boldsymbol{\nu}} - \Phi(\boldsymbol{\nu})\tilde{\Theta}_{\mathrm{H}} + \boldsymbol{\omega}_{\mathrm{H}}] + \tilde{\Theta}_{\mathrm{H}}^{\mathrm{T}}\Phi^{\mathrm{T}}(\boldsymbol{\nu})\hat{\boldsymbol{z}}_2 \\
=& -\boldsymbol{z}_1^{\mathrm{T}}\mathbf{K}_1\boldsymbol{z}_1 - \boldsymbol{z}_2^{\mathrm{T}}\mathbf{K}_2\boldsymbol{z}_2 + \boldsymbol{z}_2^{\mathrm{T}}(\mathbf{K}_2 - \mathbf{D})\tilde{\boldsymbol{\nu}} + \boldsymbol{z}_2^{\mathrm{T}}\boldsymbol{\omega}_{\mathrm{H}} - \tilde{\Theta}_{\mathrm{H}}^{\mathrm{T}}\Phi^{\mathrm{T}}(\boldsymbol{\nu})\tilde{\boldsymbol{\nu}} \\
\leq& -\boldsymbol{z}_1^{\mathrm{T}}\mathbf{K}_1\boldsymbol{z}_1 - \boldsymbol{z}_2^{\mathrm{T}}(\mathbf{K}_2 - \frac{1+\lambda_{kd}^2}{2}\mathbf{I})\boldsymbol{z}_2 - \frac{1}{2}(\lambda_{kd}\boldsymbol{z}_2 - \tilde{\boldsymbol{\nu}})^{\mathrm{T}}(\lambda_{kd}\boldsymbol{z}_2 - \tilde{\boldsymbol{\nu}}) \\
&+ \frac{1}{2}\tilde{\boldsymbol{\nu}}^{\mathrm{T}}\tilde{\boldsymbol{\nu}} - \frac{1}{2}(\boldsymbol{z}_2 - \boldsymbol{\omega}_{\mathrm{H}})^{\mathrm{T}}(\boldsymbol{z}_2 - \boldsymbol{\omega}_{\mathrm{H}}) + \frac{1}{2}\boldsymbol{\omega}_{\mathrm{H}}^{\mathrm{T}}\boldsymbol{\omega}_{\mathrm{H}} - \tilde{\Theta}_{\mathrm{H}}^{\mathrm{T}}\Phi^{\mathrm{T}}(\boldsymbol{\nu})\tilde{\boldsymbol{\nu}} \\
\leq& -\boldsymbol{z}_1^{\mathrm{T}}\mathbf{K}_1\boldsymbol{z}_1 - \boldsymbol{z}_2^{\mathrm{T}}(\mathbf{K}_2 - \frac{1+\lambda_{kd}^2}{2}\mathbf{I})\boldsymbol{z}_2 + \tilde{\boldsymbol{\nu}}^{\mathrm{T}}\tilde{\boldsymbol{\nu}} + \frac{1}{2}\boldsymbol{\omega}_{\mathrm{H}}^{\mathrm{T}}\boldsymbol{\omega}_{\mathrm{H}} - \frac{1}{2}\|\tilde{\Theta}_{\mathrm{H}}\|^2 \\
\leq& -\rho V_{\mathrm{H}} + C
\end{aligned}$$

where λ_{kd} is the maximum eigenvalue of $\mathbf{K}_2 - \mathbf{D}$. ρ and C are defined as

$$\rho = \min[2\lambda_{min}(\mathbf{K}_1), \frac{2\lambda_{min}(\mathbf{K}_2 - \frac{1+\lambda_{kd}^2}{2}\mathbf{I})}{\lambda_{max}(\mathbf{M})}, \frac{1}{\lambda_{max}(\mathbf{K}_3^{-1})}] \tag{6.37}$$

$$C = \varepsilon^2 h_2^2 + \frac{1}{2}\boldsymbol{\omega}_{\mathrm{H}}^{\mathrm{T}}\boldsymbol{\omega}_{\mathrm{H}} \tag{6.38}$$

where $\lambda_{min}(\mathbf{A})$ and $\lambda_{max}(\mathbf{A})$ denote the minimum and maximum eigenvalues of matrix $\mathbf{A}$. To ensure $\rho > 0$, the gain matrix $\mathbf{K}_1$ and $\mathbf{K}_2$ are chosen such that $\lambda_{min}(\mathbf{K}_1) > 0$

and $\lambda_{min}(\mathbf{K}_2 - (1+\lambda_{kd}^2)\mathbf{I}/2) > 0$. Hence, the signals $\boldsymbol{z}_1$, $\boldsymbol{z}_2$ and $\tilde{\Theta}_{\mathrm{H}}$ are semiglobally uniformly bounded, and other signals involved are also bounded. Multiplying $\dot{V}_{\mathrm{H}} \leq -\rho V_{\mathrm{H}} + C$ by $e^{\rho t}$ yields

$$\frac{d}{dt}(V_{\mathrm{H}} e^{\rho t}) \leq C e^{\rho t}.$$

Integrating the above inequality yields

$$V_{\mathrm{H}} \leq (V_{\mathrm{H}}(0) - \frac{C}{\rho}) e^{-\rho t} + \frac{C}{\rho} \leq V_{\mathrm{H}}(0) + \frac{C}{\rho}.$$

Substituting V_{H} in (6.19) into the above inequality,

$$\frac{1}{2}\|\boldsymbol{z}_1\|^2 \leq V_{\mathrm{H}}(0) + \frac{C}{\rho}. \tag{6.39}$$

Hence, $\boldsymbol{z}_1$ is bounded by the compact set Ω_{z_1}. Bounds of $\boldsymbol{z}_2$ and $\tilde{\Theta}_{\mathrm{H}}$ can be similarly shown and this concludes the proof. ∎

Remark 6.2 *Theorem 6.2 is applicable to the situations where the faults described in subsection 6.1.3 occur. The proof procedures are similar to the proof of Theorem 6.2.*

Remark 6.3 *In this chapter, a rigorous theoretical treatment of the output feedback problem is proposed using high-gain observer. The theorem is obtained based on the assumption that the position measurements are perfect. If the position measurements are contaminated with zero mean Gaussian white noise within tolerance, careful implementation is necessary through designing ε to be sufficiently small. In this case, the transient performance may degrade.*

6.3 Simulation Studies

MSS as reviewed in [99], which is a Matlab/Simulink library developed in Norwegian University of Science and Technology, is employed as the platform for the simulation studies. Sea current with speed $V_c = 0.2$ m/s and direction $\beta_c = 30^\circ$ is included in the simulations, although ignored during the controller design. The ITTC wave spectrum with significant wave height $H_s = 3$ m and peak frequency $\omega_0 = 0.56$ rad/s is used to imitate rough sea with large waves. The encounter angle, which is the angle between the heading of the vessel and the direction of the wave, is set as $\beta = 30^\circ$. The container ship S-175 as shown in [37] is used as case study. Its main particulars are shown in Table 3.1. Similar to the setting in previous chapter, the sinusoidal trajectory is chosen as $\boldsymbol{\eta}_d = [x_d, y_d, \psi_d]^{\mathrm{T}}$, where $x_d = 8t$, $y_d = 200\cos(0.005\pi t)$, and $\psi_d = \arctan(y_d/x_d)$. The initial states are set as $[\boldsymbol{\eta}_0^{\mathrm{T}}, \boldsymbol{\nu}_0^{\mathrm{T}}] = [10, 210, 0, 0, 0, 0]$. All the IT2 FLSs in the state feedback controller (6.17) and (6.18) and the output feedback controller (6.32) and (6.33) are configured same as those in previous chapter.

6.3.1 State Feedback

In this subsection, the state feedback fault-tolerant adaptive backstepping IT2 FLC (6.17) and (6.18) is evaluated. Three conditions, i.e., no fault, faults in the plant, and faults in the controller are considered.

- No fault

If there is no fault, the control law expressed as (6.17) can be used for tracking control

$$\boldsymbol{\tau} = -\mathbf{J}^{\mathrm{T}}(\boldsymbol{\eta})\boldsymbol{z}_1 - \mathbf{K}_2\boldsymbol{z}_2 + \mathbf{D}\boldsymbol{\nu} + \Phi(\boldsymbol{\nu})\hat{\Theta}_{\mathrm{H}} + \mathbf{M}\dot{\boldsymbol{\alpha}}_1.$$

The desired and actual trajectory of the vessel under the state feedback fault-tolerant adaptive backstepping IT2 FLC, when $\mathbf{K}_1 = \mathrm{diag}[0.02, 0.02, 0.02]$, $\mathbf{K}_2 = \mathrm{diag}[4.3 \times 10^8, 4.3 \times 10^8, 4.3 \times 10^8]$, $k_{31} = 10^8$, $k_{32} = 10^9$ and $k_{33} = 10^{10}$, is shown in Fig. 6.1. The tracking errors of the vessel's actual trajectories to the desired trajectories are shown as solid line in Fig. 6.2. It can be observed that when there is no fault, the tracking errors under the proposed controller asymptotically converge to zero despite the time-varying hydrodynamic disturbances and the IT2 FLSs effectively approximate the complex disturbances $\boldsymbol{\tau}_H$.

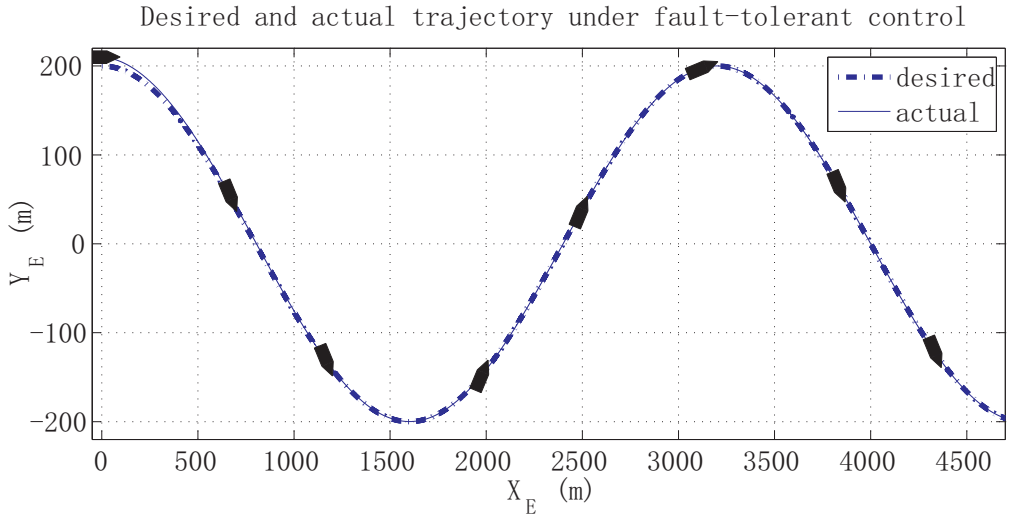

Figure 6.1: The desired and actual trajectory of the container ship under state feedback fault-tolerant adaptive backstepping IT2 FLC.

- Fault in the plant

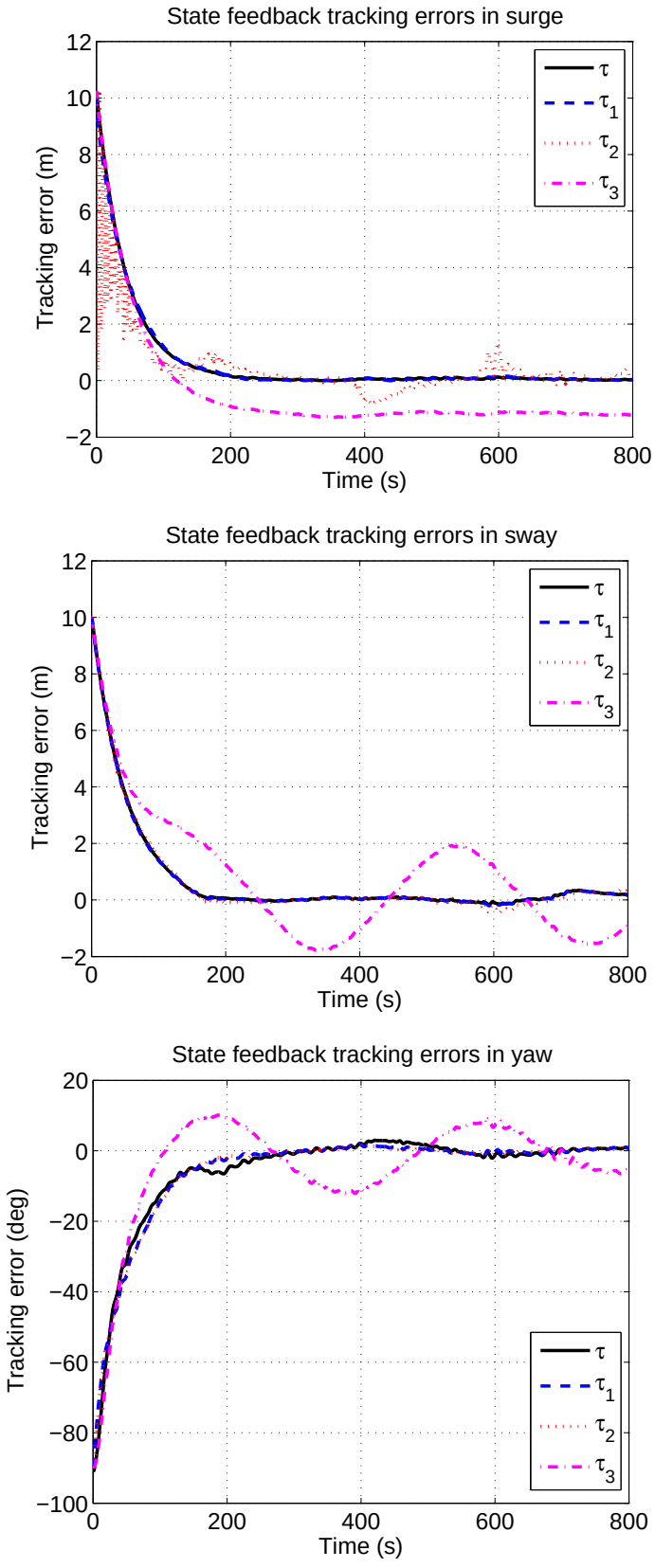

Figure 6.2: Tracking errors of state feedback adaptive backstepping IT2 FLC.

If there are faults in the plant as explained in subsection 6.1.3, the control law could be expressed as in (6.21) as

$$\boldsymbol{\tau}_1 = -\mathbf{J}^{\mathrm{T}}(\boldsymbol{\eta})\boldsymbol{z}_1 - \mathbf{K}_2\boldsymbol{z}_2 + \Phi(\boldsymbol{\nu})\hat{\Theta}_{\mathrm{H1}}.$$

Now the parameters $\mathbf{M}$ and $\mathbf{D}$ in (6.17) are unknown and set as $\mathbf{M} = \mathbf{0}$ and $\mathbf{D} = \mathbf{0}$. The tracking errors, when $\mathbf{K}_2 = \mathrm{diag}[4.3 \times 10^8, 4.3 \times 10^8, 4.3 \times 10^8]$, $k_{31} = 10^8$, $k_{32} = 10^9$ and $k_{33} = 10^{10}$, are shown as dash line in Fig. 6.2. It can be seen when there is modeling error or the loading condition and the trimming of the vessel change, the proposed controller can maintain satisfactory performance.

- Fault in the controller

As mentioned, the control law of the fault-tolerant adaptive backstepping IT2 FLC (6.17) can be viewed as a combination of two parts, a model based control law $-\mathbf{J}^{\mathrm{T}}(\boldsymbol{\eta})\boldsymbol{z}_1 - \mathbf{K}_2\boldsymbol{z}_2 + \mathbf{D}\boldsymbol{\nu} + \mathbf{M}\dot{\boldsymbol{\alpha}}_1$ and a compensator $\Phi(\boldsymbol{\nu})\hat{\Theta}_{\mathrm{H}}$. Imagine the model based control law and the compensator are implemented on two separate computers. If there are faults in the computer that operating the model based control law, the control law could be expressed as in (6.25) as

$$\boldsymbol{\tau}_2 = \Phi(\boldsymbol{\nu})\hat{\Theta}_{\mathrm{H2}}.$$

Now only the compensator is working. The tracking errors, when $k_{31} = 10^8$, $k_{32} = 10^9$ and $k_{33} = 10^{10}$, are shown as dot line in Fig. 6.2. It can be observed that the performance degrades a little. Small fluctuations in the tracking error of surge direction are observed, that is because the function to be modeled is more complex, but the structures of the IT2 FLSs are the same.

If there are faults in the computer that operating the compensator, the control law could be expressed as

$$\boldsymbol{\tau}_3 = -\mathbf{J}^{\mathrm{T}}(\boldsymbol{\eta})\boldsymbol{z}_1 - \mathbf{K}_2\boldsymbol{z}_2 + \mathbf{D}\boldsymbol{\nu} + \mathbf{M}\dot{\boldsymbol{\alpha}}_1.$$

The tracking errors, when $\mathbf{K}_1 = \mathrm{diag}[0.02, 0.02, 0.02]$, $\mathbf{K}_2 = \mathrm{diag}[4.3 \times 10^8, 4.3 \times 10^8, 4.3 \times 10^8]$, are shown as dot dash line in Fig. 6.2. It can be seen that the performance degrades very much. This is because $\boldsymbol{\tau}_3$ does not have any disturbance compensation due to the lack of information. However, in order to have better performance one can estimate a conservative bound of the disturbances and include the bound in $\boldsymbol{\tau}_3$ to dominate the disturbances. Meanwhile, a fault detection and isolation unit may be needed to switch the control laws when the compensator fails.

6.3.2 Impact of Control Gains

There are three control gains $\mathbf{K}_i$ $(i = 1, \ldots, 3)$ in the fault-tolerant adaptive backstepping IT2 FLC (6.17) and (6.18). The control gain $\mathbf{K}_1$ determines the relative convergence speed of vessel displacement and velocity and should be chosen first. The choice of the value of $\mathbf{K}_1$ depends on the plant. For container ship S-175 in the simulation studies, $\mathbf{K}_1$ is set as $\mathbf{K}_1 = \mathrm{diag}[0.02, 0.02, 0.02]$. The control gain $\mathbf{K}_3$ determines the convergent speed of adaptive law. To investigate the impact of the control gains in the proposed controller, simulations with the following three cases are conducted:

- Case 1: $\mathbf{K}_2 = \mathrm{diag}[4.3 \times 10^7, 4.3 \times 10^7, 4.3 \times 10^7]$, $k_{31} = 10^7$, $k_{32} = 10^8$ and $k_{33} = 10^9$;

- Case 2: $\mathbf{K}_2 = \text{diag}[4.3 \times 10^8, 4.3 \times 10^8, 4.3 \times 10^8]$, $k_{31} = 10^8$, $k_{32} = 10^9$ and $k_{33} = 10^{10}$;
- Case 3: $\mathbf{K}_2 = \text{diag}[4.3 \times 10^9, 4.3 \times 10^9, 4.3 \times 10^9]$, $k_{31} = 10^9$, $k_{32} = 10^{10}$ and $k_{33} = 10^{11}$.

The tracking errors of the vessel's actual trajectories to the desired trajectories under the the fault-tolerant adaptive backstepping IT2 FLC (6.17) and (6.18) for different control gains are shown in Fig. 6.3. It could be seen that as the values of control gains increase, the steady state errors decrease. And the performance improvement between Case 1 and Case 2 is more obvious than that between Case 2 and Case 3. In practice, large control gains are not recommended as they require larger actuators. Thus, the choice of control gains should consider both performance requirement and practical limitation.

6.3.3 Output Feedback

In this subsection, the high-gain observer (6.30) and (6.31) is used to obtain the velocity estimate $\hat{\boldsymbol{\nu}} = \mathbf{J}^{\mathrm{T}}(\boldsymbol{\eta})(\boldsymbol{\pi}_2/\varepsilon)$ with $\lambda_1 = 2$ and $\epsilon = 0.04$. Corresponding to subsection 6.3.1, the output feedback fault-tolerant adaptive backstepping IT2 FLC

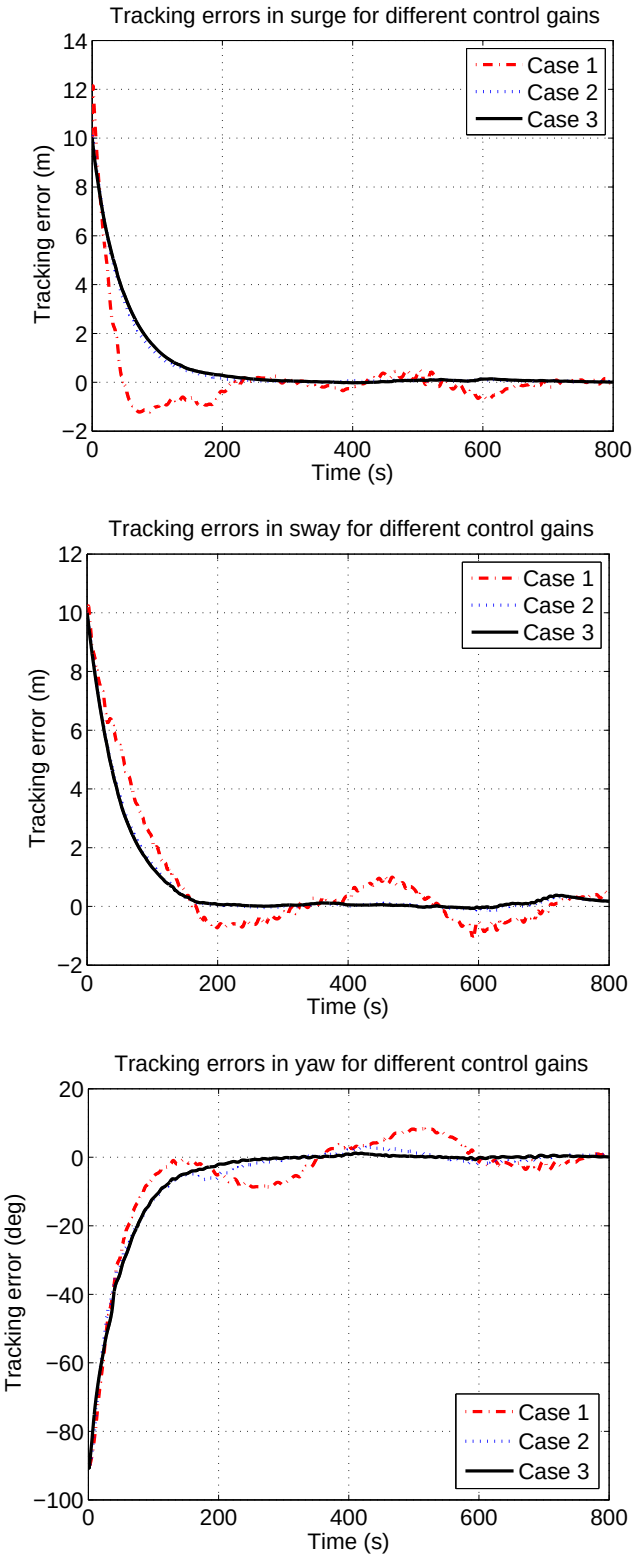

Figure 6.3: Tracking errors of fault-tolerant adaptive backstepping IT2 FLC with different control gains.

(6.32) and (6.33) is evaluated. Four different cases considered are as follows.

$$\boldsymbol{\tau}_o = -\mathbf{J}^{\mathrm{T}}(\boldsymbol{\eta})\boldsymbol{z}_1 - \mathbf{K}_2\hat{\boldsymbol{z}}_2 + \mathbf{D}\hat{\boldsymbol{\nu}} + \Phi(\hat{\boldsymbol{\nu}})\hat{\Theta}_{\mathrm{H}} + \mathbf{M}\dot{\boldsymbol{\alpha}}_1$$

$$\boldsymbol{\tau}_{o1} = -\mathbf{J}^{\mathrm{T}}(\boldsymbol{\eta})\boldsymbol{z}_1 - \mathbf{K}_2\hat{\boldsymbol{z}}_2 + \Phi(\hat{\boldsymbol{\nu}})\hat{\Theta}_{\mathrm{H1}}$$

$$\boldsymbol{\tau}_{o2} = \Phi(\hat{\boldsymbol{\nu}})\hat{\Theta}_{\mathrm{H2}}$$

$$\boldsymbol{\tau}_{o3} = -\mathbf{J}^{\mathrm{T}}(\boldsymbol{\eta})\boldsymbol{z}_1 - \mathbf{K}_2\hat{\boldsymbol{z}}_2 + \mathbf{D}\hat{\boldsymbol{\nu}} + \mathbf{M}\dot{\boldsymbol{\alpha}}_1$$

The simulation results for the above four cases, when $\mathbf{K}_1 = \mathrm{diag}[0.02, 0.02, 0.02]$, $\mathbf{K}_2 = \mathrm{diag}[4.3 \times 10^8, 4.3 \times 10^8, 4.3 \times 10^8]$, $k_{31} = 10^8$, $k_{32} = 10^9$ and $k_{33} = 10^{10}$, are shown in Fig. 6.4. From the performance of the proposed controller $\boldsymbol{\tau}_o$, it can be observed that the tracking errors under the output feedback controller converge to and remain within a small neighborhood of zero despite the time-varying hydrodynamic disturbances. If the tracking errors are desired to be lower, it can be reduced by several means to decrease C/ρ in Theorem 6.2. From the performance of the control law $\boldsymbol{\tau}_{o1}$, it can be seen similar to the state feedback case, the proposed controller can well handle modeling error and the changes of the loading condition and the trimming of the vessel. When the model based control law or the compensator in the proposed controller fails, it can be observed that the performance degrades very much in the output feedback cases. The reasons are similar to those for the sate feedback cases. In conclusion, the proposed state and output feedback controllers can well accommodate the faults in the plant, and maintain some "acceptable" level of performance when the faults in the controller occur.

The small time convergence of the high-gain observer estimates to the velocity signals for the four output feedback cases is clearly shown in Fig. 6.5. Within about

1 s, the estimates peak at their respective values. Here, saturation functions are used to overcome the peaking phenomenon of the high-gain observer. After saturation, the observer estimates converge rapidly to the actual velocity signals. Thereafter, the estimates remain in a small neighborhood of the velocity signals.

6.4 Conclusions

In this chapter, both state feedback and output feedback fault-tolerant adaptive backstepping IT2 FLCs have been designed for tracking control of fully actuated surface vessels in face of time-varying hydrodynamic disturbances. For the state feedback case, the sufficient condition, under which the tracking errors will semiglobally asymptotically converge to zero, is proposed. For the output feedback case, a high-gain observer is used to estimate the unmeasurable states. The closed-loop signals under this case are semiglobally uniformly bounded and converge to a compact set which can be made small through appropriate choice of design parameters. Simulation results have demonstrated that the proposed state and output feedback controllers are effective in reducing the tracking errors, and able to accommodate certain faults in the plant and the controllers.

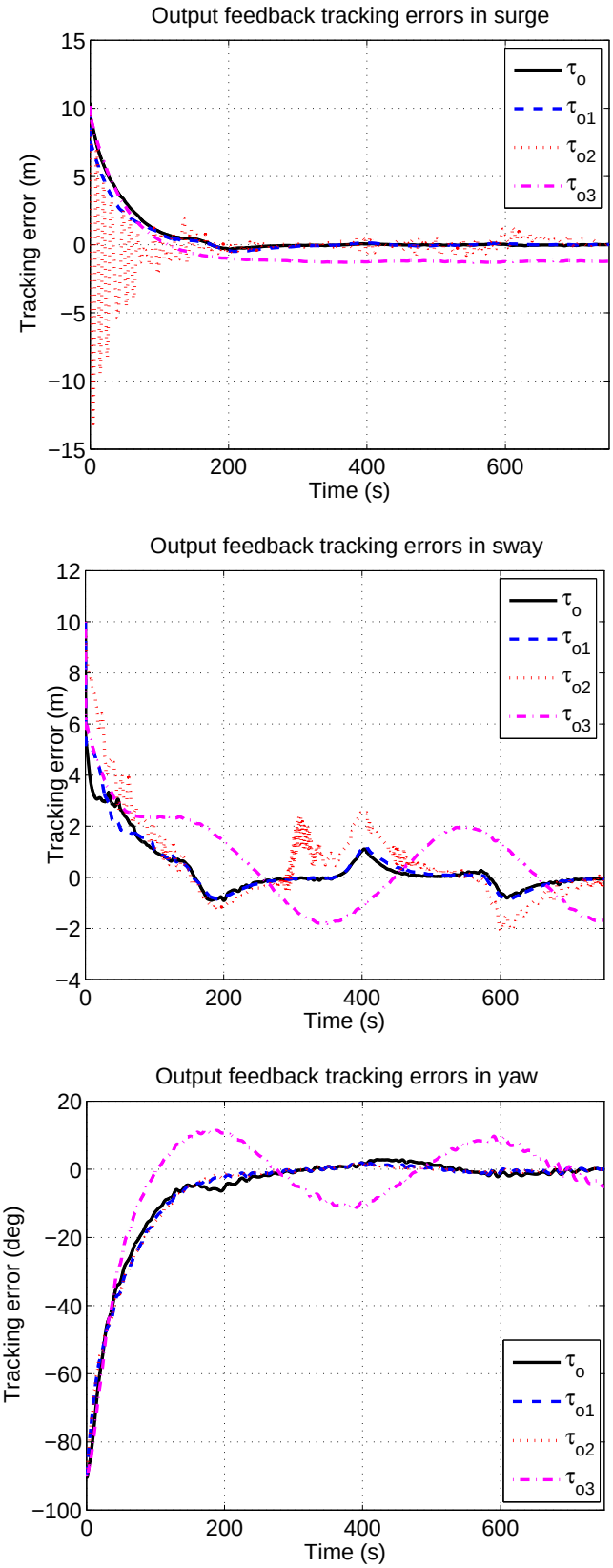

Figure 6.4: Tracking errors of output feedback adaptive backstepping IT2 FLC.

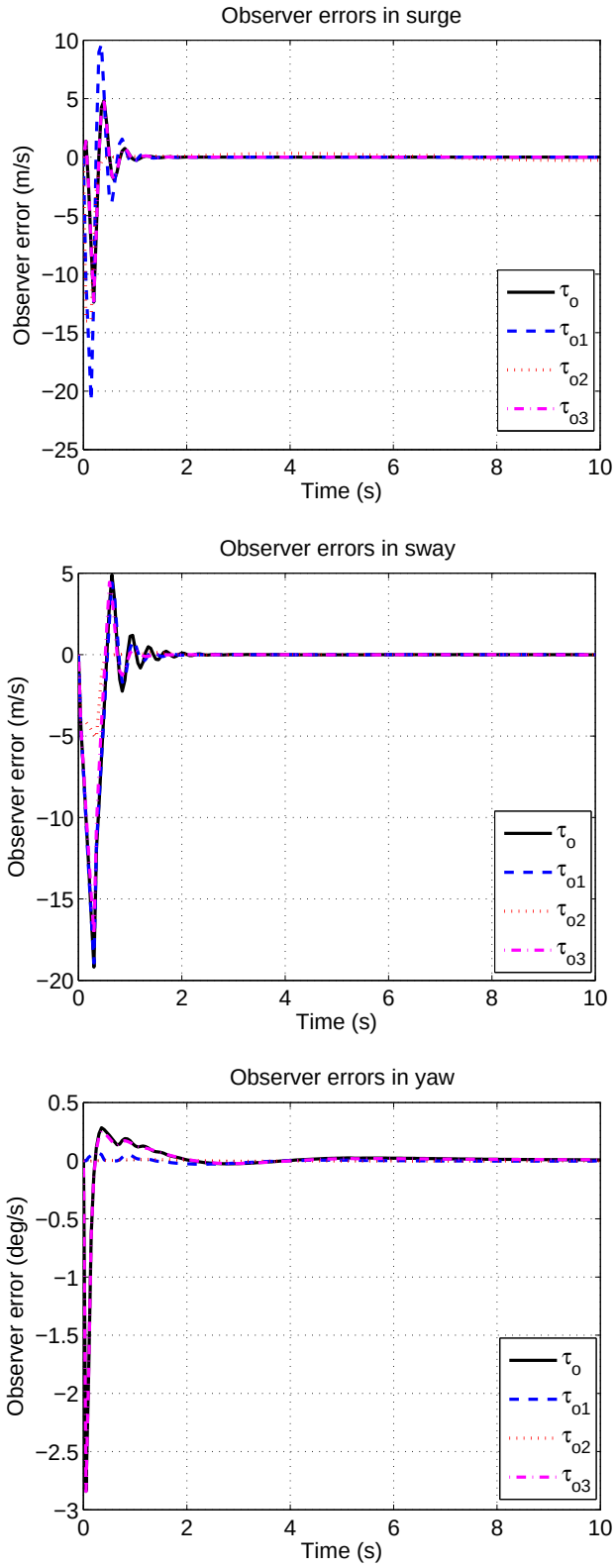

Figure 6.5: The errors $\tilde{\boldsymbol{\nu}}$ between actual velocity signals and their estimates for four output feedback control cases.

Chapter 7

Conclusions

7.1 General Conclusions

This thesis focused on marine control system design by means of adaptive IT2 fuzzy logic control to handle the time-varying disturbances and uncertainties presented in marine operations. The key results are as follows:

- **Dynamic Positioning**

In this thesis, an indirect adaptive IT2 FLC and a passive adaptive IT2 fuzzy observer have been designed for DP vessels with attached thrusters in the presence of time-varying hydrodynamic disturbances. The combination of approximation-based adaptive technique and IT2 FLS allows the time-varying hydrodynamic disturbances in the vessel model to be handled without exact information on them. The stabilities of the adaptive IT2 fuzzy controller and observer were explored separately through Lyapunov and passive analyses where the regulation errors of the adaptive IT2 fuzzy controller would semiglobally asymptotically converge to zero, if the IT2 FLS adequately approximates the underlying function. And the estimation errors of the adaptive IT2 fuzzy observer are semiglobally uniformly ultimately bounded. Rigorous analysis showed that the adaptive IT2 fuzzy controller generated a passive

closed-loop system and the adaptive IT2 fuzzy observer resulted in a passive observer error dynamics. Simulation results with a container ship have shown that both the adaptive IT2 fuzzy controller and observer are efficient and robust. IT2 FLS has comparable universal approximation property with type-1 FLS in DP application. As the kinematics and dynamics of vessels are very typical in mechanical systems, the proposed method could be used in regulation control of other mechanical systems such as mobile vehicle and unmanned aerial vehicle. The main contributions of this piece of work are: (i) the combination of approximation-based adaptive technique and IT2 FLS is proposed to handle disturbances and uncertainties in regulation and observer design problem; (ii) a control scheme including both controller and observer, which is able to adjust its parameters subject to the variations in vessel loading condition and sea state, is introduced for DP; (iii) the stabilities of the adaptive IT2 fuzzy controller and observer for DP are rigorously analyzed; (iv) passive nonlinear observer [25] is extended and better estimation performance is achieved.

- **Trajectory Tracking Control**

The problem of tracking control of fully actuated surface vessels along a desired trajectory in the presence of time-varying hydrodynamic disturbances was investigated in this thesis. The combination of approximation-based adaptive technique and IT2 FLS was also used to handle time-varying hydrodynamic disturbances and uncertainties in the tracking control problem. An indirect adaptive IT2 FLC as well as a direct adaptive IT2 FLC were first proposed. Although designed through different approaches, the closed-loop systems for both indirect and direct IT2 FLCs are

similar and passive. The semiglobal asymptotic convergence of the tracking errors in the closed-loop systems was shown by means of passive analysis and Lyapunov synthesis. Simulation results have demonstrated that the indirect and direct adaptive IT2 fuzzy techniques are effective, and reduce the integral of time-weighted absolute tracking errors for the indirect adaptive FLC by at least 21.9% and 18.0% for the direct adaptive case compared to type-1 FLCs. It was also shown that the IT2 FLS has comparable approximation property even with fewer fuzzy rules when compared to its type-1 counterpart in tracking control application. Although possessing good performance, both the indirect and direct IT2 FLCs show their limitations in the situations where the velocities of the surface vessels are not measurable. This is because both the indirect and direct IT2 FLCs were designed based on the assumption that all the state variables of the vessel, i.e. displacements and velocities are measured by its own on-board devices. To overcome this limitation and improve the reliability of the tracking controller, a state feedback fault-tolerant adaptive backstepping IT2 FLC was then introduced, with the option of high-gain observer for output feedback. Through backstepping and Lyapunov synthesis, the stabilities of the closed-loop systems were explored where sufficient condition for guaranteeing semiglobal asymptotic convergence of the tracking errors in sate feedback control was proposed, whereas semiglobal uniform boundedness of the closed-loop signals in output feedback control was guaranteed. The combination of backstepping control and approximation-based adaptive technique allows the proposed controller to be able to accommodate faults such as the changes of the loading conditions and trimming of the vessels, and failure of some parts of the control law. Simulation studies with a container ship were con-

ducted. Results showed both the state and output feedback controllers are effective and robust. Similarly, the proposed method could be used in tracking control of other mechanical systems such as mobile vehicle and unmanned aerial vehicle. The main contributions of this piece of work are: (i) the combination of approximation-based adaptive technique and IT2 FLS is proposed to handle disturbances and uncertainties in tracking control problem; (ii) an indirect and a direct adaptive IT2 FLC, which have similar passive and stable closed-loop systems, are proposed for tracking control; (iii) both a state feedback and an output feedback fault-tolerant adaptive backstepping IT2 FLC are constructed for tracking control; (iv) detailed stability analyses of all the proposed controller are described.

7.2 Future Research

The efficiency of the control algorithms designed for DP and tracking control of marine vessels are verified by means of simulation. Whether their performances could be guaranteed in practice is not very clear. It would be laudable if experiments with real vessels in sea [25, 112] or scaled models of vessels in towing tank [33] could be conducted to test the performances of the algorithms.

In [113], a separation principle of PD-like controller and passive nonlinear observer was proposed for DP of ships based on cascaded nonlinear systems and Lyapunov theory. Further study is needed to propose a similar separation principle for the adaptive IT2 fuzzy controller and observer in DP.

Due to the developments in computer science, propulsion systems and modern

sensor technology, more and more attentions are paid on the reliability of marine control systems. Although the fault-tolerant marine control systems are explored in this thesis, the faults that the proposed control algorithm can accommodate are limited. In order to make the marine control systems more reliable, future research should attempt to propose more complex fault-tolerant marine control systems which include fault detection and isolation unit and supervision system.

In DP and tracking control of marine vessels, it is shown that IT2 FLS has comparable approximation property with type-1 FLS. However, due to the obstacle caused by switch points in type-reduction of IT2 FLS, there is still a lack of theoretical analysis showing the reason behind this. It will be interesting to extend the works [89]– [91] to investigate the universal approximation property of IT2 FLS rigorously in future study.

Bibliography

[1] S. Bennet, *A History of Control Engineering 1800-1930*. London: Peter Peregrinus, 1979.

[2] N. Minorsky, "Directional stability of automatically steered bodies," *Journal of American Sociaty of Naval Engineers*, vol. 34, no. 2, pp. 280–309, May 1922.

[3] R. E. Kalman, "A new approach to linear filtering and prediction problems," *ASME Transactions, Series D: Journal of Basic Engineering*, vol. 82, no. 1, pp. 35–45, 1960.

[4] R. E. Kalman and R. S. Bucy, "New results in linear filtering and prediction theory," *ASME Transactions, Series D: Journal of Basic Engineering*, vol. 83, no. 1, pp. 95–108, 1961.

[5] T. Koyama, "On the optimum automatic steering system of ships at sea," *Society of Naval Architects of Japan*, vol. 4, pp. 142–156, 1970.

[6] J. V. Amerongen and H. R. V. N. Lemke, "Criteria for optimum steering of ships," in *Proceedings of Symposium on Ship Steering Automatic Control*, Genova, Italy, 1980.

[7] T. I. Fossen, *Guidance and Control of Ocean Vehicles*. Trondheim, Norway: John Wiley and Sons Ltd, 1994.

[8] ——, *Marine Control Systems: Guidance Navigation and Control of Ships Rigs and Underwater Vehicles*. Trondheim, Norway: Marine Cybernetics, 2002.

[9] J. S. Sargent and P. N. Cowgil, "Design considerations for dynamically positioned utility vessels," in *Proceedings of 8th Offshore Technology Conference*, Houston, USA, 1976.

[10] J. G. Balchen, N. A. Jensen, and S. Sælid, "Dynamic positioning using kalman filtering and optimal control theory," in *IFAC/IFIP Symposium on Automatic Offshore Oil Field Operation*, Amsterdam, The Netherlands, 1976, pp. 183–186.

[11] J. G. Balchen, N. A. Jenssen, E. Mathisen, and S. Sælid, "Dynamic positioning system based on kalman filtering and optimal control," *Modeling, Identification and Control*, vol. 1, no. 3, pp. 135–163, 1980.

[12] P. T.-K. Fung and M. J. Grimble, "Dynamic ship positioning using a self tuning kalman filter," *IEEE Transactions on Automatic Control*, vol. 28, no. 3, pp. 339–349, 1983.

[13] T. I. Fossen, S. I. Sagatun, and A. J. Sørensen, "Identification of dynamically positioned ships," *Control Engineering Practice*, vol. 4, no. 3, pp. 369–376, 1996.

[14] A. J. Sørensen and J. P. Strand, "Positioning of small waterplane area marine constructions with roll and pitch damping," *Control Engineering Practice*, vol. 8, no. 2, pp. 205–213, 2000.

[15] S. K. Volovodov, M. G. Chernjaev, A. J. Kaverinsky, S. S. Volovodov, and B. P. Lampe, "Control princiiple for dynamic positioning of offshore drilling platforms and ships," in *Proceedings of 11th Symposium on Maritime Elek-*

trotechnik, Elektronik and informationstechnik, Rostock, Germany, 2004.

[16] T. Perez and A. Donaire, "Constrained control design for dynamic positioning of marine vehicles with control allocation," *Modelling, Identification and Control*, vol. 30, no. 2, pp. 57–70, 2009.

[17] R. I. Stephens, K. J. Burnham, and P. J. Reeve, "A practical approach to the design of fuzzy controllers with application to dynamic ship positioning," in *Proceedings of IFAC Conference on Control Applications in Marine Systems*, Trondheim, Norway, 1995.

[18] M. F. Aarset, J. P. Strand, and T. I. Fossen, "Nonlinear vectorial observer backstepping with integral action and wave filtering for ships," in *Proceedings of IFAC Conference on Control Applications in Marine Systems*, Fukuoka, Japan, 1998.

[19] T. I. Fossen and Å. Grøvlen, "Nonlinear output feedback control of dynamically positioned ships using vectorial observer backstepping," *IEEE Transactions on Control Systems Technology*, vol. 6, no. 1, pp. 121–128, 1998.

[20] D. S. Bertin, S. M. Bittanti, and S. M. Savaresi, "Dynamic positioning of a single-thruster vessel by feedback linearization," in *Proceedings of IFAC Conference on Manoeuvring and Control of Marine Craft*, Aalborg, Denmark, 2000.

[21] J. J. Slotine and W. Li, *Applied Nonlinear Control*. Englewood Cliffs, NJ: Prentice Hall, 1991.

[22] A. Isidori, *Nonlinear Control Systems*. London: Springer, 1995.

[23] T. I. Fossen, "A survey on nonlinear ship control: From theory to practise," in *Proceedings of 5th IFAC Conference on Manoeuvring and Control of Marine Craft*, Aalborg, Denmark, 2000.

[24] H. K. Khalil, *Nonlinear Systems*. London: Prentice Hall, 2002.

[25] T. I. Fossen and J. P. Strand, "Passive nonlinear observer design for ships using lyapunov mehtods: Experimental results with a supply vessel," *Automatica*, vol. 35, no. 1, pp. 3–16, 1999.

[26] A. J. Sørensen, B. J. Leira, J. P. Strand, and C. M. Larsen, "Optimal setpoint chasing in dynamic positioning of deep-water drilling and intervention vessels," *Journal of Robust and Nonlinear Control*, vol. 11, pp. 1187–1205, 2001.

[27] B. J. Leira, A. J. Sørensen, P. I. Berntsen, and O. M. Aamo, "Structure reliability criteria and dynamic positioning of marine vessels," *International Journal of Materials and Structural Reliability*, vol. 4, no. 2, pp. 161–174, 2006.

[28] T. I. Fossen and J. P. Strand, "Nonlinear passive weather optimal positioning control system for ships and rigs: experimental results," *Automatica*, vol. 37, no. 5, pp. 701–715, 1999.

[29] H. M. Morithita and B. J. Cornet, "Dynamics of a turret-fpso and shuttle vessel due to current," in *Proceedings of IFAC Conference on Control Applications in Marine Systems*, Fukuoka, Japan, 1998.

[30] H. M. Morithita, E. A. Tannuri, and T. T. Bravin, "Methodology for dynamic analysis of offloading operations," in *Proceedings of IFAC Conference on Control Applications in Marine Systems*, Ancona, Italy, 2004.

[31] E. A. Tannuri, A. C. Saad, and H. M. Morishita, "Offloading operation with a dp shuttle tanker: comparision between full scale measurements and numerical simulation results," in *Proceedings of IFAC Conference on Manoeuvring and Control of Marine Craft*, Guarujá, Brazil, 2009.

[32] A. J. Sørensen, S. T. Quek, and T. D. Nguyen, "Improved operability and safety of dp vessels using hybrid control concept," in *Proceedings of International Conference on Technology and Operation of Offshore Support Vessels*, Singapore, 2005.

[33] T. D. Nguyen, "Design of hybrid marine control systems for dynamic positioning," Ph.D dissertation, Dept. Civil Eng., NUS, Singapore, 2006.

[34] T. D. Nguyen, A. J. Sørensen, and S. T. Quek, "Design of hybrid controller for dynamic positioning from calm to extreme sea conditions," *Automatica*, vol. 43, no. 5, 2007.

[35] ——, "Multi-operational hybrid controller structure for station keeping and transit operations of marine vessels," *IEEE Transactions on Control Systems Technology*, vol. 16, no. 3, pp. 491–498, 2008.

[36] D. T. Nguyen and A. J. Sørensen, "Switching control for thruster-assisted position mooring," *Control Engineering Practice*, vol. 17, no. 9, pp. 985–994, 2009.

[37] T. I. Fossen, "Nonliear time-domain strip theory formulation for low speed manoeuving and station-keeping," *Modelling, Identification and Control*, vol. 25, no. 4, pp. 201–221, 2004.

[38] T. Perez and T. I. Fossen, "Kinematic models for manoeuvring and seakeeping

of marine vessels," *Modelling, Identification and Control*, vol. 28, no. 1, pp. 19–30, 2007.

[39] K. S. Narendra and A. M. Annaswamy, *Stable Adaptive Systems*. Englewood Cliffs, NJ: Prentice-Hall, 1989.

[40] K. J. Åström and B. Wittenmark, *Adaptive Control*. Addison-Wesley, 1995.

[41] L. X. Wang, "Stable adaptive fuzzy control of nonlinear systems," *IEEE Transactions on Fuzzy Systems*, vol. 1, no. 2, pp. 146–155, May 1993.

[42] S. S. Ge, C. C. Hang, T. H. Lee, and T. Zhang, *Stable Adaptive Neural Network Control*. Boston, MA: Kluwer, 2001.

[43] J. H. Park, G. T. Park, S. H. Kim, and C. J. Moon, "Direct adaptive self-structuring fuzzy controller for nonaffine nonlinear system," *Fuzzy Sets and Systems*, vol. 153, pp. 429–445, 2005.

[44] J. A. Farrell and M. M. Polycarpou, *Adaptive Approximation Based Control: Unifying Neural, Fuzzy and Traditional Adaptive Approximation Approaches*. USA: Wiley-Interscience, 2007.

[45] M. Wang, B. Chen, X. P. Liu, and P. Shi, "Adaptive fuzzy tracking control for a class of perturbed strict-feedback nonlinear time-delay systems," *Fuzzy Sets and Systems*, vol. 159, pp. 949–967, 2008.

[46] Y. J. Liu, S. C. Tong, and T. S. Li, "Observer-based adaptive fuzzy tracking control for a class of uncertain nonlinear mimo systems," *Fuzzy Sets and Systems*, vol. 164, pp. 25–44, 2011.

[47] M. W. Nie and W. W. Tan, "Stable adaptive fuzzy pd plus pi controller for nonlinear uncertain systems," *Fuzzy Sets and Systems*, vol. 179, pp. 1–19, 2011.

[48] T. C. Lin and M. C. Chen, "Adaptive hybrid type-2 intelligent sliding mode control for uncertain nonlinear multivariable dynamical systems," *Fuzzy Sets and Systems*, vol. 171, pp. 44–71, 2011.

[49] T. Holzhüter and R. Schultze, "On the experience with a high precision track controller for commercial ships," *Control Engineering Practice*, vol. 4, no. 3, pp. 343–350, 1996.

[50] T. Holzhüter, "LQG approach for the high precision track control of ships," *IEEE Proceedings on Control Theory and Application*, vol. 144, no. 2, pp. 121–127, 1997.

[51] J. M. Godhavn, T. I. Fossen, and S. P. Berge, "Nonlinear and adaptive backstepping designs for tracking control of ships," *International Journal of Adaptive Control Signal Processing*, vol. 12, pp. 649–670, 1998.

[52] K. D. Do and J. Pan, *Control of Ships and Underwater Vehicles*. Australia: Springer, 2009.

[53] M. Wondergem, E. Lefeber, K. Y. Petersen, and H. Nijmeijer, "Output feedback tracking of ships," *IEEE Transactions on Control Systems Technology*, vol. 19, no. 2, pp. 442–448, Mar. 2011.

[54] R. J. Patton, "Fault tolerant control systems: the 1997 situation," in *Proceedings of IFAC Symposium on Fault Detection, Supervision and Safety for Technical Processes*, Brussels, 1997, pp. 1033–1054.

[55] M. Blanke, M. Staroswiecki, and N. E. Wu, "Concepts and methods in fault tolerant control," in *Proceedings of 2001 Americal Control Conference*, Arlington, VA, 2001, pp. 2606–2620.

[56] R. Skjetne, T. I. Fossen, and P. V. Kokotović, "Adaptive maneuvering, with experiments, for a model ship in a marine control laboratory," *Automatica*, vol. 41, pp. 289–298, 2005.

[57] A. J. Sørensen, *Marine Cybernetics: Modelling and Control*, 5th ed. Trondheim, Norway: Dept. Marine Technology, NTNU, 2005.

[58] L. A. Zadeh, "Fuzzy sets," *Information and Control*, vol. 8, pp. 338–353, 1965.

[59] K. M. Passino and S. Yurkovich, *Fuzzy Control*. Menlo Park, CA: Addison Wesley Longman, 1998.

[60] I. S. Shaw, *Fuzzy Control of Industrial Systems: Theory and Applications*. Norwell, USA: Kluwer Academic Publishers, 1998.

[61] D. Driankov and R. Palm, *Advances in Fuzzy Control*. Germany: Springer-Verlag, 1998.

[62] K. Tanaka and H. O. Wang, *Fuzzy control systems design and analysis: a linear matrix inequality approach*. Singapore: John Wiley and Sons, 2001.

[63] K. Michels, F. Klawonn, R. Kruse, and A. Nürnberger, *Fuzzy Control: Fundamentals, Stability and Design of Fuzzy Controllers*. New York: Springer, 2006.

[64] L. Zadeh, "The concept of a linguistic variable and its application to approxi-

mate reasoning," *Information Sciences*, vol. 8, pp. 199–249, 1975.

[65] M. Mizumoto and K. Tanaka, "Fuzzy sets of type 2 under algebraic product and algebraic sum," *Fuzzy Sets and Systems*, vol. 5, pp. 277–290, 1981.

[66] D. Dubois and H. Prade, *Fuzzy Sets and Systems: Theory and Applications*. New York: Academic Press, 1982.

[67] M. B. Gorzalczany, "A method of inference in approximate reasoning based on interval valued fuzzy sets," *Fuzzy Sets and Systems*, vol. 21, pp. 1–17, 1987.

[68] I. B. Türkşen, "Fuzzy normal forms," *Fuzzy Sets and Systems*, vol. 69, pp. 319–346, 1995.

[69] D. G. Schwartz, "The case for an interval-based representation of linguistic truth," *Fuzzy Sets and Systems*, vol. 17, pp. 153–165, 1985.

[70] G. Klir and T. Folger, *Fuzzy Sets, Uncertainty, and Information*. Prentice-Hall, 1988.

[71] N. Karnik and J. Mendel, "Centroid of a type-2 fuzzy set," *Information Sciences*, vol. 132, pp. 195–220, 2001.

[72] Q. Liang and J. M. Mendel, "Interval type-2 fuzzy logic systems: theory and design," *IEEE Transactions on Fuzzy Systems*, vol. 8, pp. 535–549, 2000.

[73] N. N. Karnik, J. M. Mendel, and Q. Liang, "Type-2 fuzzy logic systems," *IEEE Transactions on Fuzzy Systems*, vol. 7, no. 6, pp. 643–658, Dec. 1999.

[74] J. M. Mendel, *Uncertain Rule-Based Fuzzy Logic System: Introduction and New Directions*. Upper Saddle River, NJ: Prentice-Hall, 2001.

[75] J. M. Mendel and R. I. John, "Type-2 fuzzy sets made simple," *IEEE Transactions on Fuzzy Systems*, vol. 10, no. 2, pp. 117–127, Apr. 2002.

[76] R. John and S. Coupland, "Type-2 fuzzy logic: A historical view," *IEEE Computational Intelligence Magazine*, vol. 2, no. 1, pp. 57–62, Feb. 2007.

[77] T. Dereli, A. Baykasoglu, K. Altun, A. Durmusoglu, and I. B. Türksen, "Industrial applications of type-2 fuzzy sets and systems: a concise review," *Computers in Industry*, vol. 62, pp. 125–137, 2011.

[78] Q. Liang, N. N. Karnik, and J. M. Mendel, "Connection admission control in atm networks using survey-based type-2 fuzzy logic systems," *IEEE Transactions on Fuzzy Systems*, vol. 30, no. 3, pp. 329–339, Aug. 2000.

[79] H. Hagras, "A hierarchical type-2 fuzzy logic control architecture for autonomous mobile robots," *IEEE Transactions on Fuzzy Systems*, vol. 12, no. 4, pp. 524–539, Aug. 2004.

[80] D. R. Wu and W. W. Tan, "A type-2 fuzzy logic controller for the liquid-level process," in *Proceedings of 2004 IEEE International Conference on Fuzzy Systems*, Budapest, 2004, pp. 953–958.

[81] H. Hagras, F. Doctor, V. Callaghan, and A. Lopez, "An incremental adaptive life long learning approach for type-2 fuzzy embedded agents in ambient intelligent environments," *IEEE Transactions on Fuzzy Systems*, vol. 15, no. 1, pp. 41–55, 2007.

[82] E. A. Jammeh, M. Fleury, C. Wagner, H. Hagras, and M. Ghanbari, "Interval type-2 fuzzy logic congestion control for video streaming across ip networks,"

IEEE Transactions on Fuzzy Systems, vol. 17, no. 5, pp. 1123–1142, Oct. 2009.

[83] J. M. Mendel and D. Wu, *Perceptual Computing: Aiding People in Making Subjective Judgments*. Wiley-IEEE Press, 2010.

[84] X. T. Chen and W. W. Tan, "A type-2 fuzzy logic controller for dynamic positioning systems," in *Proceedings of 2010 IEEE International Conference on Control and Automation*, Xiamen, China, 2010, pp. 1013–1018.

[85] L. X. Wang and J. M. Mendel, "Fuzzy basis functions, universal approximation, and orthogonal least-squares learning," *IEEE Transactions on Neural Networks*, vol. 3, no. 5, pp. 807–814, Sep. 1992.

[86] J. L. Castro, "Fuzzy logic controllers are universal approximators," *IEEE Transactions on System, Man and Cybernetics*, vol. 25, no. 4, pp. 629–635, Apr. 1995.

[87] X. J. Zeng and M. G. Singh, "Approximation accuracy analysis of fuzzy systems as function approximators," *IEEE Transactions on Fuzzy Systems*, vol. 4, no. 1, pp. 44–63, Jan. 1996.

[88] H. Ying, *Fuzzy Control and Modeling: Analytical Foundations and Applications*. New York: IEEE Press, 2000.

[89] ——, "General interal type-2 mamdani fuzzy systems are universal approximators," in *Proceedings of 27th North American Fuzzy Information Processing Society Conference*, New York, 2008.

[90] ——, "Interal type-2 takagi-sugeno fuzzy systems with linear rule consequent are universal approximators," in *Proceedings of 28th North American Fuzzy*

Information Processing Society Conference, Cincinnati, Ohio, 2009.

[91] F. You and H. Ying, "Interal type-2 boolean fuzzy systems are universal approximators," in *Proceedings of 29th North American Fuzzy Information Processing Society Conference*, Toronto, Canada, 2010.

[92] T. I. Fossen, *Handbook of Marine Craft Hydrodynamics and Motion Control*. United Kingdom: Wiley-Blackwell, 2011.

[93] SNAME, "Nomenclature for treating the motion of a submerged body through a fluid," The Society of Naval Architects and Marine Engineers, Technical and Research Bulletin 1-5, 1950.

[94] M. A. Abkowitz, *Lectures on Ship Hydrodynamics: Steering and Maneuverability*. Denmark: Hydro- and Aerodynamic's Laboratory, 1964.

[95] T. I. Fossen, "Nonlinear modeling and control of underwater vehicles," Ph.D dissertation, Department of Engineering Cybernetics, Norwegian University of Sciency and Technoloty, Trondheim, 1991.

[96] S. I. Sagatun and T. I. Fossen, "Lagrangian formulation of underwater vehicles' dynamics," in *Proceedings of 1991 IEEE International Conference on System, Man and Cybernetics*, Charlottesville, VA, 1991, pp. 1029–1034.

[97] S. P. Berge and T. I. Fossen, "On the properties of the nonlinear ship equations of motion," *Journal of Mathematical and Computer Modelling of Dynamical Systems*, vol. 6, no. 4, pp. 365–381, Dec. 2000.

[98] MSS, "Marine systems simulator. viewed 27.07.2011," 2010,

http://www.marinecontrol.org.

[99] T. Perez, Ø. N. Smogeli, T. I. Fossen, and A. J. Sørensen, "An overview of the marine system simulator (MSS): a simulink toolbox for marine control system," *Modelling, Identification and Control*, vol. 27, no. 4, pp. 259–275, 2006.

[100] V. Kreinovich, G. C. Mouzouris, and H. T. Nguyen, "Fuzzy rule based modeling as a universal approximation tool," *Fuzzy Systems, Modeling and Control*, pp. 135–196, May 1998.

[101] I. B. Türkşen, "Type-2 representation and reasoning for CWW," *Fuzzy Sets and Systems*, vol. 127, pp. 17–36, 2002.

[102] J. Aisbett, J. T. Richard, and D. Morgenthaler, "Multivariate modeling and type-2 fuzzy sets," *Fuzzy Sets and Systems*, vol. 163, pp. 78–95, 2011.

[103] J. M. Mendel, "Computing derivatives in interval type-2 fuzzy logic system," *IEEE Transactions on Fuzzy Systems*, vol. 12, no. 1, pp. 84–98, Feb. 2004.

[104] C. F. Juang, R. B. Huang, and Y. Y. Lin, "A recurrent self-evolving interval type-2 fuzzy neural network for dynamic system processing," *IEEE Transactions on Fuzzy Systems*, vol. 17, no. 5, pp. 1092–1105, Oct. 2009.

[105] B. Brogliato, R. Lozano, B. Maschke, and O. Egeland, *Dissipative Systems Analysis and Control: Theory and Applications*, 2nd ed. London: Springer Verlag, 2007.

[106] J. Mendel and F. Liu, "Super-exponential convergence of the Karnik-Mendel algorithms for computing the centroid of an interval type-2 fuzzy set," *IEEE*

Transactions on Fuzzy Systems, vol. 15, no. 2, pp. 309–320, Apr. 2007.

[107] C. Lynch and H. Hagras, "Developing embedded type-2 fuzzy logic controllers for handling the uncertainties in marine diesel engine speed control," *International Journal of Computational Intelligence Research*, vol. 4, no. 4, pp. 402–420, Oct. 2008.

[108] S. Sælid, N. A. Jenssen, and J. G. Balchen, "Design and analysis of a dynamic positioning system based on kalman filtering and optimal control," *IEEE Transactions on Automatic Control*, vol. 28, no. 3, pp. 331–339, 1983.

[109] S. S. Ge and C. Wang, "Adaptive neural network control of uncertain mimo non-linear system," *IEEE Transactions on Neural Networks*, vol. 15, no. 3, pp. 674–692, May 2004.

[110] E. E. Mitropoulos, "E-navigation; a glimpse into the future?" *IMO NEWS*, vol. 2, pp. 4–4, 2006.

[111] S. Behtash, "Robust output tracking for nonlinear system," *International Journal of Control*, vol. 51, no. 6, pp. 931–933, 1990.

[112] A. J. Sørensen, S. I. Sagatun, and T. I. Fossen, "Design of a dynamic positioning system using model based cotrol," *Control Engineering Practice*, vol. 4, no. 3, pp. 359–368, 1996.

[113] A. Loria, T. I. Fossen, and E. Panteley, "A separation princeple for dynamic positioning of ships: theoretical and experimental results," *IEEE Transactions on Control Systems Technology*, vol. 8, no. 2, pp. 332–343, 2000.

List of Publications

The contents of this thesis are based on the following papers that have been published, accepted, or submitted to the peer-reviewed journals and conferences.

- Journal papers:

    1. X. Chen and W. W. Tan, "Tracking control of surface vessels via fault-tolerant adaptive backstepping interval type-2 fuzzy control," submitted to *Ocean Engineering*.
    2. X. Chen and W. W. Tan, "Passive adaptive interval type-2 fuzzy observer design for dynamic positioning," submitted to *Ocean Engineering*.
    3. X. Chen and W. W. Tan, "Tracking control of surface vessels via adaptive interval type-2 fuzzy logic control," submitted to *Fuzzy Sets and Systems*.

- Conference papers:

    1. X. Chen and W. W. Tan, "Tracking control of surface vessels via adaptive backstepping interval type-2 fuzzy logic control," accepted by *2012 IEEE International Conference on Fuzzy Systems*, Brisbane, Australia, 2012.
    2. X. Chen and W. W. Tan, "Adaptive interval type-2 fuzzy logic observer for dynamic positioning," accepted by *2012 IEEE International Conference on Fuzzy Systems*, Brisbane, Australia, 2012.

3. X. Chen and W. W. Tan, "Tracking control of surface vessels via adaptive type-2 fuzzy logic control," in *Proceedings of 2011 IEEE International Conference on Fuzzy Systems*, Taipei, Taiwan, 2011, pp. 1538-1545.

4. X. Chen and W. W. Tan, "A adaptive type-2 fuzzy logic controller for dynamic positioning," in *Proceedings of 2011 IEEE International Conference on Fuzzy Systems*, Taipei, Taiwan, 2011, pp. 2147-2154.

5. X. Chen and W. W. Tan, "A type-2 fuzzy logic controller for dynamic positioning systems," in *Proceedings of 2010 IEEE International Conference on Control and Automation*, Xiamen, China, 2010, pp. 1013-1018.